Interaction of Biomolecules at the Air-Water Interface: Evaluating the Role of Lipid Composition when Interacting with Lung Surfactant Proteins and Engineered Carbon Nanodiamonds

By

Aishik Chakraborty

Submitted to the department of Chemical & Petroleum Engineering and the Graduate Faculty of the University of Kansas in partial fulfillment of the requirements for the degree of Doctor of Philosophy

Chairperson: Dr. Prajnaparamita Dhar

Dr. Stevin Henry Gehrke

Dr. Kevin Charles Leonard

Dr. Arghya Paul

Dr. Gibum Kwon

Date Defended: 23rd July 2019

The Dissertation Committee for Aishik Chakraborty attests that this is the approved version of the following dissertation:

Interaction of Biomolecules at the Air-Water Interface: Evaluating the Role of Lipid Composition when Interacting with Lung Surfactant Proteins and Engineered Carbon Nanodiamonds

_____

Chairperson: Dr. Prajnaparamita Dhar

Date approved:

ABSTRACT

Lung surfactants (LSs) are a complex mixture of lipids and proteins that are found in the alveolar lining of the lungs. Their primary objective lies in lowering the surface tension of the aqueous layer on which they reside. By doing so, LSs reduce the energy involved in breathing, and any loss/ dysfunction of the surfactants can cause fatal respiratory complications. Successful treatment methods require a thorough understanding of the biophysical properties of the LSs, and their interaction with any material that may come in contact. This dissertation aims at evaluating the interaction of the different lipids found in the surfactant pool with such plausible candidates at the air-water interface. Engineered carbon nanodiamonds (ECNs) is selected because of their potential in becoming a candidate for drug delivery through the respiratory tract. Therefore, it is necessary to evaluate any possible toxic outcome from ECNs. Here, we observe that both the lipid headgroup charge and the tail saturation impact the biophysical properties of the monolayer. We also evaluate the impact of the protein, Mini-B, which is a synthetic analog of the native surfactant protein, SP-B, on the biophysical properties of the LSs. Mini-B is a suitable candidate for surfactant replacement therapy (SRT), which is associated with lung diseases. Thus, Mini-B needs a thorough biophysical analysis. Lastly, we observe the effectiveness of Mini-B in countering the deleterious effects of cholesterol. Cholesterol is found in the native mixture and helps in fluidizing the monolayer. However, cholesterol has been reported to have some harmful impact on the LSs. Thus, it is a highly disputed component in SRT, with some formulations removing cholesterol from their product. We observe that 1 to 5 wt.% of Mini-B can counter the harmful effects of small quantities of cholesterol, providing a wholesome mixture.

Dedicated to my beloved parents:

Dr. Nibedita Chakrabarti and Dr. Manoj Kumar Chakrabarti

ACKNOWLEDGEMENT

My journey through graduate school would not have been possible without the tireless contribution of my beloved advisor, Dr. Prajnaparamita Dhar. She has been the primary source of positive influence throughout my professional life as well as personal, and I cannot thank her enough for her kind guidance. She is an inspiring individual and is extremely hard working. Her style of conducting research, solving problems, and teaching students have made a lasting impression on me, and I am grateful to have been a part of her laboratory.

At this point, I would also like to express my sincere gratitude to Dr. Stevin Gehrke. I was fortunate enough to have worked with him closely on both research and class. I am grateful for his kind mentorship. Other than research, I would like to point out his style of teaching courses. I adored the way he communicated complex material through real-life examples taken from the surroundings. I hope to implement such teaching philosophy in the future, and I am grateful to have been his teaching assistant.

I would also like to thank the rest of my phenomenal committee members, Dr. Kevin Leonard, Dr. Arghya Paul and Dr. Gibum Kwon for their kind counsel. They have lent their helping hands throughout my graduate studies.

I have also had the pleasure of being a teaching assistant to Dr. Karen Nordheden, and I immensely enjoyed working with her. I would also like to acknowledge the contributions of all the professors, including Dr. Laurence Weatherley, and the members of the administration, especially Ms. Martha Kehr, of Chemical & Petroleum Engineering, University of Kansas, for their constant

support. They have provided me with the right ambiance needed for the completion of my dissertation.

I am also thankful to my colleagues, both past and present, in Dr. Dhar's lab for supporting me throughout this journey. I express special thanks to Dr. Nabil Alhakamy for helping me so much both with research and personal life. I would also like to thank Dr. Saba Ghazvini, Nico Mucci, Rachel Hattaway, Dr. Lorena Napolitano, Joe Scalet, Coleman Vaclaw, and Valerie Pringle for being so supportive. I would also like to thank the undergraduate researchers, who have worked with me, especially, Erica Hui, Monica Ketchum, Mason Choitz, and Hayley Ditmars.

It is needless to say that I have been blessed with amazing friends, in the likes of Aveek Dhar, Ankit Verma, and Aparna Chakravarti, whose company has helped me through the thick and thin of this long journey. I would also like to thank Dr. Animesh Dhar, KU Medical Center, and Dr. Minati Dhar, Children's Mercy Hospital. They have been a loving presence during my graduate studies.

Lastly, it would be impossible to end this section without acknowledging the contributions of my parents, Dr. Manoj Kumar Chakrabarti and Dr. Nibedita Chakrabarti. They have helped me consistently through all my struggles. A countless number of times, I troubled them when the going got tough, and they were there every time, without losing hope, and cheerfully motivating me to pick myself up. It is with all humility that I dedicate this thesis to my loving parents.

TABLE OF CONTENTS

LIST OF FIGURES

Chapter 1

Chapter 2

Chapter 3

Chapter 4

Chapter 1: Introduction

1. INTRODUCTION:

1.1.Origin of lung surfactants:

Lung surfactants [LSs] are a complex mixture of lipids and proteins. Through the process of exocytosis of vesicles, called Lamellar Bodies [LBs], LSs are released into the alveolar space from Alveolar Type II [AT II] cells [1, 2]. Prior to birth, a glycogen pool acts as the source of carbon for the LSs, however, after birth the phospholipids are synthesized in the endoplasmic reticulum. The various components of the surfactants are then transported to the lamellar bodies [LBs], which act as a storage location for the surfactants. In addition to the phospholipids, two major surfactant proteins are also present in the LBs. These surfactants, namely, SP-B and SP-C, are synthesized in the endoplasmic reticulum, and then via the Golgi apparatus, transported to the LBs. LBs are bound by a limiting membrane that fuses with the plasma membrane. Eventually, from the LBs, the LSs are released into the extracellular region [3, 4]. However, not all the components of the surfactants are present in the LBs. Surfactant proteins, namely SP-A and SP-D are secreted independently. Once the surfactants are released in the extracellular region, the complex components give rise to three dimensional, lattice-like macromolecular aggregates, called Tubular Myelin [TM], in the alveolar lining fluid [ALF]. The ALF is thin and continuous over the surface of the alveoli, ranging between 0.1 μm to several μms in thickness [5]. The lipophilic nature of the surfactants combined with contribution from SP-A and divalent ions (Ca^{2+}) help in the formation of TM [6, 7]. However, TM is not the only structure that appears in the ALF. Several other microstructures such as

small vesicles [SVs] are also present in the alveolar lining fluid [8]. From these aggregates the surfactants finally make their way to the surface of the liquid lining.

Once reaching the surface of the ALF, the surfactants form a film. The primary function of this film is to lower the surface tension. The molecules at the surface face forces that are not balanced. The attractive forces at the interface try to minimize the area covered. While exhaling, these forces can be strong enough to collapse the alveoli, which in turn reduces the area for gas exchange. The surfactants displace the water molecules at the interface, which reduces the attractive forces acting at the surface. This result in the lowering of surface tension, thereby, avoiding the collapse of the alveoli [9]. Therefore, the role of surfactant is paramount in the proper physiological functioning of the lungs, and any lack or dysfunction of the surfactants results in a multitude of diseases. Most commonly, neonatal respiratory distress syndrome [NRDS] and hyaline membrane disease has been linked with lung surfactant disorder [10]. Additionally, many obstructive pulmonary diseases have been linked with lung surfactant disorder [11]. The list includes asthma, chronic obstructive pulmonary disorder [COPD], cystic fibrosis, and pneumonia. Furthermore, interstitial lung diseases such as idiopathic pulmonary fibrosis, sarcoidosis, pulmonary alveolar proteinosis, and hypersensitivity pneumonitis have also been associated with surfactant disorders. Thus studying the biophysical properties of the surfactants is of utmost importance. In fact, surfactant replacement therapy has been clinically successful in the case of newborn babies suffering from respiratory

distress syndrome [12]. However, most clinically approved surfactants at present are animal derived, and these natural surfactants are given preference over the synthetic ones. Studies have shown a marginal decrease in the risk of mortality with animal derived surfactants but at the same time, an increase in intra ventricular hemorrhage was reported with these surfactants [13]. Thus, further research is needed to come up with effective synthetic surfactants. More compositions need to be tested, and their biophysical properties and molecular interactions at the interface must be evaluated.

1.2 Composition of Natural Lung Surfactants:

Natural lung surfactants primarily consist of lipids [14]. Among the different components of lipids, the phospholipids form the primary constituent. Trace amounts of phosphatidylinositol, phosphatidylserine and plasmalogen analog of phosphatidylcholine are found in the surfactants. However, the bulk of the phospholipids are made up of Phosphatidylcholine, of which dipalmitoylphosphatidylcholine, DPPC accounts for 41-70% of the phosphatidylcholine. Furthermore, 10 mol% of phosphatidylglycerol forms another significant component of the surfactants. Other than phospholipids, neutral lipids also are a part of the surfactant mixture, particularly, cholesterol. Cholesterol makes up for 8 weight % of the lung surfactants. Lastly, surfactant proteins contribute to about 10% of the mixture. SP-A and SP-D comprises of the majority of the surfactant proteins, however, even at lower concentrations, SP-B and SP-C contributes significantly to the proper physiological functioning of the

lung surfactants. The composition of bovine surfactant has been given in Fig 1 [15].

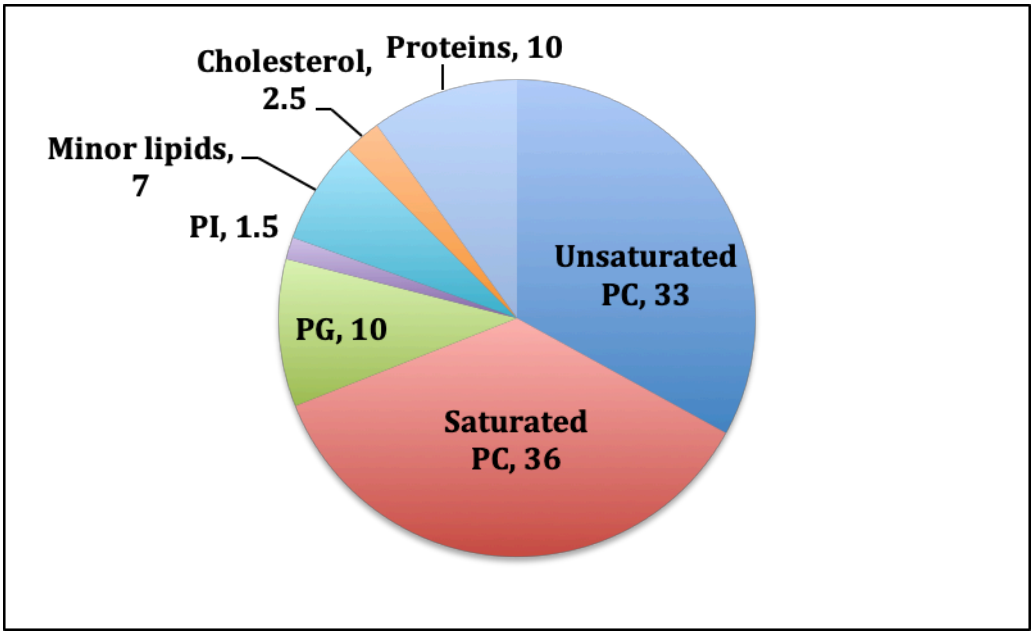

Fig 1. *Composition of the bovine lung: The saturated DPPC, at 36%, forms the major component of the lung surfactants. The unsaturated PC group of phospholipids comes in second at 33%. Thus, PC headgroup comprises of most of the surfactant pool. The PG headgroup contributes to 10% of the total composition. This includes both saturated and unsaturated PG lipids. Phosphatidylinositol, PI, lipids form around 1.5% whereas, cholesterol stands around 2.5%. The minor components consist of phosphatidylethanolamine, PE, lyso-bis-phosphatidic acid, sphingomyelin and diacylglycerol.*

1.3 Function of Natural Lung Surfactants:

The main objective of the surfactants is to reduce the surface tension of the alveolar fluid lining. Surfactant vesicles in the alveolar fluid lining adsorb highly rapidly to the surface, and during exhalation, the surfactants are capable of lowering the value of surface tension to near zero values [16]. However, lung surfactants also promote gas exchange and alveolar stability among other functions. Table 1 lists the biophysical functions of the lung surfactants.

Biophysical Function
1. Lung surfactants prevent the collapse of the alveoli during expiration. 2. Lung surfactants prevent the formation of lung edema by balancing hydrostatic filtration forces. 3. They are responsible for stabilizing and keeping small airways unobstructed. 4. The surfactants also enhance mucociliary transport and assists in the inspiratory opening of the lungs. 5. The surfactants also assist in the translocation of particles under 6mm into the hypo-phase of the alveolar lining fluid. 6. By lowering the surface tension, the surfactants also help in removing particles and cellular debris from the alveoli.

Table 1: *The biophysical functions of lung surfactants have been taken from ref [10], lists the different physiological functions of the lung surfactants.*

Other than the biophysical functions listed above, the surfactants also serve an important role in defending against foreign invasions. Specifically, the proteins SP-A and SP-D help in opsonizing microorganisms for their effective removal through phagocytosis. Thus, SP-A and SP-D help modulate is involved with modulating phagocytosis, oxidative bursts of macrophages and chemotaxis.

Additionally, SP-A and SP-D also bind and capture bacterial toxin for their swift removal. Furthermore, the phospholipids of the lung surfactants also inhibit the release of endotoxin-stimulated cytokine from macrophages [10]. Therefore, lung surfactants play a vital role in the proper functioning of the lungs along with carrying out immunological tasks.

1.4. Function of individual components:

1.4.1 Phospholipids: The saturated phospholipid, DPPC, is the only component in the surfactant pool that can lower the surface tension to near zero values at the air/water interface of the alveoli at the end of each respiratory cycle [17]. Fig 2 shows the molecular structure of DPPC.

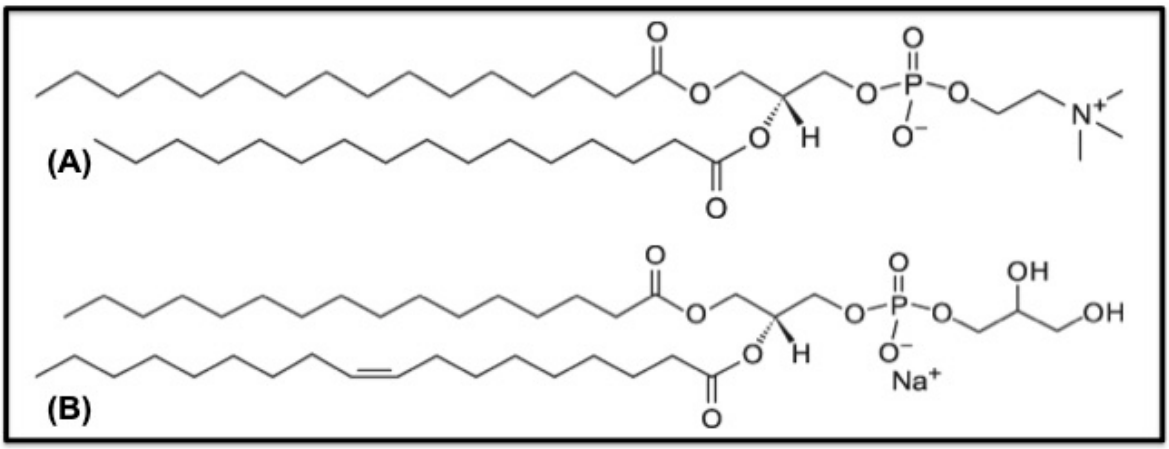

Fig 2. *The image represents the molecular make up of two major components of the lung surfactants, (A) DPPC and (B) POPG. (Source: Avanti Polar Lipids)*

The two 16 carbon acyl chains in DPPC are devoid of any unsaturation. Therefore, when compressed, the acyl chains can line up perfectly and form a

highly packed monolayer. The ability of DPPC to pack tightly allows it to remain at the interface at high compression, which eventually lowers the surface tension. Furthermore, in vitro studies suggest two theories for DPPC build-up at the surface. One is the addition of new DPPC into the monolayer and the other one is the squeeze-out of unsaturated lipids from the surface and the subsequent enrichment of the monolayer with DPPC [18]. A modified squeeze out method has also been proposed where the formation of multiple layers was observed with Langmuir studies [19]. Here, the monolayer, while getting enriched with saturated phospholipids, removes the unsaturated components from the surface. These unsaturated lipids then form multilayered stacks that remain associated with the surface because of the surfactant proteins. Although DPPC serves the primary purpose of lowering the surface tension, it has been observed that vesicles of DPPC films form monolayers extremely slowly at temperatures lower than its gel-to-fluid phase transition temperature of 41^{o}C. Therefore, at body temperature, DPPC is too rigid to be able to adsorb rapidly to the interface. Additionally, DPPC on it's own is also incapable spreading quickly on the surface. These disadvantages associated with DPPC gives rise to the necessity of other components that are more fluid than the saturated ones. In this regard, the acidic phospholipids play an important part. As discussed earlier, unsaturated PG and PI also contribute to the mixture, and a combination of the unsaturated phospholipids along with DPPC enhances the adsorption and respreading of material at the interface. Furthermore, the acidic unsaturated components can also interact with surfactant proteins, which further improves the properties of the

surfactants. Lower quantities of PG lipids decrease the biophysical activities of the surfactants, and have also been linked with acute respiratory distress syndrome. However, the unsaturation in the acyl chain, as can be seen in Fig 2B, prevents these molecules from packing tightly at the interface when compressed, and usually, they collapse within a surface pressure of 50 mN/m. Other than the PC, PG and PI lipids, there are some minor constituents in the native surfactant mixture. But it is unlikely that these molecules provide a significant contribution towards the biophysical activity of the mixture.

1.4.2 Neutral Lipids: Finally, some neutral lipids, most notably cholesterol, is also present in the native mixture. Cholesterol primarily increases the fluidity of the mixture. Low quantities of cholesterol have been shown to be effective in surfactant mixtures. However, the presence of a high concentration of cholesterol fails to lower the surface tension to zero [20-24]. The biophysical activity of the surfactants is lowered because cholesterol cannot be squeezed out of the monolayer with ease [25]. Therefore, the monolayer is no longer enriched in DPPC, making it impossible to reach near zero surface tension. Furthermore, in vivo studies have also shown the presence of elevated quantities of cholesterol in the case of ventilator-induced lung injury. This form of injury also leads to a reduction in the biophysical activity of the lung surfactants [26]. However, as mentioned earlier, native surfactant contains cholesterol. Additionally, it has been observed that small quantities of cholesterol can improve the biophysical properties of the lung surfactants [27]. Essentially, small quantities of cholesterol are capable of lowering the viscosity of the surfactants, thus increasing the

spreadability of the surfactants at the interface. Additionally, studies with captive bubble surfactometer have shown that cholesterol has negligible impact on BLES [28]. Strikingly, inconsistency in the formulation of medicinal surfactants can be observed. Some formulations used in surfactant replacement therapy consist of cholesterol, while others actively remove the cholesterol component. Therefore, there is little consensus in the composition of the synthetic or animal derived surfactants. In practice, commercial surfactants like, Survanta ® (bovine lung mince) has less than 0.2% cholesterol, whereas, Curosurf ® (Porcine lung mince) has no cholesterol at all. The same is the case for entirely synthetic compositions where no cholesterol is added to the mixture. On the contrary, Infasurf ® (calf lung lavage), BLES ® (bovine lung lavage) and BNS (Bovine Lung Lavage) contain up to 8% cholesterol [29]. Therefore, the purpose and use of cholesterol in the formulations for replacement therapy is extensively debated.

1.4.3 Surfactant Proteins: The four surfactant proteins plays specific functions related to the biophysical activity of the surfactants and the promotion of immune response. The surfactant proteins can be divided into two categories, namely, the hydrophobic group, and the other one being the hydrophilic group.

1.4.3.1 Hydrophobic Proteins: The surfactant proteins SP-B and SP-C are the two hydrophobic proteins found in the surfactant pool. The 17 kDa SP-B contains 79-amino acid in its molecular construct. This amphipathic peptide is prepared in the type II epithelial cells [30, 31]. It belongs to the sphingolipid activator saposin family of proteins. SP-B has a longer, 381 amino acids precursor. However, it goes through a proteolytic cleavage of the N- and C- terminals to get into the final

sequence. The mature SP-B is highly cationic with a net positive charge of +7. Additionally, dimerization of the monomeric form occurs with the formation of intermolecular disulfide bond at Cys48. After the completion of the cleavage of the proprotein in the type II epithelial cell, the dimerization takes place. In native surfactants, SP-B is present in quantities less than 1.5% of the total weight. However, even at a small concentration, SP-B is capable of significantly enhancing the properties of the native surfactants. In fact, absence of SP-B has been shown to be severely detrimental [32-35]. On the other hand, the SP-C is a smaller peptide with a molecular mass of 4.2 kDa and containing 35 amino acid residue [36]. SP-C is also a positively charged peptide alongside having over 70% non-polar residues, making it highly hydrophobic. Both SP-B and SP-C have been intensively studied to find out their significance in the surfactant mixture. SP-B and SP-C help with lipid insertion into the monolayer [37]. Furthermore, it has also been shown that at low surface pressures, SP-B fluidizes the monolayer, whereas at high surface pressures, SP-C increases the compressibility of the monolayers [38]. Additionally, because they promote the insertion of lipid molecules into the air/water interface, they help with lowering the surface tension and prevent the insertion of serum into the monolayer. Overall, SP-B helps with the reconstitution of the tubular myelin, enhances adsorption of the phospholipid to the interface and helps with respiratory function. On the other hand, SP-C aids in stabilizing surface-associated surfactant reservoirs. SP-C also promotes the adsorption of phospholipids to the air/water interface [39]. The following table lists the known functions of both SP-B and SP-C.

Protein	Function
SP-B	Interacts selectively with the PG headgroup of phospholipid bilayers
	Promotes the aggregation of phospholipids
	Also interacts with the superficial region of the bilayer
	Helps with stabilizing phospholipid monolayers
	Promotes squeeze out
	Promotes the exchange of phospholipids between vesicles and bilayers
	Helps in incorporating phospholipid molecules into the air/water interface
SP-C	
	Interacts with bilayers
	Helps with squeeze out
	Helps in creating three-dimensional structures
	Helps in respreading of films

Table 2: *The table summarizes the functions of SP-B and SP-C in the surfactant mixture [39].*

1.4.3.2. Hydrophilic Proteins: SP-A and SP-D are two hydrophilic members of the surfactant pool, with significantly larger size than that of SP-B and SP-C [40]. SP-A is a 630 kDa protein, whereas SP-D is a 520 kDa protein. Both SP-A and SP-D have been attributed with immunogenic functions. It has been shown to have anti-viral, anti-bacterial, anti-fungal properties among others.

1.4.3.3. Synthetic Proteins: First generation synthetic medicinal surfactants composed only of lipids. Alec, a mixture of DPPC along with egg PG, and Exosurf, a mixture of DPPC with hexadecanol and tyloxapol, were two synthetic mixtures devoid of any surfactant protein [41]. However, they found little clinical success. Thus, second generation medicinal surfactants have focused on preparing alternatives that contain synthetic analogs of SP-B and SP-C. Surfaxin and Venticute are two such examples, which have employed synthetic analog of SP-B, KL4 (Surfaxin) and recombinant human surfactant protein C, rhSP-C (Venticute). Truncated SP-B mimics with 1-25 amino acid residues, SP-B_{1-25}, and 49-66 amino acid residues, SP-B_{49-66}, have also shown potency similar to that of their native parent protein [42, 43]. Mini-B is one such synthetic alternative that has been biophysically characterized in this work.

Mini-B is a synthetic analog of SP-B containing 34 amino acid residue [44]. It is based on the predicted N- and C- terminals of SP-B. Similar to SP-B, Mini-B has a charge of +7. Containing four of the six conserved cysteines, which define the saposin fold, Mini-B is capable of forming disulfide bridge, C1-C33 and C4-27, between the two helices when oxidized. The amino acid sequence of Mini-B is as follows: -CWLCRALIKRIQAMIPKGGRMLPQL VCRLVLRCS, and it is synthesized by solid phase chemical synthesis via *O*-fluorenylmethyloxycarbonyl (Fmoc) chemistry with partial ^{15}N-labeling. The disulfide linkages are synthesized by the selective deprotection of the cysteine residues at C1 and C33 through trityl side-chain protecting protocol. Finally, air-mediated oxidation of Mini-B forms the disulfide links at the desired location.

Mini-B is also effective in mimicking the in vitro and in vivo characteristics of SP-B. It has been shown that the oxidized form of Mini-B containing the disulfide linkage is more potent at reducing surface tension than the reduced counterpart [45]. Furthermore, we had also shown the capability of Mini-B to counter the deleterious effects of cholesterol [46], which forms part of the current thesis.

1.5. Impairment of lung surfactant activity:

Pulmonary immaturity in the case of prematurely born infants leads to an absence of lung surfactants. This is a fatal condition, which needs an immediate clinical response. However, lung immaturity is not the only source of surfactant impairment [47]. A loss in the activity of lung surfactants may occur at any age because of an injury to the type II alveolar cells. Furthermore, the presence of inhibitors may also cause abnormalities in the lungs. These abnormalities then trigger an increase in the surface tension of the aqueous-lining in the alveoli, which in turn, severely impacts the breathing process. Degradation of the components may also cause similar irregularities. Degrading agents like phospholipases, released during pulmonary inflammation, may trigger respiratory distresses. Thus, the properties of the individual components along with their interaction with foreign agents must be thoroughly studied to devise necessary medical intervention.

Among the different components in the surfactant pool, cholesterol is a disputed one because of its potential detrimental impact on the biophysical properties of the lung surfactants [48, 49]. The function of cholesterol in the

native surfactant mixture is still relatively unknown. Even at low concentrations, cholesterol is capable of altering the morphology and dynamics of phospholipid monolayers [27]. Furthermore, elevated concentrations of cholesterol have been found in lung diseases [26, 50]. Therefore, cholesterol is removed from most commercial surfactant mixtures. However, some studies have indicated that at physiological concentrations, cholesterol has less impact compared to that at elevated conditions [20, 23, 24]. Additionally, native surfactant mixture contains cholesterol and is capable of lowering surface tension to near zero values. Moreover, cholesterol is capable of lowering the phase transition temperature of the lipids [28]. Highly ordered, rigid lipid in the gel phase transitions to a more fluid, liquid-crystalline phase in the presence of cholesterol, meaning, cholesterol enhances the fluidity of the lung surfactant mixture, which in turn improves the spreadability of the surfactants [51]. Thus, a balanced lung surfactant mixture is needed, which can lower surface tension to near zero and at the same time be fluid enough to spread rapidly. Cholesterol can therefore be a critical component in surfactant-mediated intervention. To counter the deleterious effects of cholesterol, SP-A has been used in the past [52]. Additionally, the protein SP-C has also been shown to counter the negative effects of cholesterol [53]. In our work [46], we investigated the role of the synthetic protein, Mini-B, in countering the adverse impact of cholesterol on the biophysical properties of the surfactant monolayer.

Another component that may alter the functions of lung surfactants are foreign particles that are small enough to reach the inner linings of the alveoli.

Once reaching the alveoli, these nano-sized particles encounter the lung surfactants, which act as a line of defense against such particles. However, there are cases where nanoparticles maybe added to the lungs as a means of drug delivery. Artificially inserted or not, the toxicity of these particles must be evaluated, and any material that can adversely impact the functioning of the lungs must be discarded. The following section briefly introduces the use of nanoparticles and highlights the necessity to evaluate the potential toxic behavior of such particles.

Nanotechnology, which involves the formulation, characterization and application of nano-sized solid particles, has been gaining ground rapidly over the past several decades. The nano-scale size of these particles makes their properties different from that of their bulk counterpart. These properties provide some unique advantages to the nanoparticles. They have a large ratio of surface area to volume. Additionally, the surface properties of these particles can be easily modified. Furthermore, related to therapy and diagnostics, the shape and the size of these particles allow them to reach locations that are otherwise impregnable. Thus, nanoparticles are regularly used in medicine, cosmetics, solar cells, agriculture and food sector, water treatment, oil and gas industry, textile industry, construction industry to name a few of the sectors [54-69]. From brake pads in vehicles to manufacturing plants, nanoparticles are widely present [70, 71]. Additionally, engineered nanoparticles are being constantly used in a variety of consumer products [72]. Of the various nanoparticles, carbon nanodiamonds is an emerging type of nanomaterial. The detonation synthesis of

nanodiamonds was discovered in 1963 but over the last two decades, multiple synthesis techniques have been optimized to provide the nanodiamonds with unique physical, chemical, and biological properties [73, 74]. These particles have found application in both diagnosis and therapeutics. However, the increase in use has also led to an increase in the exposure of these particles. As a consequence, there are multiple routes of entry for the nanoparticles, and owing to both systemic and local advantage related to drug delivery, the respiratory tract is one favorable port of insertion [75]. On their own, lung surfactants provide hydrophobic regions that can host therapeutic molecules and poorly soluble drugs, which can treat both respiratory and systemic diseases [76, 77]. Thus, the surfactants can act as a simple excipient for the drug when considering systemic diseases, and in the case of local respiratory illness, the surfactants can act as a therapeutic agent along with being carriers. However, the combination of surfactants with nanoparticles has also been considered for the purpose of drug delivery. Recently, a combination of siRNA loaded with dextran nanogel and an outer nano-composite was shown to be an effective method for delivering siRNA [78]. Thus, it is of utmost importance to assess the interaction of nanoparticles with lung surfactants so that their combination can be used as a carrier for drug molecules.

Even though there are mechanical barriers like mucociliary apparatus and dendritic cells that capture larger particles [79], small enough materials are capable of inserting themselves into the alveoli through gravitational sedimentation, inertial impaction, interception and diffusion [80]. Thus, the size of

the particles plays a pivotal role in the location of deposition. The larger particles tend to get deposited in the upper layers of the respiratory canal, whereas the smaller ones are capable of reaching the alveoli. It has been reported that particles ranging within 100 to 200 nm in size have an approximately 15% likelihood to be deposited in the alveoli of the lungs [81]. Smaller particles that are around 20 nm in size have an even higher probability of reaching the alveoli. Furthermore, these particles may stay in the lungs for 700 days. Therefore, these particles may pose a threat to the proper functioning of the lungs. Moreover, the lung surfactants come in contact with the particles that reach the alveoli. Therefore, the surfactants form a barrier of resistance against both the unwanted and the medicinal nanomaterial. Furthermore, the behavior of the material in their nano form can be very different from their microform. For example, TiO_2 nanoparticles inhibited the biophysical function of surfactants as a function of concentration, but the micro-particles of TiO_2 didn't have the same effect [82]. As a result, it is necessary to monitor the possible toxic impact of the nanoparticles on the lung surfactants. Over the last several years, studies have focused on the biophysical interaction of lung surfactants with metallic and polymeric nanomaterial varying in size, composition, modifications in surface chemistry and surface potential. However, the results have been contradictory, and thus, making it even more necessary to continue investigating the nature of the interaction.

Fan *et al.* showed that even small concentrations of Hydroxyapatite nanoparticles can hinder the biophysical function of lung surfactants [83]. Here, a

progressive decay in the surface tension lowering capability of Infasurf was observed with time when 1 wt.% Hydroxyapatite nanoparticle was added. In two separate studies, Guzman *et al.* showed the impact of silica nanoparticles on the phase behavior of different model lung surfactant system [84, 85]. Valle *et al* suggested that hydrophobicity of polymeric nanoparticles plays a role when interacting with infasurf [86]. Increase in the hydrophobicity of the nanoparticles showed an increased deterioration in the biophysical properties of the nanoparticles. Furthermore, Harishchandra *et al.* showed the impact of organosiloxane nanoparticles on model lung surfactant systems [87]. Here, the nanoparticles caused a notable change in the phase behavior of the lung surfactants. Additionally, the lipid domain structure at the interface was also impacted by the nanoparticles. However, the damage to the biophysical properties of the surfactants was dependent on the concentration of the nanoparticle. Another study by Beck-Broichsitter *et al.* demonstrated the impact of polymeric nanoparticles on lung surfactant mixtures [88]. Higher concentration of the nanoparticles deteriorated the biophysical properties of the surfactants. The type of surfactant also impacted the biophysical behavior. This was previously observed by the same group, where only negatively charged polymeric nanoparticles notably deteriorated the biophysical properties of the surfactants [89]. Impact of metallic nanoparticles has also been investigated [82, 90, 91]. In the case of gold nanoparticles, samples containing even less than 1 wt.% of gold drastically inhibited the biophysical function of DPPC/POPG/SP-B monolayers [90]. But, the study by Tatur *et al.* displays that 0.2 mol% of the

hexadecanethiolate-capped gold nanoparticles didn't have any effect on the surface tension lowering capability of DPPC but notably modified the lipid domains at the interface [91]. Even 16 wt.% of the nanoparticle had no effect on the clinical surfactant, Survanta. Survanta is a more complex lipid system than DPPC. Thus, there were discrepancies in the behavior of the same set of nanoparticles in the presence of different phospholipid systems. Studies so far focused on the properties of the nanoparticles like surface charge, size, shape, and type, but the difference in the behavior led us to investigate the interaction of engineered carbon nanodiamond [ECN] in the presence of different model lung surfactant systems [92].

1.6. Thesis organization:

The primary theme of the thesis is to evaluate the role of the phospholipids when interacting with other components that can come in contact with lung surfactants. Often times, the contribution of the phospholipids is neglected, having the focus predominantly on the foreign agents. However, the role of the phospholipids, and the overall composition, should not be neglected when determining the effectiveness of the surfactants in the presence of the foreign components. Furthermore, the knowledge from this thesis can be extended to lipid systems outside that of the lungs. For instance, the behavior of the engineered carbon nanodiamonds is dependent on the lipid mixture to which they are introduced. Therefore, even though these particles aren't toxic to certain compositions in moderate quantities, they can be detrimental to some other

compositions. So, the route of entry of these particles has a notable impact on their behavior. The following section outlines the topics to be discussed in this dissertation.

Chapter 2 focuses on the impact of cholesterol on a model lung surfactant mixture. Furthermore, the synthetic protein, Mini-B, has been applied to counter the deleterious effects of cholesterol. Here, emphasis has been placed on two biophysical functions of the surfactants. The ability of the surfactants to lower surface tension to near zero values is the primary objective, whereas, the ability of the surfactants to readsorb and retain material at the interface after each cycle of compression and expansion is the second objective. Based on the performance of the compositions, the concentration of the mixture has been optimized. Smaller quantities of cholesterol can have a positive role in fluidizing the monolayer. We observe that 1% to 5% of Mini-B is capable of countering the deleterious effect of smaller concentrations of cholesterol. Increasing the concentration, however, still proves to be malicious for the surfactant mixture.

Chapter 3, on the other hand, discusses the impact of ECN on the biophysical properties of the lung surfactant monolayers. We primarily focus on the phospholipid composition when interacting with the ECN. Model mixtures containing two phospholipids have been studied in this chapter. Disaturated phosphatidylcholine has been kept constant for all the mixtures tested. The second phospholipid has been altered to modify the behavior of the monolayers. Altering the lipid headgroup charge and the lipid tail saturation also makes an

impact on the way the monolayers behave in the presence of ECN. The most profound negative influence is seen with mixtures that contain the neutral, mono-unsaturated phosphatidylcholine. On the other hand, negatively charged disaturated phosphatidylglycerol shows favorable properties in the presence of ECN. The chapter also concludes that the anionic lipids are better suited to interact with ECN than their zwitterionic counterpart.

Chapter 4 investigates the role of the phospholipid composition when interacting with the synthetic protein, Mini-B. Here too, lowering of surface tension as well as the ability to readsorb and retain material at the surface has been considered as the key properties of the surfactants. We observed that a zwitterionic mixture with 5% Mini-B has the best response. Furthermore, we speculate that the vesicles formed in the case of the zwitterionic mixture get reincorporated into the interface. Lastly, we believe that the location of insertion of the protein into the interface plays a part in modifying the behavior of the surfactant mixtures.

1.7. References:

1. Haller, T., et al., *Dynamics of surfactant release in alveolar type II cells.* Proceedings of the National Academy of Sciences, 1998. **95**(4): p. 1579.
2. Andreeva, A.V., M.A. Kutuzov, and T.A. Voyno-Yasenetskaya, *Regulation of surfactant secretion in alveolar type II cells.* American Journal of Physiology-Lung Cellular and Molecular Physiology, 2007. **293**(2): p. L259-L271.
3. Dietl, P., et al., *Mechanisms of Surfactant Exocytosis in Alveolar Type II Cells In Vitro and In Vivo.* Physiology, 2001. **16**(5): p. 239-243.
4. Haagsman, H.P. and L.M.G. Van Golde, *Synthesis and Assembly of Lung Surfactant.* Annual Review of Physiology, 1991. **53**(1): p. 441-464.
5. Bastacky, J., et al., *Alveolar lining layer is thin and continuous: low-temperature scanning electron microscopy of rat lung.* Journal of Applied Physiology, 1995. **79**(5): p. 1615-1628.
6. Hawgood, S., B.J. Benson, and R.L. Hamilton, *Effects of a surfactant-associated protein and calcium ions on the structure and surface activity of lung surfactant lipids.* Biochemistry, 1985. **24**(1): p. 184-190.
7. Poulain, F.R., et al., *Effects of surfactant apolipoproteins on liposome structure: implications for tubular myelin formation.* American Journal of Physiology-Lung Cellular and Molecular Physiology, 1992. **262**(6): p. L730-L739.
8. Gross, N.J., *Extracellular Metabolism of Pulmonary Surfactant: The Role of a New Serine Protease.* Annual Review of Physiology, 1995. **57**(1): p. 135-150.

9. Lopez-Rodriguez, E. and J. Pérez-Gil, *Structure-function relationships in pulmonary surfactant membranes: From biophysics to therapy.* Biochimica et Biophysica Acta (BBA) - Biomembranes, 2014. **1838**(6): p. 1568-1585.

10. Griese, M., *Pulmonary surfactant in health and human lung diseases: state of the art.* European Respiratory Journal, 1999. **13**(6): p. 1455.

11. Devendra, G. and R.G. Spragg, *Lung surfactant in subacute pulmonary disease.* Respiratory research, 2002. **3**(1): p. 19-19.

12. Richard A. Polin, W.A.C., *Surfactant Replacement Therapy for Preterm and Term Neonates With Respiratory Distress.* PEDIATRICS 2014. **133**(1): p. 156-163.

13. Ardell, S., R.H. Pfister, and R. Soll, *Animal derived surfactant extract versus protein free synthetic surfactant for the prevention and treatment of respiratory distress syndrome.* Cochrane Database of Systematic Reviews, 2015(8).

14. Goerke, J., *Pulmonary surfactant: functions and molecular composition.* Biochimica et Biophysica Acta (BBA) - Molecular Basis of Disease, 1998. **1408**(2): p. 79-89.

15. Zuo, Y.Y., et al., *Current perspectives in pulmonary surfactant — Inhibition, enhancement and evaluation.* Biochimica et Biophysica Acta (BBA) - Biomembranes, 2008. **1778**(10): p. 1947-1977.

16. Rugonyi, S., S.C. Biswas, and S.B. Hall, *The biophysical function of pulmonary surfactant.* Respiratory physiology & neurobiology, 2008. **163**(1-3): p. 244-255.

17. Veldhuizen, R., et al., *The role of lipids in pulmonary surfactant.* Biochimica et Biophysica Acta (BBA) - Molecular Basis of Disease, 1998. **1408**(2): p. 90-108.

18. Jesu¨s Pe¨rez-Gil , K.M.W.K., *Interfacial properties of surfactant proteins.* Biochimica et Biophysica Acta, 1998. **1408**(2-3): p. 203-217.

19. Keating, E., et al., *A modified squeeze-out mechanism for generating high surface pressures with pulmonary surfactant.* Biochimica et Biophysica Acta (BBA) - Biomembranes, 2012. **1818**(5): p. 1225-1234.

20. Keating, E., et al., *Effect of Cholesterol on the Biophysical and Physiological Properties of a Clinical Pulmonary Surfactant.* Biophysical Journal, 2007. **93**(4): p. 1391-1401.

21. Diemel, R.V., et al., *Effects of Cholesterol on Surface Activity and Surface Topography of Spread Surfactant Films.* Biochemistry, 2002. **41**(50): p. 15007-15016.

22. Gunasekara, L., et al., *A comparative study of mechanisms of surfactant inhibition.* Biochimica et Biophysica Acta (BBA) - Biomembranes, 2008. **1778**(2): p. 433-444.

23. Gunasekara, L., et al., *Pulmonary surfactant function is abolished by an elevated proportion of cholesterol.* Biochimica et Biophysica Acta (BBA) - Molecular and Cell Biology of Lipids, 2005. **1737**(1): p. 27-35.

24. Leonenko, Z., et al., *An Elevated Level of Cholesterol Impairs Self-Assembly of Pulmonary Surfactant into a Functional Film.* Biophysical Journal, 2007. **93**(2): p. 674-683.

25. Yu, S.-H. and F. Possmayer, *Interaction of pulmonary surfactant protein A with dipalmitoylphosphatidylcholine and cholesterol at the air/water interface.* Journal of Lipid Research, 1998. **39**(3): p. 555-568.

26. Vockeroth, D., et al., *Role of cholesterol in the biophysical dysfunction of surfactant in ventilator-induced lung injury.* American Journal of Physiology-Lung Cellular and Molecular Physiology, 2009. **298**(1): p. L117-L125.

27. Kim, K., et al., *Effect of cholesterol nanodomains on monolayer morphology and dynamics.* Proceedings of the National Academy of Sciences, 2013. **110**(33): p. E3054.

28. Orgeig, S. and C.B. Daniels, *The roles of cholesterol in pulmonary surfactant: insights from comparative and evolutionary studies.* Comparative Biochemistry and Physiology Part A: Molecular & Integrative Physiology, 2001. **129**(1): p. 75-89.

29. Zhang, H., et al., *Comparative study of clinical pulmonary surfactants using atomic force microscopy.* Biochimica et biophysica acta, 2011. **1808**(7): p. 1832-1842.

30. Haagsman, H.P. and R.V. Diemel, *Surfactant-associated proteins: functions and structural variation.* Comparative Biochemistry and Physiology Part A: Molecular & Integrative Physiology, 2001. **129**(1): p. 91-108.

31. Serrano, A.G. and J. Pérez-Gil, *Protein–lipid interactions and surface activity in the pulmonary surfactant system.* Chemistry and Physics of Lipids, 2006. **141**(1): p. 105-118.

32. Nogee, L.M., et al., *A mutation in the surfactant protein B gene responsible for fatal neonatal respiratory disease in multiple kindreds.* The Journal of clinical investigation, 1994. **93**(4): p. 1860-1863.

33. Clark, J.C., et al., *Targeted disruption of the surfactant protein B gene disrupts surfactant homeostasis, causing respiratory failure in newborn mice.* Proceedings of the National Academy of Sciences, 1995. **92**(17): p. 7794.

34. Stefan Kurath-Koller, B.R., Raimund Kraschl, Christian Windpassinger, Ernst Eber, *Surfactant Protein B Deficiency Caused by Homozygous C248X Mutation—A Case Report and Review of the Literature.* American Journal of Perinatology Reports, 2015. **05**(1): p. e053-e059.

35. Wilder, M.A., *Surfactant protein B deficiency in infants with respiratory failure.* The Journal of perinatal & neonatal nursing, 2004. **18**(1): p. 61-67.

36. Johansson, J., *Structure and properties of surfactant protein C.* Biochimica et Biophysica Acta (BBA) - Molecular Basis of Disease, 1998. **1408**(2): p. 161-172.

37. Oosterlaken-Dijksterhuis, M.A., et al., *Characterization of lipid insertion into monomolecular layers mediated by lung surfactant proteins SP-B and SP-C.* Biochemistry, 1991. **30**(45): p. 10965-10971.

38. Ross, M.K., Silke ; Janshoff, Andreas ; Galla, Hans-Joachim, *Kinetics of phospholipid insertion into monolayers containing the lung surfactant proteins SP-B or SP-C.* European biophysics journal, 2001. **31**(1): p. 52-61.

39. Pérez-Gil, J., *LIPID-PROTEIN INTERACTIONS OF HYDROPHOBIC PROTEINS SP-B AND SP-C IN LUNG SURFACTANT ASSEMBLY AND DYNAMICS.* Pediatric pathology & molecular medicine, 2001. **20**(5): p. 445-469.

40. Kishore, U., et al., *Surfactant proteins SP-A and SP-D: Structure, function and receptors.* Molecular Immunology, 2006. **43**(9): p. 1293-1315.

41. Walther, F.J., L.M. Gordon, and A.J. Waring, *Advances in synthetic lung surfactant protein technology.* Expert Review of Respiratory Medicine, 2019: p. 1-3.

42. Frans J. Walther, J.M.H.-J., Larry M. Gordon, *Dimeric surfactant protein B peptide sp-b(1-25) in neonatal and acute respiratory distress syndrome.* Experimental lung research, 2002. **28**(8): p. 623-640.

43. Longo, M.L., A. Waring, and J.A. Zasadzinski, *Lipid bilayer surface association of lung surfactant protein SP-B, amphipathic segment detected by flow immunofluorescence.* Biophysical journal, 1992. **63**(3): p. 760-773.

44. Sarker, M., et al., *Structure of Mini-B, a Functional Fragment of Surfactant Protein B, in Detergent Micelles.* Biochemistry, 2007. **46**(39): p. 11047-11056.

45. Waring, A.J., et al., *The role of charged amphipathic helices in the structure and function of surfactant protein B.* The Journal of Peptide Research, 2005. **66**(6): p. 364-374.

46. Chakraborty, A., et al., *Combined effect of synthetic protein, Mini-B, and cholesterol on a model lung surfactant mixture at the air–water interface.* Biochimica et Biophysica Acta (BBA) - Biomembranes, 2016. **1858**(4): p. 904-912.

47. Christmann, U., et al., *Role of Lung Surfactant in Respiratory Disease: Current Knowledge in Large Animal Medicine.* Journal of Veterinary Internal Medicine, 2009. **23**(2): p. 227-242.

48. Taneva, S. and K.M.W. Keough, *Cholesterol Modifies the Properties of Surface Films of Dipalmitoylphosphatidylcholine plus Pulmonary Surfactant-Associated Protein B or C Spread or Adsorbed at the Air–Water Interface.* Biochemistry, 1997. **36**(4): p. 912-922.

49. Possmayer, S.-H.Y.a.F., *Dipalmitoylphosphatidylcholine and cholesterol in monolayers spread from adsorbed films of pulmonary surfactant.* Journal of lipid research, 2001. **42**(9): p. 1421-1429.

50. Karagiorga, G., et al., *Biochemical parameters of bronchoalveolar lavage fluid in fat embolism.* Intensive Care Medicine, 2006. **32**(1): p. 116-123.

51. R.W. Evans, M.A.W., & J. Tinoco, *Surface viscosities of phospholipids alone and with cholesterol in monolayers at the air-water interface.* Lipids, 1980. **15**(7): p. 524–533.

52. Qua Hiansen, J., et al., *Cholesterol-mediated surfactant dysfunction is mitigated by surfactant protein A.* Biochimica et Biophysica Acta (BBA) - Biomembranes, 2015. **1848**(3): p. 813-820.

53. Gómez-Gil, L., et al., *Pulmonary Surfactant Protein SP-C Counteracts the Deleterious Effects of Cholesterol on the Activity of Surfactant Films under Physiologically Relevant Compression-Expansion Dynamics.* Biophysical Journal, 2009. **97**(10): p. 2736-2745.

54. Wilkinson, J., *Nanotechnology applications in medicine.* Medical device technology, 2003. **14**(5): p. 29—31.

55. Sozer, N. and J.L. Kokini, *Nanotechnology and its applications in the food sector.* Trends in Biotechnology, 2009. **27**(2): p. 82-89.

56. Qu, X., P.J.J. Alvarez, and Q. Li, *Applications of nanotechnology in water and wastewater treatment.* Water Research, 2013. **47**(12): p. 3931-3946.

57. Kapusta, S., L. Balzano, and P.M. Te Riele, *Nanotechnology Applications in Oil and Gas Exploration and Production*, in *International Petroleum Technology Conference*. 2011, International Petroleum Technology Conference: Bangkok, Thailand. p. 5.

58. Silva, G.A., *Introduction to nanotechnology and its applications to medicine.* Surgical Neurology, 2004. **61**(3): p. 216-220.

59. Caruthers, S.D., S.A. Wickline, and G.M. Lanza, *Nanotechnological applications in medicine.* Current Opinion in Biotechnology, 2007. **18**(1): p. 26-30.

60. Y. W. H. Wong, C.W.M.Y., M. Y. S. Leung, S. K. A. Ku, and H. L. I. Lam, *Selected Applications of Nanotechnology in Textiles.* AUTEX Research Journal, 2006. **6**(1): p. 1-8.

61. Raki, L., J.J. Beaudoin, and R. Alizadeh. *Nanotechnology Applications for Sustainable Cement-Based Products*. in *Nanotechnology in Construction 3*. 2009. Berlin, Heidelberg: Springer Berlin Heidelberg.

62. Sanchez, F. and K. Sobolev, *Nanotechnology in concrete – A review.* Construction and Building Materials, 2010. **24**(11): p. 2060-2071.

63. Mu, L. and R.L. Sprando, *Application of Nanotechnology in Cosmetics.* Pharmaceutical Research, 2010. **27**(8): p. 1746-1749.

64. Kwong, C.Y., et al., *Poly(3-hexylthiophene):TiO2nanocomposites for solar cell applications.* Nanotechnology, 2004. **15**(9): p. 1156-1161.

65. Mokhatab, S., M.A. Fresky, and M.R. Islam, *Applications of Nanotechnology in Oil and Gas E&P.* Journal of Petroleum Technology, 2006. **58**(04): p. 48-51.

66. Stark, W.J., et al., *Industrial applications of nanoparticles.* Chemical Society Reviews, 2015. **44**(16): p. 5793-5805.

67. Suphiya Parveen, R.M.a.S.K.S., *Nanoparticles: a boon to drug delivery, therapeutics, diagnostics*

and imaging. Nanomedicine, 2012. **8**(2): p. 147-166.

68. Zhang, L., et al., *Nanoparticles in Medicine: Therapeutic Applications and Developments.* Clinical Pharmacology & Therapeutics, 2008. **83**(5): p. 761-769.

69. Rai, M., et al., *Strategic role of selected noble metal nanoparticles in medicine.* Critical Reviews in Microbiology, 2016. **42**(5): p. 696-719.

70. Kukutschová, J., et al., *On airborne nano/micro-sized wear particles released from low-metallic automotive brakes.* Environmental Pollution, 2011. **159**(4): p. 998-1006.

71. Demou, E., P. Peter, and S. Hellweg, *Exposure to Manufactured Nanostructured Particles in an Industrial Pilot Plant.* Annals of Work Exposures and Health, 2008. **52**(8): p. 695-706.

72. Kessler, R., *Engineered nanoparticles in consumer products: understanding a new ingredient.* Environmental health perspectives, 2011. **119**(3): p. a120-a125.

73. Danilenko, V.V., *On the history of the discovery of nanodiamond synthesis.* Physics of the Solid State, 2004. **46**(4): p. 595-599.

74. Whitlow, J., S. Pacelli, and A. Paul, *Multifunctional nanodiamonds in regenerative medicine: Recent advances and future directions.* Journal of Controlled Release, 2017. **261**: p. 62-86.

75. Sung, J.C., B.L. Pulliam, and D.A. Edwards, *Nanoparticles for drug delivery to the lungs.* Trends in Biotechnology, 2007. **25**(12): p. 563-570.

76. Hidalgo, A., A. Cruz, and J. Pérez-Gil, *Barrier or carrier? Pulmonary surfactant and drug delivery.* European Journal of Pharmaceutics and Biopharmaceutics, 2015. **95**: p. 117-127.

77. Guagliardo, R., et al., *Pulmonary surfactant and drug delivery: Focusing on the role of surfactant proteins.* Journal of Controlled Release, 2018. **291**: p. 116-126.

78. De Backer, L., et al., *Bio-inspired pulmonary surfactant-modified nanogels: A promising siRNA delivery system.* Journal of Controlled Release, 2015. **206**: p. 177-186.

79. Nicod, L.P., *Lung defences: an overview.* European Respiratory Review, 2005. **14**(95): p. 45.

80. Malgorzata Smola, T.V., Adam Sokolowski, *Nanocarriers as pulmonary drug delivery systems to treat and to diagnose respiratory and non respiratory diseases.* International journal of nanomedicine, 2008. **3**(1): p. 1-19.

81. Günter Oberdörster, E.O., Jan Oberdörster, *Nanotoxicology: An Emerging Discipline Evolving from Studies of Ultrafine Particles.* Environmental health perspectives, 2005. **113**(7): p. 823-839.

82. Schleh, C., et al., *The effect of titanium dioxide nanoparticles on pulmonary surfactant function and ultrastructure.* Respiratory Research, 2009. **10**(1): p. 90.

83. Fan, Q., et al., *Adverse Biophysical Effects of Hydroxyapatite Nanoparticles on Natural Pulmonary Surfactant.* ACS Nano, 2011. **5**(8): p. 6410-6416.

84. Guzmán, E., et al., *DPPC–DOPC Langmuir monolayers modified by hydrophilic silica nanoparticles: Phase behaviour, structure and rheology.* Colloids and Surfaces A: Physicochemical and Engineering Aspects, 2012. **413**: p. 174-183.

85. Guzmán, E., et al., *Mixed DPPC–cholesterol Langmuir monolayers in presence of hydrophilic silica nanoparticles.* Colloids and Surfaces B: Biointerfaces, 2013. **105**: p. 284-293.

86. Valle, R.P., et al., *Increasing Hydrophobicity of Nanoparticles Intensifies Lung Surfactant Film Inhibition and Particle Retention.* ACS Sustainable Chemistry & Engineering, 2014. **2**(7): p. 1574-1580.

87. Harishchandra, R.K., M. Saleem, and H.-J. Galla, *Nanoparticle interaction with model lung surfactant monolayers.* Journal of the Royal Society, Interface, 2010. **7 Suppl 1**(Suppl 1): p. S15-S26.

88. Beck-Broichsitter, M., et al., *Biophysical inhibition of synthetic vs. naturally-derived pulmonary surfactant preparations by polymeric nanoparticles.* Biochimica et Biophysica Acta (BBA) - Biomembranes, 2014. **1838**(1, Part B): p. 474-481.

89. Moritz Beck-Broichsitter, C.R., Thomas Schmehl, Andreas Guenther, Thomas Betz, Udo Bakowsky, Werner Seeger, Thomas Kissel and Tobias Gessler *Biophysical investigation of pulmonary surfactant surface properties upon contact with polymeric nanoparticles in vitro.* Nanomedicine, 2011. **7**(3): p. 341-350.

90. Bakshi, M.S., et al., *Metal nanoparticle pollutants interfere with pulmonary surfactant function in vitro.* Biophysical journal, 2008. **94**(3): p. 855-868.

91. Tatur, S. and A. Badia, *Influence of Hydrophobic Alkylated Gold Nanoparticles on the Phase Behavior of Monolayers of DPPC and Clinical Lung Surfactant.* Langmuir, 2012. **28**(1): p. 628-639.

92. Chakraborty, A., et al., *Phospholipid Composition Modulates Carbon Nanodiamond-Induced Alterations in Phospholipid Domain Formation.* Langmuir, 2015. **31**(18): p. 5093-5104.

Chapter 2: Combined Effect of Synthetic Protein, Mini-B, and Cholesterol on A Model Lung Surfactant Mixture at the Air-Water Interface

Aishik Chakraborty[1], Erica Hui[1], Alan J Waring[2], Prajnaparamita Dhar[1]*

[1] Department of Chemical Engineering, University of Kansas, KS 66045

[2] Department of Medicine, Harbor UCLA Medical Center – LA BioMed, CA 90502 and Department of Physiology and Biophysics, University of California, Irvine, CA 92697

2.1. INTRODUCTION

Lung surfactant [LS], produced by Type II epithelial cells, is a complex mixture of lipids and proteins present primarily in the alveolar lining of the lungs [1, 2]. LS help in lowering surface tension at the air-water interface with expiration, thereby reducing the energy needed for breathing and improving lung compliance [3, 4]. They also form a line of defense against any foreign particle that is small enough to make its way through the air canal [5]. It has been firmly established that there is a lack of LS in cases of Neonatal Respiratory Distress Syndrome [NRDS] occurring in infants [6]. Currently NRDS is treated with a high success by using exogenous surfactant, referred to as Surfactant Replacement Therapy (SRT) [7]. In comparison to NRDS, a dysfunction/ impairment of the surfactant may lead to Acute Respiratory Distress Syndrome (ARDS)/ Acute Lung Injury (ALI). Each year, a staggering 50,000-190,000 case of ALI/ARDS are reported in USA itself [8]. While SRT has also been proposed for treating this condition as well, the success of SRT is currently debated, possibly because of a lack of complete understanding of the biophysical interactions between different LS components [9]. Lack of complete understanding of the biophysical role of the different constituents in combination has resulted in a lack of consensus on the composition of lung surfactants used in SRT, and forms the main motivation of this work.

Although native surfactants differ by species in their detailed composition, almost all contain about 90% by weight lipid and 10 wt. % of the surfactant specific proteins SP-A, SP-B, SP-C and SP-D [10, 11]. The dominant

phospholipid component is disaturated dipalmitoylphosphatidylcholine (DPPC, 30-70%), along with some unsaturated phosphatidylcholine (PC, 25-35%), anionic phospholipids like phosphatidylglycerol (PG), saturated fatty acids like palmitic acid, neutral lipids like cholesterol as well as minor fractions of phosphatidylethanolamine (PE) and sphingomyelin [12-14]. Although less in quantity, surfactant proteins play a crucial part. The hydrophobic SPB and SPC are involved in enhancing adsorption of LS to the air-water interface, whereas, the hydrophilic SPA and SPD mainly play a part in immune response [15].

Among the different constituents, the presence of cholesterol in SRT is highly disputed, primarily because its biophysical function in the proper functioning of the lung surfactant remains mostly unknown. Early experimental studies using Langmuir troughs and pulsating bubble surfactometer suggested that any amount of cholesterol is detrimental to the proper functioning of the lung, since the ability of the lung surfactant to reach a low surface tension (16-19) was inhibited in most of these studies. Cholesterol changes the morphology of DPPC domains even at low concentrations, which in turn can alter the surface tension lowering ability of DPPC [20].

On the other hand, it is important to note that cholesterol forms the major neutral lipid component of endogenous lung surfactants (3-10 wt. %), yet near zero surface tensions have been measured in the lung(21), suggesting that physiological amounts of cholesterol do not interfere with the proper functioning of the lung. Lessons learned from evolutionary studies on mammalian lung show that high amounts of cholesterol are present in more primitive animals with sac-

like lungs(22). The cholesterol content has been found to be 1.5 fold higher in hetero-thermic animals undergoing torpor(22). Kim *et al* showed that even small amounts (1 wt. %) can alter the surface viscosity of DPPC films, suggesting that addition of cholesterol to LS mixtures can be beneficial during intra-tracheal delivery of LS and enhance efficient spreading of synthetic LS, once it adsorbs to the interface. Interestingly, Gunasekara *et al.*, found that physiological amount of cholesterol has no effect on the surface activity of a natural surfactant BLES (Bovine Lipid Extract Surfactant) and only concentrations as high as 20% by weight, imposed harmful effects on the function of this natural LS [23]. This suggests the highly plausible explanation that minor components in native LS mixtures can counter some of the deleterious effects of cholesterol that was observed for early studies. Therefore, in order to use cholesterol in the replacement mixtures, any deleterious effects must be countered with other components. For example, Gomez-Gil *et al.* showed that surfactant protein SP-C can counter the deleterious effects of cholesterol, if used in the right proportions, suggesting that controlled amounts of cholesterol and proteins should be considered while developing future surfactants.

SP-B is the only one among the four surfactant proteins that is essential for effective breathing. Therefore, in this paper, we focus on developing a biophysical understanding of protein interactions with the neutral lipid composition of the lung surfactant. Specifically, we report on biophysical properties of DPPC:POPG films containing different amounts of cholesterol, in the absence or presence of 1, 2.5 or 5 wt. % Mini-B. Mini-B, a synthetic analog

of the surfactant protein SP-B, is a 34 amino acid residue of the full length native protein with enhanced in vivo and in vitro surfactant properties, where the predicted helices of the N and C terminals of the native protein are ether linked [24, 25], while maintaining the net charge (+7) of the native protein [26]. Mini-B can also aid an artificial phospholipase-resistant surfactant, diether phosphonolipid (DEPN) in lowering surface tension efficiently [27], with possible application in treating ALI/ARDS. Since an elevated amount of cholesterol is also associated with impaired surfactant activity in ALI/ARDS [28], this study also aims to address if addition of Mini-B is sufficient to counter the negative effects of elevated amounts of cholesterol.

In addition to investigating the surface tension lowering ability of these model LS mixtures, we report on the changes in the compressibility modulus of the lipid films, and correlate these changes with changes in the lipid domain morphology and line tension. Domain morphology has an impact on the viscoelasticity and the compressibility of a monolayer [29], which in turn controls spreading, and the ability of these different monomolecular films to undergo reversible collapse. Reversible collapse is an important feature of LS, believed to be essential for efficient incorporation of material during the breathing cycle, by forming “surface-associated reservoirs” [30] at ultra-low surface tension. Further, some of us have also previously shown that SP-B causes an increase in the line tension of a clinical lung surfactant, an important biophysical property of phospholipid films at the air-water interface, which can control the overall energy of the lipid films [29]. By correlating high-resolution atomic force microscopy

(AFM) images to calculations of line tension changes in different binary lipid films, we have also recently shown that a change in line energy can be directly related to the tendency of a molecule to act as a line active species [31]. Further, previous research by McConnell and co-workers has established the line tension lowering ability of cholesterol [32]. However, quantitative information on how Mini-B and cholesterol alter the domain morphology and therefore the line tension between lipid domains is currently not available. Therefore, by applying our recently developed theory relating domain size distributions to changes in the excess free energy between lipid domain boundaries (line tension between domains), we also report on the line tension of lipid films due to Mini-B cholesterol interactions.

At this point I would like to mention that part of this study had been communicated earlier through the Master's thesis. However, this chapter consists of some additional findings that help in providing a better picture to understand the biophysical properties of the system under consideration.

2.2. MATERIAL AND METHODS

2.2.1 Material: The lipids, 1,2-dipalmitoyl-*sn*-glycero-3-phosphocholine (DPPC), 1-palmitoyl-2-oleoyl-*sn*-glycero-3-phospho-(1'-*rac*-glycerol) (POPG) and cholesterol were purchased from Avanti Polar Lipids, Inc. (Alabaster, AL) in powder form for cholesterol and at final concentrations of either 25 mg/ml or 5 mg/ml in organic mixtures of chloroform for the others. The synthetic protein Mini-B a mimic of the native surfactant protein SPB [26, 33] was supplied by

Biopolymer Core Facility, LA BioMed at Harbor UCLA Medical Center, Torrance, California. Organic solvents, acetone, isopropanol and chloroform, were purchased from Thermo Fisher Scientific Inc. (Pittsburgh, PA). The fluorescent dye,1,2-Dihexadecanoyl-*sn*-Glycero-3-Phosphoethanolamine, Triethylammonium Salt (TXR-DHPE), was obtained from Life Technologies (Invitrogen, Grand Island, NY) in dried form. The lipids were stored at -20 ^{o}C to prevent any evaporation of the organic mixture. Water, which served as a sub-phase as well as cleaning agent, was purified (resistivity of 18.2 MΩ cm) using Direct-Q 3 UV System purchased from EMD Millipore (Billerica, MA).

4.2.2. Methods:

2.2.2.1. Sample Preparation: Organic solutions of DPPC:POPG in high performance liquid chromatography (HPLC) grade chloroform were prepared in the ratio of 7:3 by weight as DPPC is the primary composition of LS. 1wt.% dye was used for imaging purposes. Mini-B stock solutions were prepared in a 3:1 mixture of chloroform and methanol before being added to organic LS mixture. Multiple compositions of Mini-B (1, 2.5, 5 wt. %) and Cholesterol (1, 2.5, 4, 5 wt. %, which corresponds to 2, 5, 7, 9 mol %) were used along with DPPC:POPG (7:3 molar ratio).

2.2.2.2. Surface Pressure vs. Mean Molecular Area Isotherm: Surface pressure vs. area isotherms were obtained using a Langmuir trough (Biolin Scientific Inc.), with a area of 166 cm^2 and minimum area of 46 cm^2. It uses a moveable ribbon that serves as barrier to control the available area per molecule,

which thus mimics the compression and expansion process in the alveoli. Samples were added drop wise with a Hamilton glass syringe on an aqueous sub-phase and 20 minutes were given each time before running the experiment to allow the chloroform to evaporate. For isotherm experiments a compression rate of 125 cm^2/ min was chosen. Surface pressure was measured using Wilhelmy plate balance (filter paper). All experiments were repeated at least three times, to ensure reproducibility. All three sets of isotherms were found to overlap.

2.2.2.3. Fluorescence Imaging: A Nikon Eclipse fluorescence microscope was used to visualize the lipid domain formation on the air-water interface. For imaging purposes a slower, quasi-static, rate of 7 cm^2/ min was selected. The images, at intervals of 1 to 5 mN/m (in the two-phase coexistence region), were captured using CCD camera (Andor LUCA). 5 frames were used for each image sequence and the representative images are presented in this report. Images were analyzed for calculations with ImageJ (NIH) software. Two neighboring images were analyzed for each image sequence for better statistical quality. This typically meant that at least 270 domains were analyzed to obtain the domain size distribution for each lipid composition. Furthermore, the circularity of the domains can also be measured using ImageJ. All final histograms and line tension graphs were generated using Origin 8.62 (OriginLab, Northampton, MA).

2.3. THEORETICAL ANALYSIS

2.3.1. Compressibility modulus: The compressibility modulus or modulus of elasticity b, of the film is often used to describe the properties of the monolayer film. It is defined as the ability of a film to store mechanical energy as stress under a compression force and may be mathematical defined as:

$$\beta = -A\left(\frac{\partial \Pi}{\partial A}\right)_T = -A(\frac{\partial \sigma}{\partial A})$$

…1

The inverse of b yields the isothermal compressibility k of the film. Since b and k are 2nd order derivatives of the surface free energy, G, ($\sigma = -\left(\partial G / \partial A\right)_T$), discontinuities in these values confirm the presence of phase transitions. Experimentally, the phase transitions are represented as a blunt dip in the b-A profile rather than a sharp discontinuity.

The compressibility modulus is calculated from the raw isotherm data by calculating the slope m of the isotherm (P-A) at each point using the formula

$$m = \frac{1}{2}\left(\frac{y_{i+1} - y_i}{x_{i+1} - x_i} + \frac{y_i - y_{i-1}}{x_i - x_{i-1}}\right)$$

…2

The derivatives can give rise to high-frequency, low-amplitude noise arising from fluctuations in the surface pressure reading as a result of discretization, which can be safely removed by a Fourier smoothing filter. The derivative and the Fourier smoothing filter are tools that are available as in-built functions through Origin 8.62, the graphing software used here for the isotherm data analysis.

2.3.2. Condensed Area Fraction: The condensed area fraction of domains provides us with an estimate of the fraction of the monolayer that forms ordered domain structures at a given surface pressure. Mathematically, the percentage area fraction is given by:

$$\text{Percentage Condensed Region} = \frac{\text{Area of the Condensed Domain}}{\text{Total Area}} \text{ X } 100 \text{ \%} \quad \ldots 3$$

2.3.3. Determining line tension from domain size distribution:

The line tension (λ) between lipid domains depends on the difference in the height of the lipid chain, between the molecules in the liquid condensed (l_o) and liquid expanded (l_d) regions, and the interfacial tension of the hydrocarbon-air interface (γ) [i.e., $\lambda = (l_o - l_d)\gamma$]. On the other hand, the average dipole density (Δm^2), which in turn is related to the electrostatic energy of the domains, depends on the packing density and composition of the lipid domains. The shape of the condensed domains in a monolayer is thus a function of the energy associated with the line tension and electrostatic repulsion. A method to simultaneously calculate the line tension and the dipole density moment from the distribution of circular phospholipid domains has been shown previously [29]. Using this method, we have shown that the line tension, λ can be related to the domain size distribution, C_N, where C_N is the number fraction of domains with N

radius (i.e., ratio of mole fraction of molecules in N to the number of domains, N, given by X_N/N) by the following equation:

$$C_N = \left[C_M exp\left\{ -\frac{\Delta m^2 R_o}{4\varepsilon\varepsilon_o kT}\left(\frac{R_o}{R-1}\right)^2 \right\} \right]^{\frac{R^2}{R_o^2}}, where$$

…4

$$R_o = \frac{e^3\Delta}{4}\left[\exp\left(\frac{3\pi\varepsilon\varepsilon_o}{\Delta m^2}\lambda\right)\right]$$

…5

The domain distribution, which is obtained experimentally, is then fitted with equation (4). Here we use C_M, $\Delta m^2 R_o / 4\varepsilon\varepsilon_o kT$, and R_o as the three fitting parameters. Equation 5 is next used to determine the line tension.

2.4. RESULTS

2.4.1. Isotherms: Figure 1 presents the quasi-static surface pressure vs. mean molecular area isotherms of the different samples examined. Fig 1A shows how the isotherm of a mixture of DPPC:POPG was modified by varying the concentration of Mini-B. The solid line represents the control curve for DPPC:POPG. At higher mean molecular areas, the monolayer is in the gas phase and therefore at 0 surface tension. However, the surface pressure increases with decrease in the mean molecular area, until finally the monolayer reached collapse pressures (~ 72 mN/m). With the addition of 1% Mini B to the system, we observed practically no change in the isotherm.

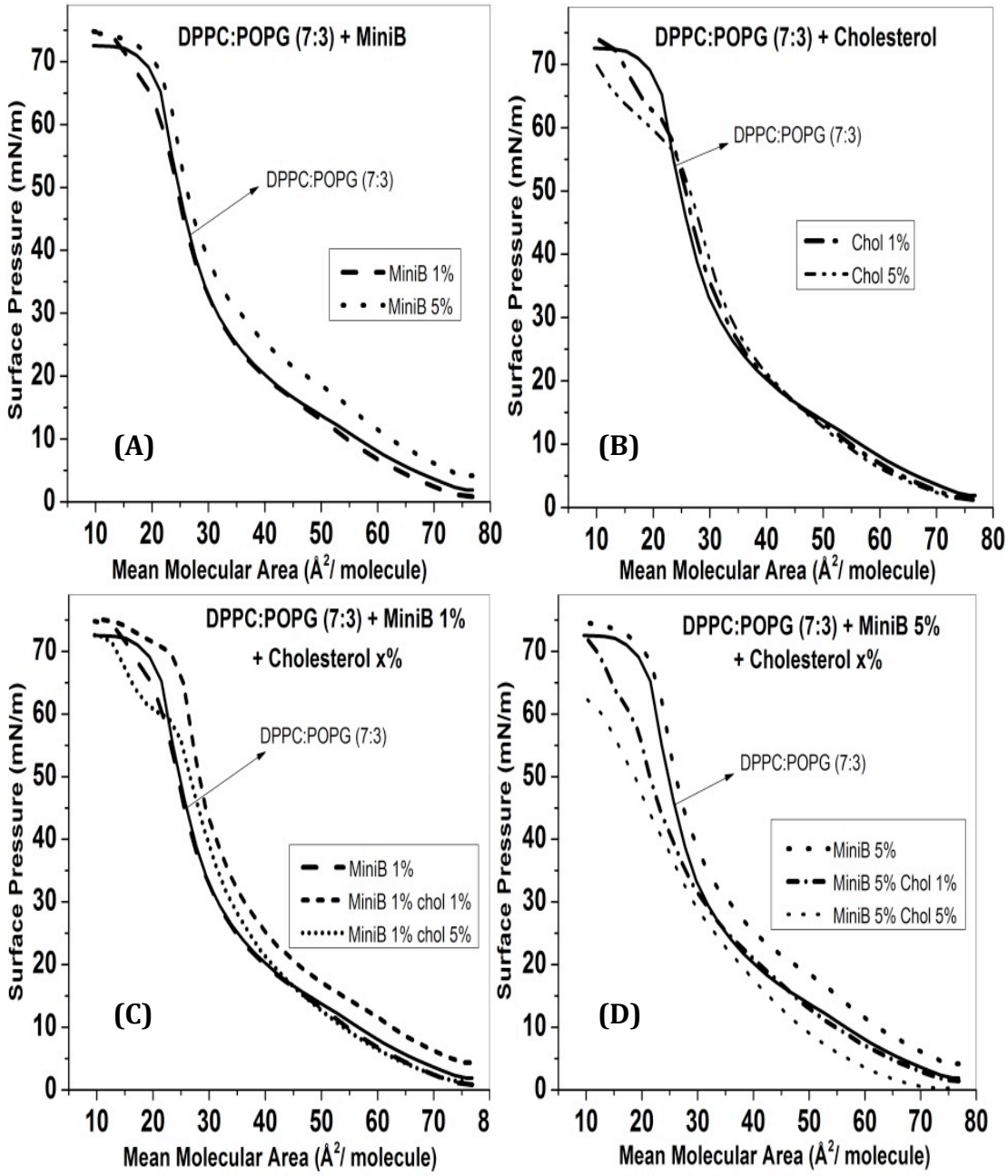

Fig 1: Surface pressure vs. mean molecular area isotherms for different lung surfactant mixtures. *(A) DPPC:POPG (7:3) with 1% and 5% Mini-B. (B) DPPC:POPG with 1% and 5% cholesterol. (C) DPPC:POPG with 1% Mini-B and varying concentration of cholesterol (D) DPPC:POPG with 5% Mini-B and different weightage of cholesterol. (Taken from the Master's thesis)*

However, when 5 % Mini B was added to DPPC:POPG, given by the dotted line, the isotherm moved to higher values of surface pressure at any given mean molecular area. Fig 1B represents the effect of varying amounts of cholesterol on the isotherm of DPPC:POPG, while Fig 1C is a plot of DPPC:POPG mixed with 1% Mini-B and varying composition of cholesterol. The isotherm for Mini-B 1% and Cholesterol 1%, given by the dashed curve, shows that the isotherm was pushed to higher values of surface pressure for the same mean molecular area. Increasing the concentration of cholesterol to 5 % caused the surface pressure vs. area curve (dotted lines) to fall back close to the control. Fig 1D represents the effect of 5% Mini-B with varying amounts of cholesterol on DPPC:POPG. The isotherms moved further to lower mean molecular areas indicating the need for higher area compression to achieve the same values of surface pressure.

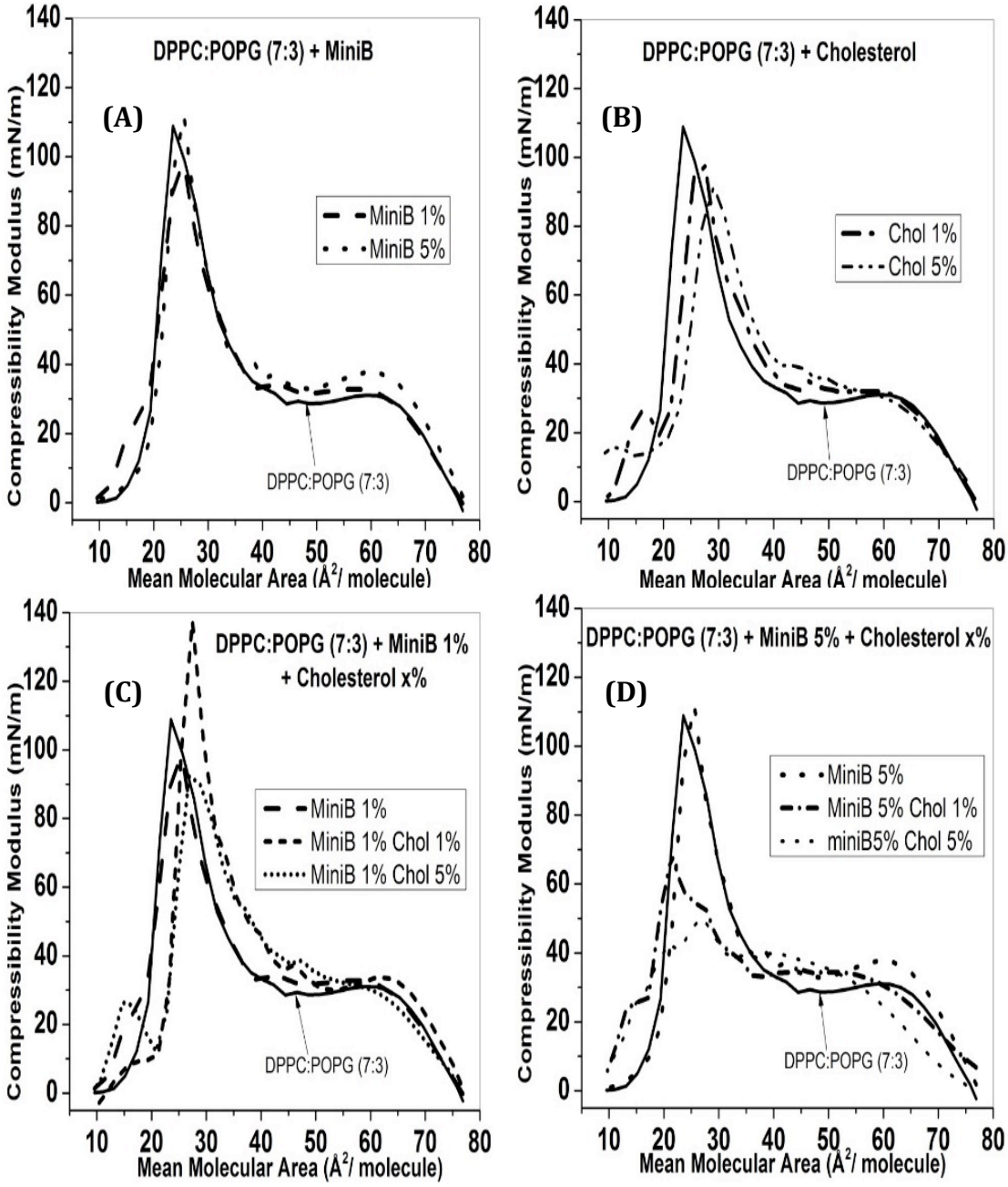

Fig 2: Compressibility Modulus for different lung surfactant mixtures. *(A) DPPC:POPG (7:3) with 1% and 5% Mini-B. (B) DPPC:POPG with 1% and 5% cholesterol. (C) DPPC:POPG with fixed Mini-B percentage (1%) and varying weightage of cholesterol (D) DPPC:POPG with 5% Mini-B and different amounts of cholesterol. (Taken from the Master's thesis)*

2.4.2. Compressibility Modulus: Fig 2 presents the compressibility modulus as a function of mean molecular area of the samples tested. The data was processed using an FFT filter over 5 points, except near the collapse. Fig 2A shows the compressibility modulus for varying composition of Mini-B with DPPC:POPG. In case of the control DPPC:POPG sample, the compressibility modulus increased gradually till it reached around 31 mN/m after which there was a slight dip in the curve. The peak value of compressibility modulus before monolayer collapse was found to be 109 mN/m. In case of DPPC:POPG monolayers containing 1% Mini-B, presented as dashed lines, there was almost no change in the compressibility modulus till 32 mN/m. In place of the dip in the curve beyond this value, like that of the control, there was a plateau until 46 $Å^2$/ molecule. The peak compressibility modulus was found to be around 98 mN/m. With 5% Mini-B, the peak compressibility modulus was measured to be 112 mN/m at 26 $Å^2$/ molecule. Fig 2B shows the effect of different concentration of cholesterol on the compressibility modulus of DPPC:POPG. In case of 1% cholesterol the peak compressibility modulus was found to be 97 mN/m and at a higher value of mean molecular area than that of the control DPPC:POPG film. DPPC:POPG films containing 5 % cholesterol showed a gradual rise in the compressibility without a dip. The maximum compressibility dropped to 91 mN/m and also shifted to even higher mean molecular areas (29 $Å^2$/ molecule). Fig 2C gives the compressibility modulus for systems containing both Mini-B and cholesterol. With Mini-B 1% and cholesterol 1% (dashed curve), there was an increase in the compressibility of the mixture. We noted the highest

compressibility in this case, (137 mN/m) at a mean molecular area of 27 $Å^2$/ molecule. For 1% Mini-B and 5 % cholesterol (dotted line), the curve increased gradually to a value of 92 mN/m at 27 $Å^2$/ molecule. Fig 2D represents the compressibility modulus of DPPC:POPG along with 5% Mini-B and varying concentration of cholesterol. In case of 5% Mini-B and 5% cholesterol, the peak was as low as 50 mN/m at 27 $Å^2$/ molecule, indicating a substantial change in the mechanical property due to Mini-B cholesterol interactions.

2.4.3. Fluorescence Images: To have a detailed understanding of the changes in the domain morphology in the monolayer, we used fluorescence microscopy imaging to monitor changes in lipid domains during the compression cycle. We present here images at surface pressures 20 mN/m. At 20 mN/m, the monolayer shows coexistence between two phases, namely the bright Liquid Expanded (LE) and the dark Liquid Condensed (LC) phases.

Fig 3A shows the images for DPPC:POPG (7:3) at surface pressures 20mN/m. In case of the control, the monolayer is well packed agreeing with that found in literature [34]. The domains were more or less circular in shape at lower surface pressure. Fig 3B shows the images for DPPC:POPG (7:3) with 1% cholesterol added to the system. Here we observed a drastic change in the domains. In place of the circular condensed regions of DPPC:POPG, we found protruding curls along the boundaries of the domains. The effect became more pronounced with the rise in the surface pressure. Fig 3C shows the effect of 5% cholesterol, where the domain morphology had transitioned from circles to thin, but not continuous, stripes.

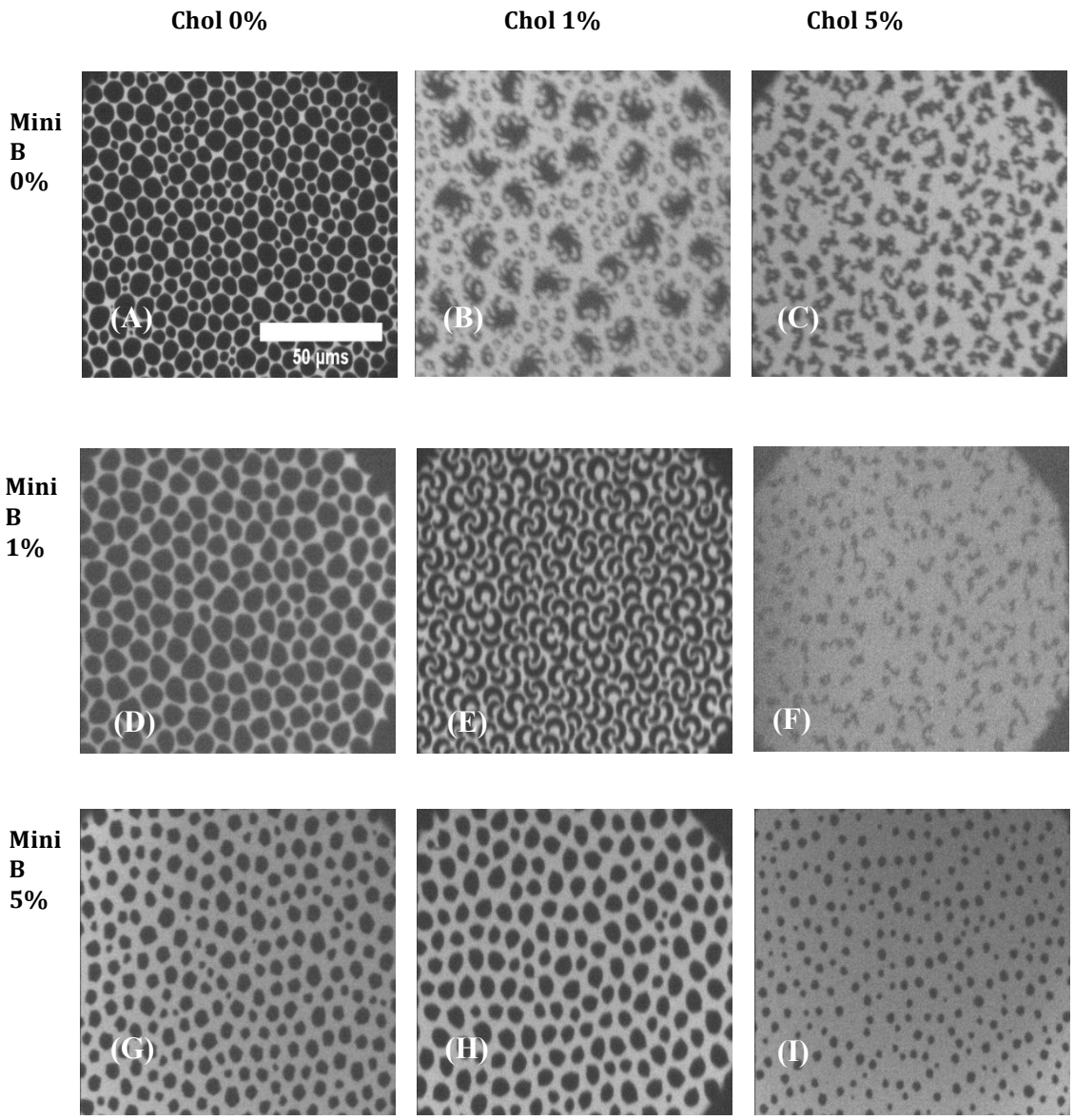

Fig 3: Fluorescence images of DPPC:POPG (7:3) along with varying concentrations of Mini-B and cholesterol. *Images A, B, C, D, E, F, G, H and I were taken at 20 mN/m, which corresponds to the two-phase coexistence region. The first row represents samples without Mini-B, the next row represents samples with 1% Mini-B in them, and the last row contains sample with 5% Mini-B. Concentration of cholesterol increases from left to right. Scale bar indicates 50 µms. (Taken from the Master's thesis)*

A noticeable decrease in dark condensed domains was recorded, that we quantified in Fig 5. Fig 3D shows that adding 1% Mini-B to DPPC:POPG shows a slight decrease in the packing density of the dark domains, which increases with increasing protein concentration, as seen in Fig 3G after addition of 5% Mini-B. Fig 3E shows the monolayer consisting of both 1% Mini-B and 1% cholesterol, where an interesting new morphology of crescent shaped domains were observed. With 1% Mini-B and 5% cholesterol (Fig 3F) the domains were completely transformed without getting packed at all. Fig 3H shows the effect of 1% cholesterol along with 5% Mini-B. There were no appreciable changes in the shape of the domains when compared to DPPC:POPG film containing Mini-B only, showing that the higher concentration of Mini-B dominated over the lower percentage of cholesterol. Finally, at 5% Mini-B with the same concentration of cholesterol added to DPPC:POPG (Fig 3I), the domains were smaller, but still circular in shape.

2.4.4. Ability to retain material during multiple compression-expansion cycles: When the monolayer is compressed to the limit of its stability, it transitions from its 2-dimensional existence to a 3-dimensional one. This phenomenon has been termed “monolayer collapse” and has been studied extensively by biophysicists due to its relevance to more efficient breathing [35, 36]. The mechanism of collapse can either be reversible or irreversible in nature. Reversible collapse typically suggests formation of surface associated reservoirs, that enable quick and efficient re-adsorption of material during multiple compression-expansion cycles, and is believed to be desirable for efficient LS

mixtures. The fluorescence-intense “streaks” seen in the images (Fig 4A-E, indicated by arrows), which are found perpendicular to the direction of compression, are the reversibly collapsed regions, commonly known as “folds” or “collapse cracks” [36]. Here, the monolayer folds into multi-layers and upon expansion, the folded component respreads. Formation of giant folds, which extends a few microns laterally, indicates lower loss of material to the sub-phase. Monolayers lacking such folds, collapses irreversibly and solubilization is the likely mechanism when fluidizing agents, such as cholesterol, is present in the monolayer. Irreversible collapse due to solubilization of material is characterized by formation of vesicles, which are visible as bright specks in the images. It has been reported earlier that DPPC:POPG (7:3) on its own produces thin folds after collapse [37**]** and Fig 4A shows similar results. Fig 4B and 4C reveals that Mini-B helped DPPC:POPG to form fluorescence-intense giant folds suggesting reversible collapse. These features are very similar to that reported for KL4 [37]. With the addition of 1% cholesterol to 1% Mini-B (Fig4D) or 5% Mini-B (Fig 4E), the monolayer collapsed reversibly. However, 5% cholesterol along with 5% Mini-B showed irreversible collapse (Fig 4F). In order to further prove that the formation of these features correspond to better incorporation of material during multiple compression cycles, we also present the surface pressure vs. area isotherms for multiple cycles. In order to represent material loss, we also plot the area of the curve.

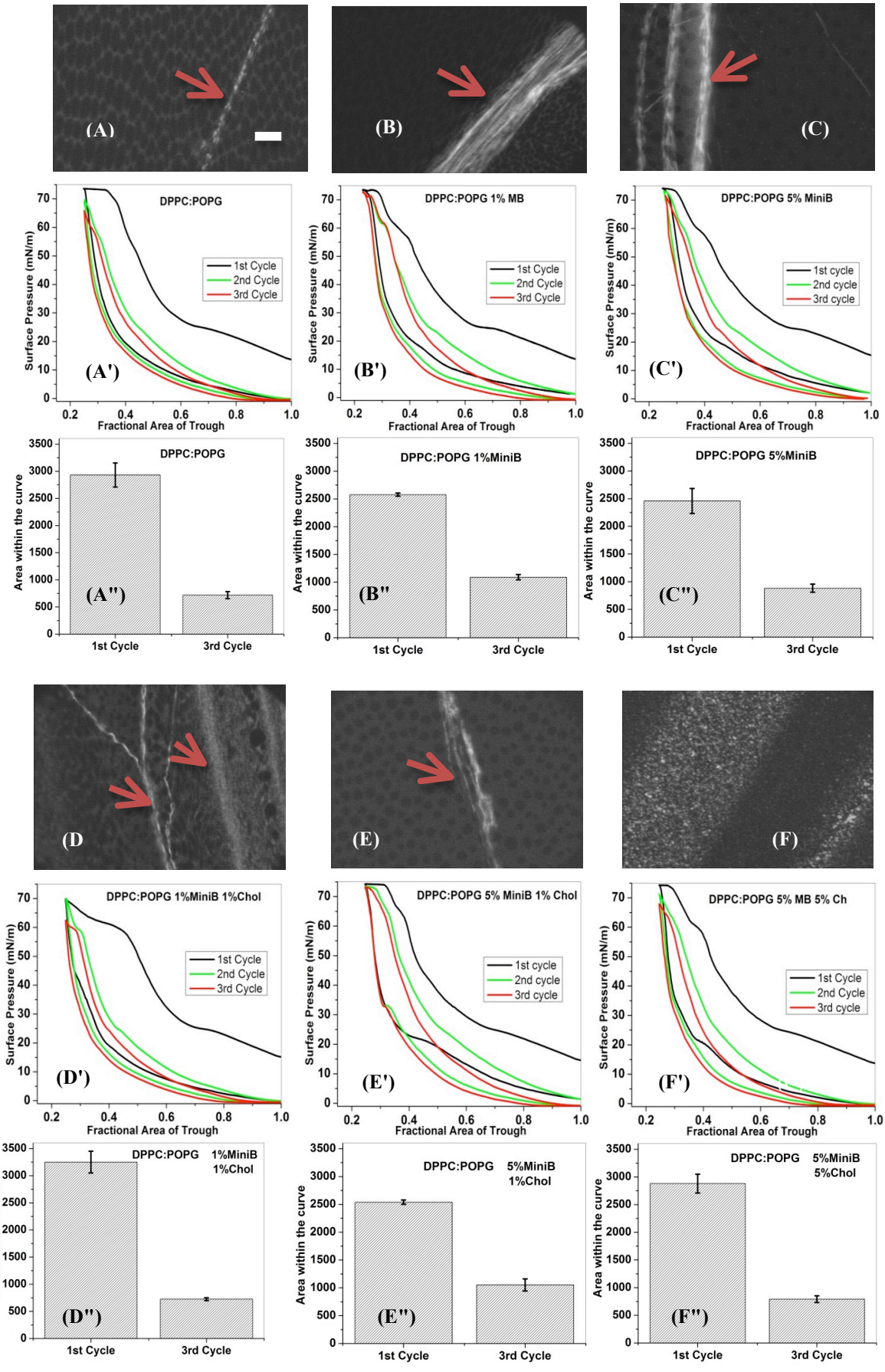
(A)
(B)
(C)
DPPC:POPG
DPPC:POPG 1% MB
DPPC:POPG 5% MiniB
Surface Pressure (mN/m)
Fractional Area of Trough
1st Cycle
2nd Cycle
3rd Cycle
(A')
(B')
(C')
Area within the curve
DPPC:POPG 1%MiniB
DPPC:POPG 5%MiniB
(A")
(B"
(C")
(D
(E)
(F)
DPPC:POPG 1%MiniB 1%Chol
DPPC:POPG 5% MiniB 1% Chol
DPPC:POPG 5% MB 5% Ch
(D')
(E')
(F')
DPPC:POPG 1%MiniB 1%Chol
DPPC:POPG 5%MiniB 1%Chol
DPPC:POPG 5%MiniB 5%Chol
(D")
(E")
(F")

Fig 4: Fluorescence images of DPPC:POPG and a combination of Mini-B and cholesterol, revealing collapse at higher surface pressures (A-F). *Arrows indicate "collapse crack".* ***(A'-F')*** *Isotherms with multiple compression cycles for the same samples (A'-F').* ***(A"- F")*** *Mean and standard deviation of the area within the curve for each cycle for the same samples. Scale bar represents 10 µms. The area under the curve is given as *10^{-4} mN-m. (Figs A-F has been taken from the Master's thesis)*

An increase in the area of the isotherm suggests more material at the surface, while a significant drop in the area within the curve suggests loss of material from the surface. Fig 4A' shows multiple compression-expansion cycles for DPPC:POPG while 4A**"** shows the corresponding area of the curve for the 1st and 3rd cycle. With multiple compressions, the isotherm shifted to lower fractional trough area. However, in case of 1% and 5% Mini-B, this loss appeared to be reduced (Fig 4B**'**, B**"** and Fig 4C**'**, C**"**). Higher concentration of Mini-B (5%) along with small concentration of cholesterol (1%) showed the least loss in material (Fig 4E**'**, E**"**).

Furthermore, One-way-ANOVA revealed a significant difference (α=0.05) in the area of the 1st cycle between the different samples ($F_{6,14}$= 9.036, p= 3.72*10^-4, R^2= 79.48%) as well as the area of the third cycle between the different samples ($F_{6,14}$ = 15.22045, p = 2.062* 10^-5, R^2= 86.71%).

2.4.5. Percentage Condensed Region: Fig 5 shows the percentage of the monolayer that was **condensed due to the addition of cholesterol and Mini-B to DPPC:POPG films. Surface pressures** 15, 20, 25 and 30 mN/m were chosen for this analysis, since at higher surface pressures analysis of individual

domains was no longer possible, and the entire field of view appeared dark. Fig 5A shows the effect of Mini-B on DPPC:POPG. The condensed domain increased from 50% to about 55% with rise in surface pressure in case of the model system. However, with the addition of Mini-B, at initial surface pressures there was a reduction in the condensed domains. The effect was more pronounced when higher percentage of Mini-B was added to the model mixture. Fig 5B shows how cholesterol alters the formation of condensed domains in the model mixture. Even in this case, there is a decrease in the area of condensed domains with the addition of cholesterol. The next two figures reveal how Mini-B and cholesterol both act together in altering the area of the dark domains. Fig 5C contains the data for 1% Mini B and varying concentrations of cholesterol. Here, with 1% of both put together, there was a steady increase in the domain area at 25 and 30 mN/m suggesting better domain packing. However, 1% Mini-B and 5% cholesterol showed a reduction in the area of the condensed domains. Fig 5D shows the effect of varying amount of cholesterol on 5% Mini-B. In this case, 5% Mini-B was able to maintain the percent of condensed domains to almost that of the control system, even in the presence of 1 wt. % cholesterol.

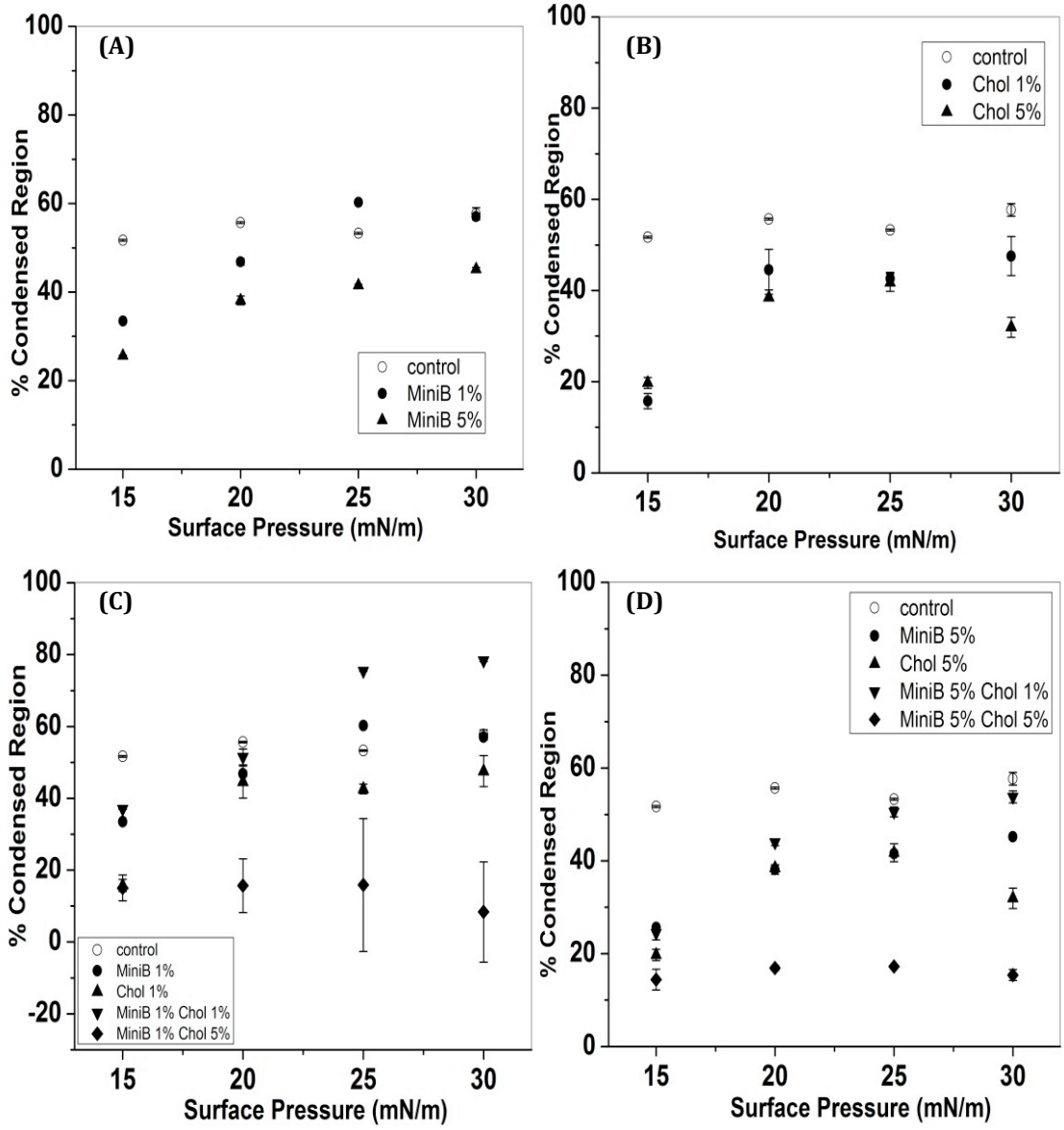

Fig 5: Percentage condensed domains for varying mixtures of DPPC:POPG (7:3). *Percentage condensed domains due to addition of (A) different weights of Mini-B on DPPC:POPG (B) cholesterol (C) 1% Mini-B with different concentrations of cholesterol (D) 5% Mini-B along with different concentrations of cholesterol. (Taken from Master's the thesis)*

However, in the presence of higher cholesterol content, the area reduced drastically. This showed the dominance of higher concentration of cholesterol even with equal amount of Mini-B. The error in measurement was particularly high for the mixture with 1% Mini-B and 5% cholesterol mainly because of the difficulty in determining the condensed area owing to the small size of the domains, which made the analysis difficult. The error for the remaining mixtures was less than 10% of the total condensed area.

2.4.6. Line Tension:

The theoretical calculations relating line tension to domain size distribution, is only feasible for lipid domains that are circular in shape. Therefore, we were limited to calculating and presenting the line tension of the domains for the control, lipid mixture with both 1% and 5% Mini-B and the mixtures that had 5% Mini-B and varying concentration of cholesterol. Surface pressure 20 mN/m was selected for the ease of analysis. The line tension of DPPC:POPG (Fig 6A) was around 2.4 x 10^{-2} pN. With the addition of 1% Mini-B, line tension increased to about 5 x 10^{-2} pN. Line tension in case of 5% Mini-B was slightly higher than that of 1%. When 1% , 2.5% and 4% cholesterol was added to 5% Mini-B (Fig 6B), no significant change in line tension was noted, even though cholesterol has been shown to reduce line tension [20]. However, increasing concentration of cholesterol to 5 wt. % showed a reduction in line tension.

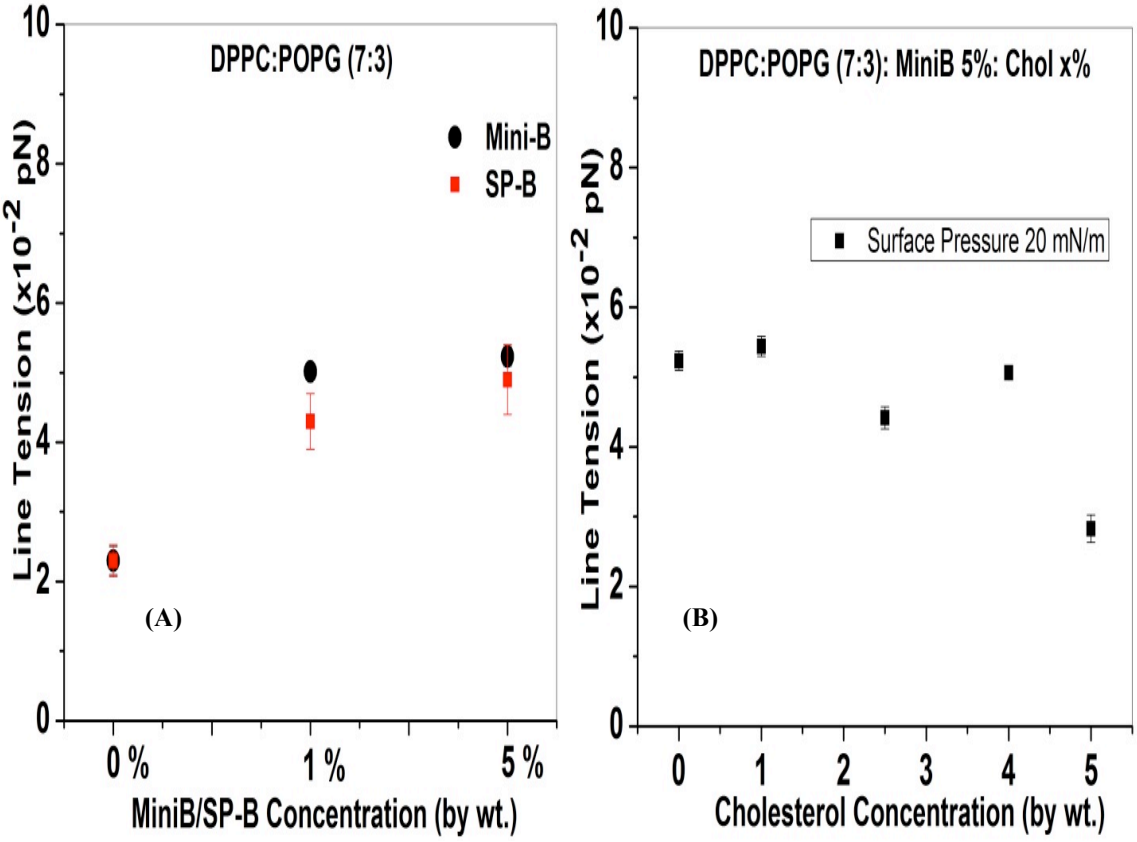

Fig 6: Changes in line tension for different mixtures. *Line tension between the domains in DPPC:POPG lipid films containing (A) different weights of Mini-B and SP-B, in the absence of cholesterol (B) 5% Mini-B with different cholesterol concentrations*

2.5. DISCUSSION

This work is motivated by the desire to understand the biophysical interactions between cholesterol and synthetic surfactant protein Mini-B in a synthetic LS mixture. Kim *et al.* have shown that even 1 wt. % cholesterol is capable of reducing the surface viscosity of DPPC monolayer by an order of magnitude whereas 2 wt. % is capable of reducing the viscosity by two orders of magnitude [20]. This characteristic feature is valuable and is therefore a desirable property in synthetic surfactant because lowering of the surface viscosity can help in uniformly distributing the LS mixture throughout the lungs, as well as re-spreading of the surfactant with the expansion of lungs. However, as noted in the introduction, cholesterol is a highly debated component of LS and most of the commercial drugs used in SRT avoid cholesterol. Our own results confirm that not surprisingly, in the absence of protein Mini-B, even physiological amounts of cholesterol cannot maintain the desirable high surface pressures necessary during exhalation in case of a synthetic binary LS mixture. Similarly, even 1% cholesterol prevent DPPC:POPG films from collapsing by forming surface associated reservoirs (reversible collapse), possibly by lowering the compressibility modulus of the film. On the other hand, 1wt. % Mini-B alone is enough to significantly improve the ability of DPPC:POPG to undergo reversible collapse. Thus Mini-B and cholesterol demonstrate seemingly opposing biophysical characteristics, which when optimized, is expected to provide synthetic surfactant mixtures with enhanced therapeutic potential. Our results show that small quantities of cholesterol and Mini-B can together enhance the

properties of LS. We discuss these results in further details in the following sub-sections.

2.5.1. Effect on Mechanical Properties:

The surfactant mixture DPPC:POPG is efficient in lowering surface tension to near zero values owing to the presence of the disaturated phospholipid which has been reported previously [38]. Pressure vs. area isotherms suggests that higher amounts of Mini-B can cause early condensation of lipid domains, leading to higher surface pressures at the same area per molecule. On the other hand, cholesterol has a negative impact on the performance of DPPC:POPG films at higher surface pressures. Here, more area compression is needed to achieve the desired high surface pressure values. However, monolayers containing 1% of both the components, Mini-B and cholesterol together, are capable of enhancing the surface activity. Moreover, compressibility modulus of the system, which can be derived directly from the pressure vs. area isotherm [39], was found to be the highest for the above mixture. A highly compressible mixture can form well-packed structure, which again is supported by the fluorescence images. The compressibility modulus is much lower in case of mixtures containing higher percentage of the two additives. Further, the isotherms for multiple cycles also show that these components together can improve the incorporation of material during multiple cycles.

2.5.2. Effect on Line Tension and Collapse:

Cholesterol and Mini-B alone have contrasting effects on the line tension of the LS films, as well as its ability to undergo reversible collapse. It is well known that cholesterol can lower the line tension between lipid domains to near zero values, as evidenced by the formation of spiral structures in the presence of cholesterol only [20]. On the other hand, our analysis of the domain size distribution shows that Mini-B increased the line tension between lipid domains. This finding is not surprising. Native SP-B was also found to increase the line tension between domains in a clinically relevant surfactant mixture [29]. We have previously attributed this increase in the line tension to the tendency of the positively charged protein to associate with the negatively charged POPG lipids that are in the fluid regions of the lipid membrane. It was interesting to note that in the presence of 5 wt. % Mini-B, 1-4 wt. % cholesterol did not lower the line tension between lipid domains, suggesting that interactions of the Mini-B with the negatively charged POPG lipid dominates over the protein cholesterol interactions, or cholesterol's tendency to associate with domain grain boundaries. Finally, the packing density between lipid domains was also high when both 1% Mini-B and 1% cholesterol were present. Further, this mixture was capable of collapsing reversibly, unlike the films containing cholesterol alone that were found to collapse irreversibly forming vesicles.

2.6. CONCLUSION

Based on our experimental observations, we conclude that any potential negative effects of low concentrations of cholesterol on the line tension, reversible collapse, and compressibility of synthetic LS mixtures, can be countered with synthetic protein Mini-B. However, higher concentration of cholesterol cannot be used as it has a greater negative impact on the model surfactant mixtures used in this study. For further exploration, smaller concentration of cholesterol along with 1% to 5% Mini-B can be tested in case of SRT to allow the surfactant to be fluid enough to effectively cover the interface at inhalation, while resisting monolayer collapse at exhalation.

2.7. ACKNOWLEDGMENT

We would like to take this opportunity to thank our funding sources: NIH (P20GM103638),

Inez Jay Award (from Higuchi Biosciences center) and from Transportation Research Institute (University of Kansas). Without their support the project would not have been possible. We would also like to acknowledge Sadie Johnson and Carlie Copeland for their line tension data for SPB.

2.8. REFERENCES

1. Robertson, B., et al, *Synthetic surfactants to treat neonatal lung disease.* Molecular Medicine Today, 2000. **6**(3): p. 119-124.
2. Notter R.H., *Lung surfactants: Basic science and clinical applications*. CRC Press, 2000. Vol. **149**
3. Zasadzinski, J.A., et al., *The physics and physiology of lung surfactants.* Current Opinion in Colloid & Interface Science, 2001. **6**(5–6): p. 506-513.
4. Dohm, M.T., et al., *Biophysical Mimicry of Lung Surfactant Protein B by Random Nylon-3 Copolymers.* Journal of the American Chemical Society, 2010. **132**(23): p. 7957-7967.
5. Zuo, Y.Y., et al., *Current perspectives in pulmonary surfactant — Inhibition, enhancement and evaluation.* Biochimica et Biophysica Acta (BBA) – Biomembranes, 2008. **1778**(10): p. 1947-1977.
6. Clements, J. et al., *Lung Surfactant and Neonatal Respiratory Distress Syndrome.* American Journal of Respiratory and Critical Care Medicine, 1998. **157**(4): p. S59-S66.
7. Stevens, T.P. et al., Sinkin, *Surfactant replacement therapy*.* Chest, 2007. **131**(5): p. 1577-1582.
8. K. Raghavendran, et. al., *Surfactant Therapy of ALI and ARDS.* Critical Care Clinics, 2011. **27**(3): p. 525-559.

9. Willson DF, Thomas NJ. Surfactant Composition and Biophysical Properties Are Important in Clinical Studies. Am J Respir Crit Care Med. 2010;181(7):762

10. Goerke, J., *Pulmonary surfactant: functions and molecular composition .* Biochimica et Biophysica Acta (BBA)- Molecular Basis of Disease, 1998. **1408**(2-3): p. 79-89.

11. Veldhuizen, R., et al., *The role of lipids in pulmonary surfactant.* Biochimica et Biophysica Acta (BBA) - Molecular Basis of Disease, 1998. **1408**(2–3): p. 90-108.

12. Veldhuizen, E.J.A., et al., *The Role of Surfactant Proteins in DPPC Enrichment of Surface Films.* Biophysical Journal, 2000. **79**(6): p. 3164-3171.

13. Keough, K.M.W., et. al., *Surface respreading after collapse of monolayers containing major lipids of pulmonary surfactant.* Chemistry and Physics of Liplds, 1988. **49**(1-2): p. 81-86.

14. Gómez-Gil, L., et al., *Cholesterol modulates the exposure and orientation of pulmonary surfactant protein SP-C in model surfactant membranes.* Biochimica et Biophysica Acta (BBA) - Biomembranes, 2009. **1788**(9): p. 1907-1915.

15. Wright, J.R., *Immunomodulatory functions of surfactant*. Physiological Reviews, 1997. **77**(4): p.931-962.

16. Yu, S. H., and F. Possmayer, *Dipalmitoylphosphatidylcholine and cholesterol in monolayers spread from adsorbed films of pulmonary surfactant*. Journal of Lipid Research, 2001. **42**:1421-1429.

17. Yu, S., P. G. R. Harding, N. Smith, and F. Possmayer, *Bovine Pulmonary Surfactant - Chemical-Composition and Physical-Properties*. Lipids, 1983. **18**:522-529.

18. Taneva, S., and K. M. W. Keough, *Cholesterol modifies the properties of surface films of dipalmitoylphosphatidylcholine plus pulmonary surfactant-associated protein B or C spread or adsorbed at the air-water interface*. Biochemistry , 1997. **36**:912-922.

19. Suzuki, Y. , *Effect of Protein, Cholesterol, and Phosphatidylglycerol on the Surface-Activity of the Lipid-Protein Complex Reconstituted from Pig Pulmonary Surfactant*. Journal of Lipid Research, 1982. **23**:62-69.

20. KyuHan Kim, S.Q.C., et al., *Effect of cholesterol nanodomains on monolayer morphology and dynamics.* Proc Natl Acad Sci U S A, 2013 **110**(33): p. 3054-3060.

21. Schurch, S., J. Goerke, and J. A. Clements,*Direct Determination of Surface-Tension in Lung*. Proceedings of the National Academy of Sciences of the United States of America, 1976. **73**:4698-4702.

22. Codd, J. R., N. C. Slocombe, C. B. Daniels, P. G. Wood, and S. Orgeig, *Periodic fluctuations in the pulmonary surfactant system in Gould's wattled bat (Chalinolobus gouldii)*. Physiol. Biochem. Zool, 2000. **73**:605-612.

23. Gunasekara, L., et al., *Pulmonary surfactant function is abolished by an elevated proportion of cholesterol.* Biochimica et Biophysica Acta (BBA) - Molecular and Cell Biology of Lipids, 2005. **1737**(1): p. 27-35.

24. Walther, F.J., et al., *Hydrophobic surfactant proteins and their analogues.* Neonatology, 2007. **91**(4): p. 303-10.

25. Walther, F.J., et al., *Critical Structural and Functional Roles for the N-Terminal Insertion Sequence in Surfactant Protein B Analogs.* PLoS ONE, 2010. **5**(1): p. e8672.

26. Waring, A.J.**,** et al., J.A. *The Role of Charged Amphipathic Helices in the Structure and Function of Surfactant Protein B (SP-B),* J. Peptide Res. 2005. **66**:364-374.

27. Walther, F.J., et al., *Dynamic Surface Activity of a Fully Synthetic Phospholipase-Resistant Lipid/Peptide Lung Surfactant.* PLoS ONE, 2007. **2**(10): p. e1039.

28. Lopez-Rodriguez, E., et al., *Structure-function relationships in pulmonary surfactant membranes: from biophysics to therapy.* Biochimica et Biophysica Acta (BBA) - Biomembranes, 2014. **1838**(6). p: 1568-1585.

29. Dhar, P., et al., *Lipid-Protein Interactions Alter Line Tensions and Domain Size Distributions in Lung Surfactant Monolayers.* Biophysical Journal, 2012. **102**(1). p: 56-65.

30. Lipp, M, Lee, et al., *Coexistance of buckled and flat monolayers*, Phys. Rev. Lett. 1998 81, 1650

31. Chakraborty, A., et al., *Phospholipid compositions modulates carbon-induced alterations in phospholipid domain formation*. Langmuir, 2015. **31**(18). p: 5093-5104.

32. McConnell, H.M., *Structures and transitions in lipid monolayers at the air-water-interface*. Annu. Rev. Phys. Chem, 1991. 42. p: 171-195.

33. Sarker, M., et al., *Structure of Mini-B, a Functional Fragment of Surfactant Protein B, in Detergent Micelle.* Biochemistry 2007. ***46***: p.11047-11056 .

34. Pocivavsek, L., et al., *Lateral stress relaxation and collapse in lipid monolayers.* Soft Matter, 2008. **4**(10): p. 2019-2029.

35. Ybert, C. et al., *Collapse of a monolayer by three mechanisms*. The Journal of Physical Chemistry 2002. 106(8): p. 2004-2008

36. Lee, K.Y.C., *Collapse mechanisms of Langmuir monolayers*. Annual Review of Pysical Chemistry 2008. **59**: p. 771-791.

37. Holten-Andersen, N. et al., *KL4 peptides induces reversible collapse structures on multiple length scales in model lung surfactants*. Biophysical Journal, 2011. **101**(12): p. 2957-2965.

38. H. Diamant, et al., *Unstable topography of biphasic surfactant monolayers.* Europhysics letters, 2000. **52**(2): p. 171 - 177.

39. Dwivedi, Mridula V., et al., *Size Influences the Effect of Hydrophobic Nanoparticles on Lung Surfactant Model Systems.* Biophysical Journal, 2014. **106**(1): p. 289-298.

Chapter 3: Impact of ECN on the Collapse Mechanism of Lung Surfactant Monolayers at the Air-Water Interface

3.1. INTRODUCTION

Langmuir monolayers of amphiphilic molecules at air-water interface go through 2D phase transitions when compressed [1]. This transition of the monolayer from the air-water interface to the aqueous sub-phase is defined as monolayer collapse. A detailed review of the different mechanisms of the monolayer collapse has been presented by Lee *et al.* [2]. The squeeze out hypothesis is one key mechanism. In this case, complex amphiphilic mixtures are prone to a rejection of molecules from the surface before reaching the limiting area of compression. Collapse following this path is deemed irreversible. In this case, a loss in the material at the interface is inevitable. However, in the case of naturally occurring lung surfactants (LSs), the molecules remain closely associated with the surface. Studies have shown that LS proteins or their synthetic analogs are capable of eliminating the squeeze out [3-5]. Thus, the collapse following this pathway is reversible, and the material is reincorporated in such monolayers upon expansion. In this report, we are concerned with the impact on the reversibility of phospholipid monolayers in the presence of Engineered Carbon Nanodiamonds [ECN]. The phenomenon of collapse and material loss is particularly interesting in the world of LSs as these monolayers undergo multiple compression/expansion cycles.

LSs are a class of amphiphilic mixtures that are present in the alveolar lining of the lungs [6, 7]. Native surfactants are made up of 90% by weight lipids and 10% by weight proteins. Because of the complexity of the native material, simple model mixtures are often used to mimic the interfacial properties of the

surfactants. The most prevalent amongst the lipids are the zwitterionic, disaturated dipalmitoylphosphatidylcholine (DPPC), and therefore DPPC is selected as the primary component of the representative LS mixtures. The other phospholipids that are usually selected are the unsaturated phosphatidylcholine as well as the negatively charged, unsaturated phosphatidylglycerol. The primary function of the LSs is to lower the surface tension of water with exhalation [8, 9]. This reduction in surface pressure, in turn, decreases the energy required for breathing, improving lung compliance. Additionally, the monolayer of LSs forms a barrier for foreign particles that are capable of reaching the alveoli [10]. Therefore, any foreign object capable of interfering with the regular functioning of LSs must be carefully examined, and this forms the primary motivation for our work.

With the advancement in nanotechnology, engineered nanoparticles have been gaining significant grounds in different areas including biomedicine [11-14]. The small size of the particles as well as relative ease in surface-tunability, these nanoparticles are suitable vehicles for targeted drug delivery amongst other biomedical applications [15, 16]. Therefore, it is highly likely for nanoparticles to either intentionally or unintentionally enter human bodies, and it is necessary to evaluate the compatibility and the toxicity of the nanoparticles when interacting with various physiological components. In this regard, the respiratory tract is one common route for the entry of the nanoparticles. The small size allows the particles to reach the depths of the alveoli [17]. Upon entering the alveoli, nanoparticles then interact with LS monolayer. Research has shown the impact

of size, hydrophobicity, and concentration of different nanoparticles on the functioning of surfactants [18-21]. In the past, we have demonstrated the effect of phospholipid headgroup charge and tail saturation on the packing and domain formation, especially in the Liquid Expanded [LE]-Condensed [C] coexistence region of the monolayer when interacting with the increasingly popular ECNs [22]. We observed that at lower surface pressures, the anionic ECNs behave as line active species when interacting with zwitterionic phospholipids. But, in the presence of anionic phospholipids, electrostatic repulsion plays a greater role. Thus, at low compressions, the composition of the phospholipids also contributes to the behavior of the nanoparticles. However, in the current report, we focus on the impact of ECNs on the collapse mechanism of LS monolayers. Reversible collapse accompanied by material preservation is ideal for LS mixtures. For our work, we selected four phospholipid mixtures that represent the two mechanisms of collapse. ECN was selected because of the growing interest in these particles for both diagnostic and therapeutic applications [23].

3.2. MATERIAL AND METHODS

3.2.1. Material. The phospholipids, 1,2-dipalmitoyl-sn-glycero-3-phosphocholine [DPPC], 1-palmitoyl-2-oleoyl-sn-glycero-3-phospho-(1'-rac-glycerol) (sodium salt) [POPG], 1-palmitoyl-2-oleoyl-glycero-3-phosphocholine [POPC], 1,2-dipalmitoyl-sn-glycero-3-phospho-(1’-rac-glycerol) (sodium salt) [DPPG], and 1,2-dipalmitoyl-sn-glycero-3-phosphoethanolamine [DPPE] were obtained from Avanti Polar Lipids (Alabaster, AL). The phospholipid mixtures were purchased in

chloroform mixtures at concentrations of 5 or 25 mg/ml. The phospholipid dye that was used in our study, Texas red 1,2-dihexadecanoyl-sn-glycero-3-phosphoethanolamine, triethylammonium salt [TXR-DHPE], was obtained from Life Technologies (Invitrogen, Grand island, NY). The engineered carbon nanodiamonds were procured from Microdiamant, Lengwil, Switzerland. The phospholipids as well as the dye were diluted to 1 mg/ml in high-performance liquid chromatography (HPLC)-grade chloroform before using them in our studies. ECN suspensions were also prepared in the chloroform:methanol solutions. Chloroform, methanol, acetone, and isopropanol used in this study for preparing samples and cleaning equipment, were purchased from Thermo Fisher Scientific Inc. (Pittsburgh, PA). The water, used as the cleaning agent and sub-phase, had a resistivity of 18.2 MΩ/cm), which was prepared in a Millipore gradient system (Billerica, MA).

3.2.2. Methods. Sample Preparation: Table 1 shows the phospholipid-ECN solutions used in our study. Solutions of DPPC:POPG, DPPC:POPC, DPPC:DPPG, and DPPC:DPPE mixtures (7:3 by weight) were prepared in chloroform. 1 weight % TXR-DHPE dye (dissolved in 4:1 chloroform:methanol mixture) was added to the lipid samples. Carbon nanodiamonds suspensions were sonicated for 2 hours, and immediately afterward, stoichiometric volumes were added to the lipid mixtures for the experiments involved in this study.

Phospholipid Composition (ratio of 7:3 by weight)	ECN percentage (wt. %)	
DPPC:POPG	0 (Control)	1
DPPC:POPC	0	1
DPPC:DPPG	0	1
DPPC:DPPE	0	1

Table 1: The table lists the samples that have been used in the study. The phospholipid mixtures were taken in the ratio of 7:3 by weight, keeping the percentage of DPPC maximum. The samples with 1 weight % ECN were compared with their counterpart, control that had no ECN in the mixture.

3.2.2.1. Langmuir Studies: Nanodiamonds were mixed with the lipid samples, sonicated for 2 hours and added dropwise on the surface of ultrapure water contained in a Langmuir Ribbon Trough, which was purchased from Biolin Scientific Inc. (Phoenix, AZ). The trough consists of movable ribbon that can compress/expand such that the molecules on the surface can go through different phases. The multiple compression and expansion cycles serve as a model that mimics the decrease and increase in the alveolar area with exhalation/inhalation. The maximum area of the trough is 166 cm^2, and the minimum area is 46 cm^2, which provided the samples with enough area to reach high surface pressure values upon compression. Furthermore, the ribbon is computer controlled to move at a uniform rate with the help of the software supplied by Biolin Scientific Inc. After spreading the sample solution on the water surface and before starting the compression/expansion cycles, the chloroform

was allowed to evaporate for 20 minutes. This waiting period also provides sufficient time for the monolayer to spread uniformly on the surface. After the 20-minute period, the ribbon was moved at the rate of 125 cm^2/min for the compression/expansion isotherms. However, in the case of fluorescence imaging, a slower rate of 7.0 cm2/min was used for clarity.

3.2.2.2. Fluorescence imaging: The trough is also coupled with a Nikon Eclipse fluorescence microscope for visualizing the surface morphology of the monolayer. The microscope is equipped with a 40X- long working distance objective lens along with motorized-focusing capabilities that allow us to monitor the surface of the monolayer continuously. A dichroic mirror/ barrier filter assembly is used in this setup to direct the excitation light perpendicular to the monolayer, whereupon, the emitted light is filtered and captured by the microscope coupled with a fast CCD camera (Andor Luca). For our purposes, we recorded images in sequences of five to observe the morphology.

3.3. THEORETICAL ANALYSIS

3.3.1. Analysis of Material Loss. Area under the curve and percentage recovery: Surface pressure versus area isotherms provides evidence of interaction between molecules at the interface. Upon compression, the monolayer transitions from one phase to the next because of an increase in the surface pressure. At high surface pressures, the monolayer no longer remains as a 2-dimensional film on the surface of the water. Instead, it becomes too unstable and excludes material to the bulk solution (ultrapure water in our case). As a

result there is a loss of material from the surface. Furthermore, with the progression of compression/expansion cycles, the isotherm shifts to lower areas, which is indicative of the aforementioned loss in material. Therefore, we focused on analyzing the area under the curve (hysteresis) of the samples tested. A lowering of such area shows the extent of material loss, which is one of the primary focuses of our study.

3.3.2. Model based on Volmer's Equation of state for the prediction of the Π-A isotherm at the region of 2-Dimensional coexistence phase: Equations of state [EOS] at the air-water interface can be used to predict the two-dimensional phase coexistence region of the Π-A isotherms of amphiphilic monolayers. Fainerman and Volhardt have described such EOS for insoluble Langmuir monolayers, which is capable of predicting the Π-A isotherms at the gaseous region as well as the 2D phase transition for single amphiphile [24]. Another theoretical model published by the same group describes the liquid expanded region of the Π-A isotherms of different amphiphilic molecules [25]. Recently, Ghazvini *et al.* used the theoretical model proposed by Feinerman and Volhardt to understand the impact of pH on the packing of phospholipid membranes [26]. Furthermore, these equations are also capable of predicting the material loss. Here, we represent the key equations that have been used in the present work to quantify the material loss at the interface.

Mathematically, Volmer's equation is expressed as follows:

$$\Pi = \frac{kT\omega}{\omega_o}\left(\frac{1}{A-\omega}\right) - \Pi_{coh}$$

…2

Here, π represents surface pressure of the monolayer, k is the Boltzmann constant, T is the temperature, ω is the average effective molecular area of the insoluble species, ω_o is the molecular area per water molecule, A is the available surface area per insoluble molecule, and π_{coh} is the cohesion pressure. However, the available surface area, A, requires the knowledge of the number of molecules, n, at the surface. Mathematically, A can be related to the trough area, A_T, as follows:

$$A = A_T/n$$

…3

Therefore, we used a modified Volmer's equation, derived by Kuo et. al. [27], represented in equation 4, to characterize material loss from the surface.

$$\Pi = \frac{kT}{\omega_o}\left(\frac{\omega_{eff}}{A_T-\omega_{eff}}\right) - \Pi_{coh}$$

…4

Here, ω_{eff} is an effective total molecular area, and is given by,

$$\omega_{eff} = n\,\omega$$

…5

Equation 4 can be directly fitted to the π-A isotherms. Additionally, ω_{eff} helps us identify the extent of material loss.

3.4. RESULTS

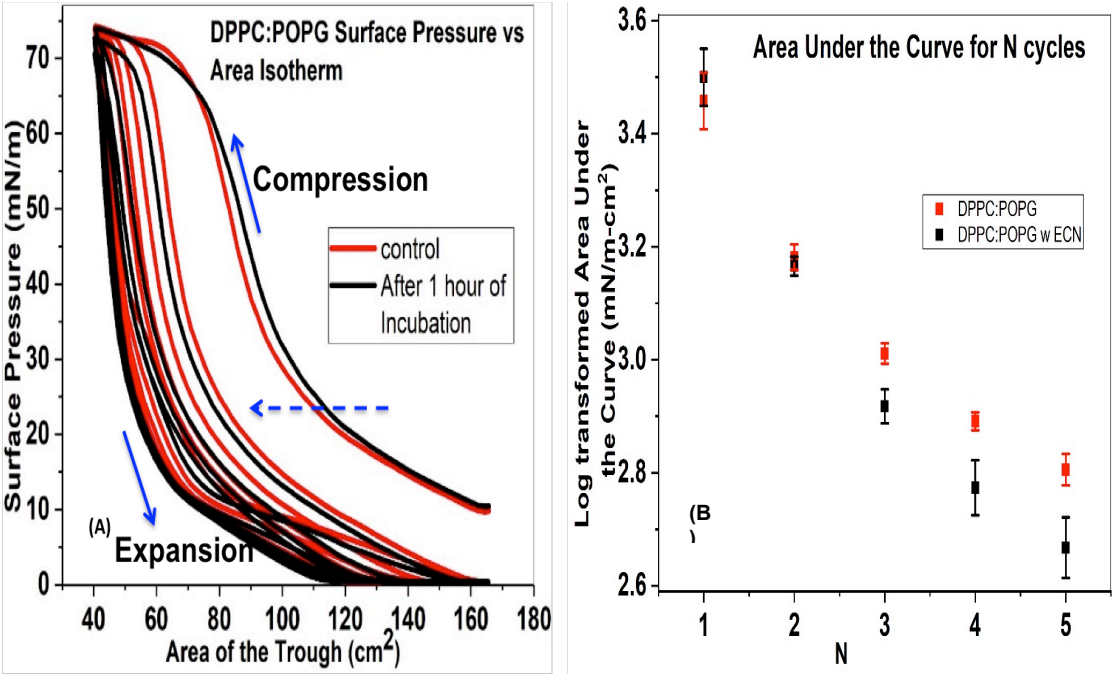

Fig 1. *(A) Surface Pressure versus area of the trough isotherms for DPPC:POPG (7:3) without (control, red solid line) and with 1 wt. % ECN (black solid line). All samples were compressed and expanded five times. The solid arrows point to the direction of compression curve and the expansion curve on the isotherms. The dashed arrow on the other hand shows the direction of advancement of the compression/expansion cycles. All data has been represented as the mean of 3 samples.* ***(B)*** *Area under the curve as a function of compression/expansion cycle for DPPC:POPG (7:3) without (control, red square) and with 1 wt. % ECN (black square). A sample size of three was used for finding the log-transformed mean and standard deviation of the sample.*

3.4.1. Isotherms and area under the curve of DPPC:POPG. Figure 1A shows the quasi-static surface pressure versus mean molecular area isotherm of DPPC:POPG monolayer without (red solid line) and with (black solid line) 1 wt% ECN. Mathematically, surface pressure can be written as,

$$\Pi = \gamma_o - \gamma \quad \ldots 6$$

Where, γ_o is the surface tension of water and γ is the surface tension of monolayer. Initially, at higher area of exposure, the molecules are spread far apart. As the film is laterally compressed, the molecules come closer together and there is an increase in the surface pressure. This leads the monolayer to transition from the gaseous phase to the LE phase. In the case of DPPC:POPG isotherms, we observe that the monolayer is in the LE phase around 10 mN/ m of surface pressure. Beyond this Π, the phase coexistence region appears, where the monolayer consists of both LE and C phase. As the surface area is further reduced, Π increases sharply until 65 mN/m. After this pressure point, the monolayer undergoes a final collapse, encountering a decreasing slope in the isotherm, and reaching pressures of around 72 mN/m eventually. Once the monolayer is fully compressed, the expansion phase begins, and the surface pressure drops rapidly without any notable change in the surface area. The drop continues around 15 mN/m after which the decrease in slope becomes gradual. Here, the expansion curve follows a different path from the compression curve, and therefore, the isotherm displays hysteresis. Multiple reasons have been considered to explain this hysteresis in the Π–A isotherm of lung surfactant

monolayers [28]. Alteration in the compositional ratio after expansion may lead to hysteresis. Also, ejection of material from the surface that fails to/ slowly reincorporates with expansion may also contribute towards hysteresis. Further compression/expansion cycles shifts the isotherms towards lower areas of the trough. This shift in the Π–A isotherm is because of a loss in material from the surface. The DPPC/POPG isotherms exposed to 1 wt% ECN shifts negligibly to higher molecular areas initially. Furthermore, the slope of the curve remains identical to that of the control. However, larger hysteresis is seen in this case. Additionally, with repeated compression/expansion cycles, the isotherm shifts to lower areas of the trough.

To quantify the material loss, we calculated the integral area under the curve for each compression/expansion cycle. The log-transformed area under the curve for DPPC:POPG has been shown in Figure 1B. In the case of the first cycle for control, the area under the curve is around 3.45 in the logarithmic scale. After the first isotherm, there is a notable drop in the area under the curve. This drop in the value indicates loss in material from the interface. For the second isotherm, the value is about 3.18, and the area keeps dropping till the fifth isotherm, where the value is as low as 2.8. With the addition of the nanodiamonds, we see an increase in the area to about 3.5 for the first isotherm. This suggests the incorporation of the nanoparticles at the interface. The subsequent cycles show decrease in the area with the fifth cycle reaching about 2.75. Further analysis of the data is reported in Figure 5.

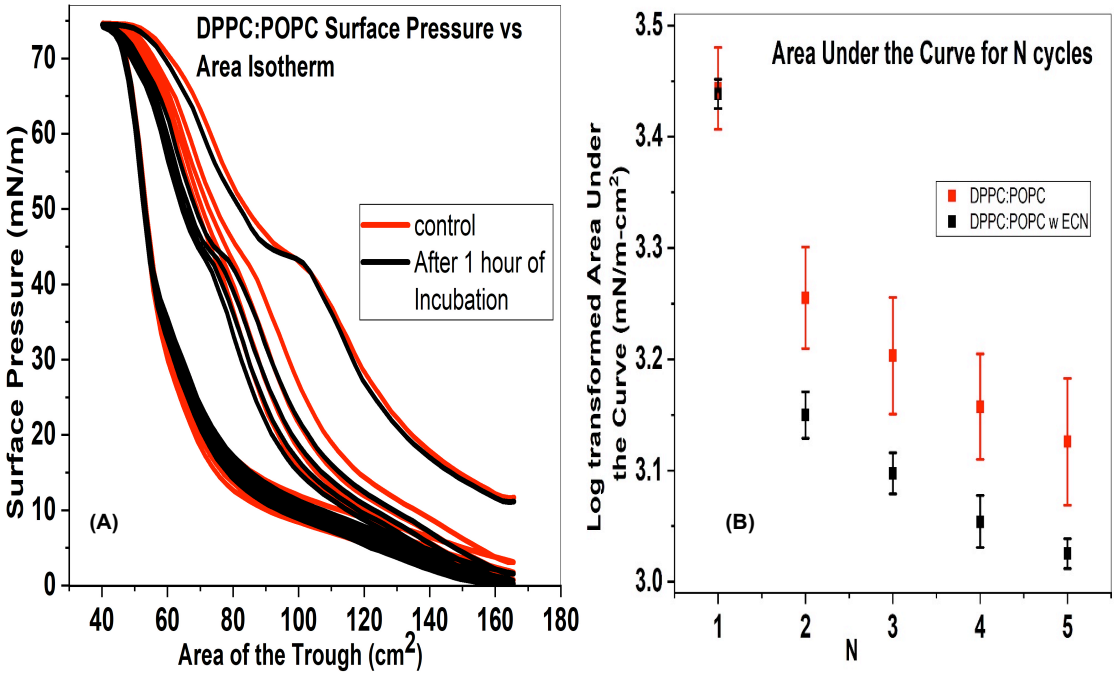

Fig 2. (A) *Surface Pressure versus area isotherms for DPPC:POPC (7:3) without (control, red solid line) and with 1 wt % ECN (black solid line). Similar to the DPPC:POPG, DPPC:POPC samples were compressed and expanded five times. The data has been represented as the mean of 3 samples.* ***(B)*** *Area under the curve as a function of compression/expansion cycle for DPPC:POPC (7:3) without (control, red square) and with 1 wt. % ECN (black square). Three samples were taken to obtain the log-transformed mean and standard deviation.*

3.4.2. Isotherms and area under the curve of DPPC:POPC. In the case of DPPC:POPC, a distinct plateau appears around 45 mN/m. This plateau corresponds to the collapse pressure of POPC, thus indicating a rejection of material from the surface. However, soon after, the refined isotherm follows a steeper slope reaching surface pressure of above 70 mN/m. Once the monolayer is expanded the surface pressure starts to plummet until it reaches values of 13 mN/m and beyond that point the slope becomes more gradual. In the case of DPPC:POPC we see smaller hysteresis than DPPC/POPG. Addition of ECN shows no change in the compression curve initially. But we do observe a larger hysteresis with ECN in the monolayer. Furthermore, we see a large shift in the isotherms with the addition of ECN, indicating loss in material. A more quantitative approach to identifying material loss will be discussed in the subsequent sections.

The area under the curve for the first cycle of DPPC:POPC control is around 3.45. We again see a large drop in the area as the isotherm goes through a second cycle of compression and expansion. Finally, after the fifth cycle, the value drops to about 3.13. When ECN is added, the first isotherm has an area very similar to that of the control. However, we see a greater reduction in the area as we go through the remaining cycles of compression/expansion. After the fifth cycle, the log-transformed value of the area reduces to 3.03.

3.4.3. Isotherms and area under the curve of DPPC:DPPG. Figure 3 shows the Π–A isotherms of DPPC:DPPG (7:3) with and without 1 wt% ECN added to the samples. Because the monolayer here comprises of two disaturated phospholipids, the surface gets well packed almost immediately after compression. The LE phase is short lived and there is a sharp rise in the surface pressure with compression. Here, the surface pressure reaches around 70 mN/m, after which the sample undergoes collapse, with a plateau appearing in the isotherm. Once the sample is expanded, the surface pressure drops to zero with almost very little change in the area of the trough. Among the four samples tested, DPPC:DPPG has the largest hysteresis along with the highest loss in material from the surface. This again is expected since the saturated components fail to respread after reaching collapse pressure. When ECN is added to the samples, there is a shift in the compression curve to higher area of trough. However, the shape of the curve is not altered in the presence of ECN, i.e., the phase transformations remain the same as that of the control. Additionally, we observe a positive influence of the ECN since less material is lost from the surface in this case. This disaturated composition shows the highest area under the curve for the first cycle at a value of about 3.75. However, in this case, much of the material from the surface is lost while undergoing the subsequent compression/expansion cycle.

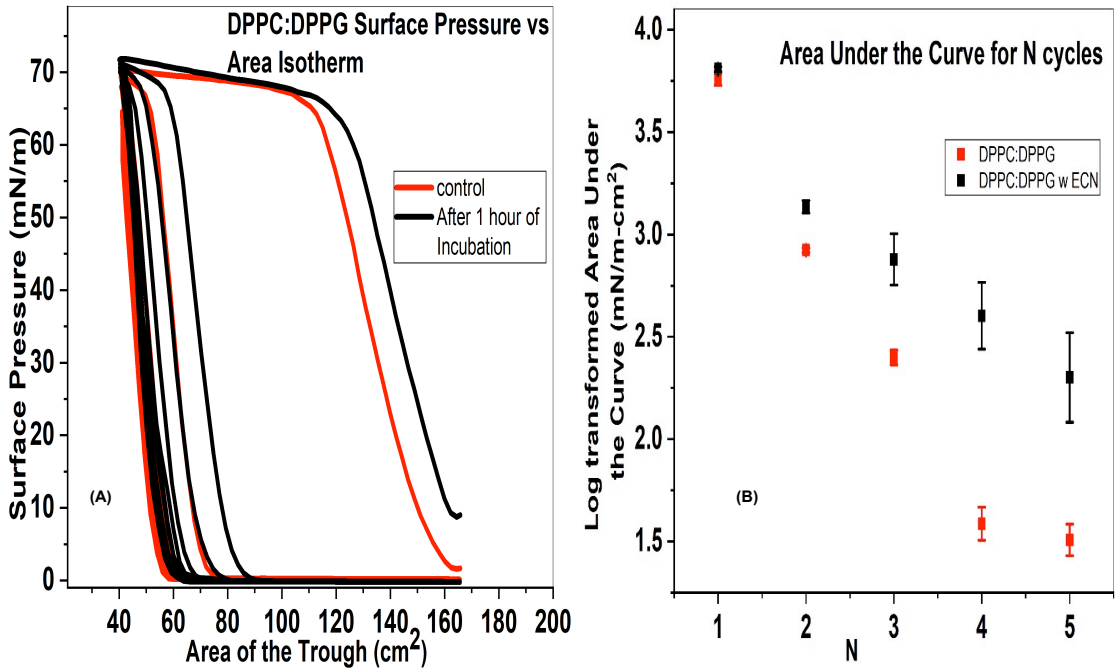

Fig 3. (A) *Surface Pressure versus area isotherms for DPPC:DPPG (7:3) without (control, red solid line) and with 1 wt % ECN (black solid line). Here again, the samples were compressed and expanded five times to understand loss of material from the surface. An average of three samples was taken to graph the data. (B) Area under the curve as a function of compression/expansion cycle for DPPC:DPPG (7:3) without (control, red square) and with 1 wt. % ECN (black square). In this case, the log-transformed mean and standard deviation of three samples has been shown in the figure.*

The fifth cycle seems to have a negligible amount remaining at the surface. Here again, we observe an increase in the area of the first cycle compared to the control when ECN is added. The log-transformed, integral area reaches a value of about 3.8 initially. But like the control, there is a drastic loss in material when the sample is compressed/expanded. Further data presented in Figure 5 shows improvement in material retention with the introduction of ECN.

3.4.4. Isotherms and area under the curve of DPPC:DPPE. Figure 4 shows the Π–A isotherms of DPPC:DPPE (7:3) with and without 1% ECN added to the sample. Here too, the monolayer gets well packed upon compression because of the presence of two disaturated components. The surface pressure rises with a steep slope, rapidly reaching high values. Upon reaching the maximum pressure, the isotherm goes through a plateau as the sample collapses. While expanding the monolayer, the surface pressure drops sharply till it reaches around 7 mN/m, and then the isotherm goes through another plateau to reach near zero values. The subsequent cycles move to lower areas of the trough, however, the loss is less than that of DPPC:DPPG. The isotherms follow a similar path when 1% ECN is added to the sample. A further analysis of the area under the curve provides a better understanding of the loss.

Figure 4B shows the area under the curve for DPPC:DPPE. For the first compression/expansion cycle of the control, the area reaches about 3.75. There is a continual loss of material with the subsequent cycles.

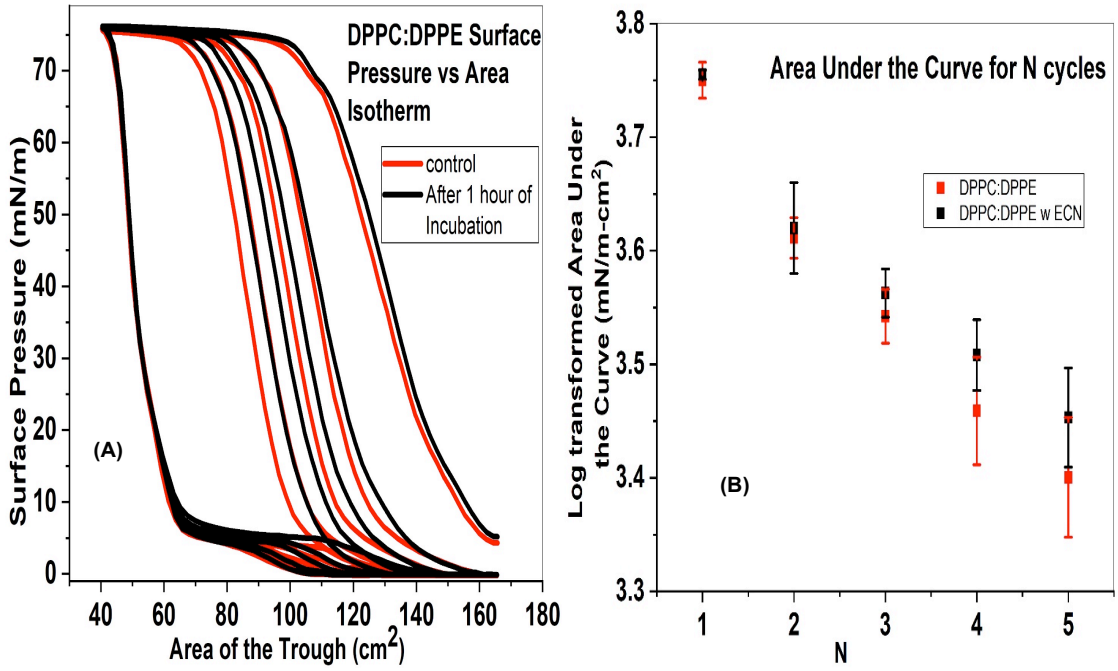

Fig 4. (A) *Surface Pressure versus area of the trough isotherms for DPPC:DPPE (7:3) without (control, red solid line) and with 1 wt % ECN (black solid line). All samples were compressed and expanded five times. The data has been represented as the mean of 3 samples.* ***(B)*** *Area under the curve as a function of compression/expansion cycle for DPPC:DPPE (7:3) without (control, red square) and with 1 wt. % ECN (black square). The log-transformed mean and standard deviation of three samples have been shown in the figure.*

Finally, for the fifth cycle, the area reduces to a value of 3.39. With the addition of ECN, the first few cycles have similar area under the curve as that of the control. However, after the third cycle we start observing deviation from the control.

Next, we obtained the differences in the area under the curve between the control and the samples containing ECN for each cycle such that we can have a better understanding of the deviation from the control once ECN is added.

3.4.5. Difference in the area under the curve for the samples tested. The difference in the integral area under the curve between the control and 1% ECN provides us with the impact of ECN on material loss. Positive values for the difference suggest the presence of less material at the interface when ECN is added, whereas, negative values imply more material is present when ECN is added to the sample. Thus, negative values for this graph is indicative of an improvement in the sample in terms of material retention. In the case of DPPC:POPG, we see mostly positive changes when ECN is added. Only for the first cycle, we have a mean value of – 0.03 mN-m. For the rest of the cycles, the deviation yields positive data. In the case of DPPC:POPC, we see positive data for all the cycles. However, when ECN is added to the disaturated material, we start observing negative values for each cycle. In the case of DPPC:DPPG, we see negative values for all the cycles. Therefore, ECN shows a beneficial impact on DPPC:DPPG. In the case of DPPC:DPPE, the mean for all the cycles has negative values.

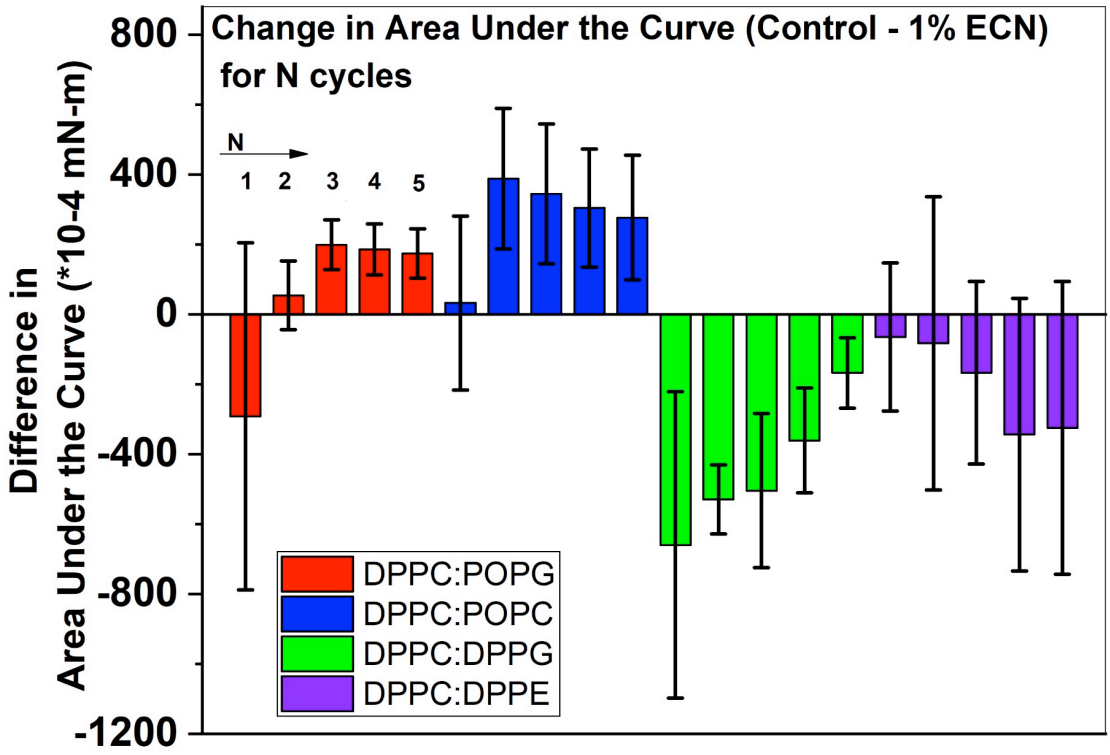

Fig 5. *Difference in the area under the curve between control and samples containing 1% ECN for each compression/expansion isotherm. DPPC:POPG is shown by the red bars, DPPC:POPC by blue, DPPC:DPPG by green and DPPC:DPPE by purple. Each bar represents the mean of 3 samples. The control data is independent from that of the samples containing ECN. Therefore, finding the total variance and subsequently taking the square root of the total variance, we obtained the standard deviation of the difference for each cycle. Mathematically,*

$$\sigma_{total} = \sqrt{(\sigma_{control}^2 + \sigma_{ECN}^2)}$$

Here, $\sigma_{control}$ *is the standard deviation of the control samples,* σ_{ECN} *is the standard deviation of the samples, which contain ECN, and* σ_{total} *is the overall standard deviation of the difference.*

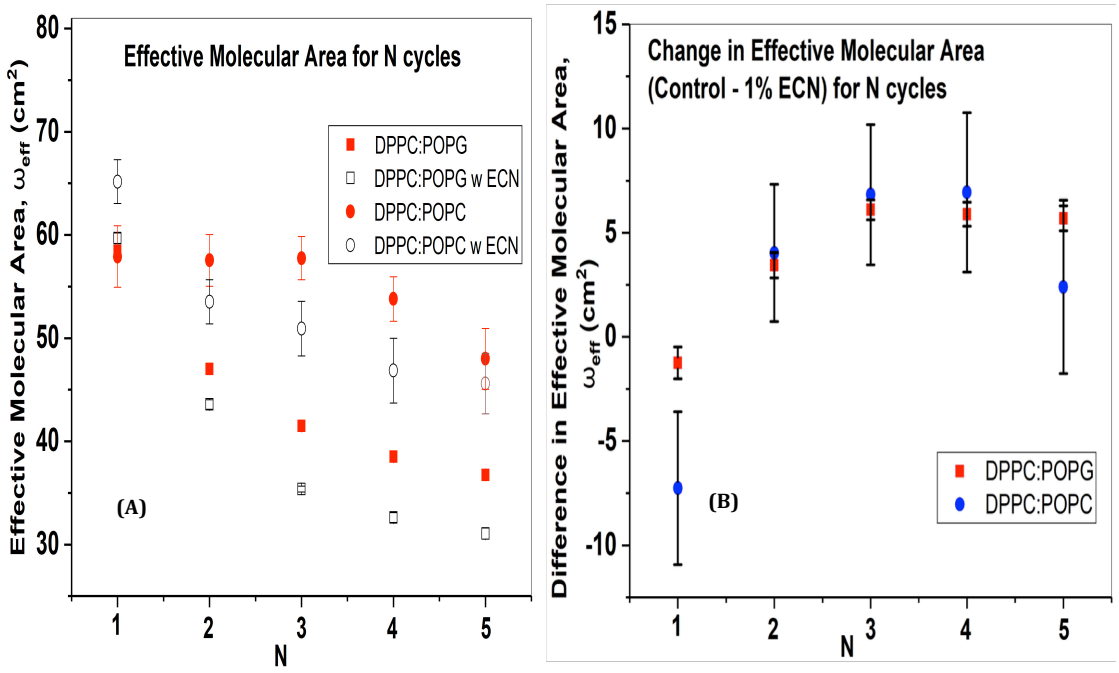

Fig 6. *Effective molecular area and difference in effective molecular area derived by fitting Volmer's equation to Π–A isotherms.* ***(A)*** *One of the parameters of equation 3 is the effective molecular area, denoted by* ω_{eff}. ω_{eff} *as a function of compression/expansion cycle was plotted for DPPC:POPG (7:3) control (closed square), DPPC:POPG (7:3) with 1% ECN (open square), DPPC:POPC (7:3) control (closed circle) and DPPC:POPC (7:3) with 1% ECN (open circle).* ***(B)*** *A difference in* ω_{eff} *between the control and1%ECN has been plotted for DPPC:POPG (7:3) (red square) and DPPC:POPC (blue circle). The data has been represented as the mean and standard deviation of 3 samples.*

3.4.6. Effective molecular area for DPPC:POPG and DPPC:POPC. Material loss can be characterized by the parameter ω_{eff}. A decrease in ω_{eff} with each subsequent cycle of compression/expansion indicates a loss in material. In the case of DPPC:POPG control, the area drops from around 58 cm^2 to 37 cm^2 over five compression/expansion cycles. With the addition of ECN to the sample, the effective molecular area drops to as low as 33 cm^2. In the case of DPPC:POPC control, the loss is smaller than that for DPPC:POPG. From around 57 cm^2 initially, ω_{eff} drops to about 48 cm^2 over 5 compression/expansion cycles. With the addition of ECN to DPPC:POPC the ω_{eff} for the first cycle is higher than that of the control. However, from 65 cm^2 at the first cycle, the ω_{eff} drops to about 47 cm^2 after the 5^{th} cycle. At this point, it should be mentioned that the disaturated mixtures transform to a condensed monolayer very quickly. For this reason, we were not able to model the disaturated systems using Volmer's equation. As our next step, we plotted the change in the effective molecular area between the control and 1% ECN for each cycle for DPPC:POPG and DPPC:POPC.

3.4.7. Change in effective molecular area for DPPC:POPG and DPPC:POPC. A difference between the effective molecular areas for the control and the samples with 1% ECN was obtained for each cycle. A larger deviation from the control suggests loss in material. Initially, more effective area is available for DPPC:POPC with 1% ECN than it's DPPC:POPG counterpart. A positive value for POPC suggests strong interaction with ECN. Therefore, charge repulsion may be a reason for the negative values in the case of DPPC:POPG. However, from the 2^{nd} cycle onwards, the value drops drastically for DPPC:POPC with 1% ECN.

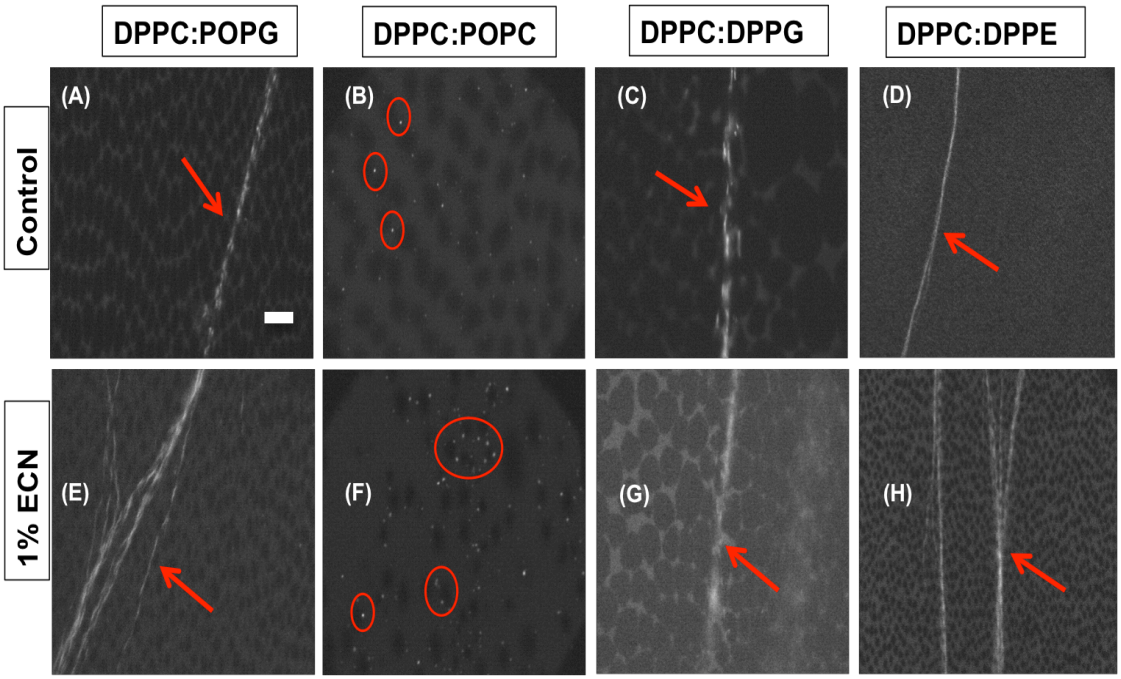

Fig 7. *Fluorescence micrographs taken after monolayer collapse.* ***(A)*** *DPPC:POPG (7:3) control,* ***(B)*** *DPPC:POPC (7:3) control,* ***(C)*** *DPPC:DPPG (7:3) control,* ***(D)*** *DPPC:DPPE (7:3) control,* ***(E)*** *DPPC:POPG (7:3) with 1 wt% ECN,* ***(F)*** *DPPC:POPC (7:3) with 1% ECN, (G) DPPC:DPPG (7:3) with 1 wt% ECN and (H) DPPC:DPPE (7:3) with 1% ECN. The arrows point out folded, reversible, collapse features on the monolayer. The circles highlight the vesicles formed in the monolayer after collapsing. Scale bar represents 10 μms.*

3.4.8. Fluorescence Micrographs of the samples tested. Figures 7(A) and (E) display the monolayer collapse for DPPC:POPG control and with 1% ECN. In the case of DPPC:POPG control (A), the monolayer collapses with the formation of folded features, which have been pointed out by the arrow. These folded structures can be easily spotted in an otherwise dark monolayer. While most of the monolayer is extremely packed, the regions where the collapse features exist appear as bright streaks, perpendicular to the direction of compression, spanning across the width of the micrograph. Fig 7E suggests that these features remain intact when ECN is added to our sample. The rest of the image appears dark because the monolayer becomes extremely packed once the surface pressure reaches high values. Similar to the DPPC:POPG monolayer, the DPPC:DPPG control (Fig 7C) collapses with the formation of reversible collapse features. Moreover, addition of ECN (Fig 7G) to DPPC:DPPG doesn't alter the collapse mechanism in this case. Furthermore, Fig 7D shows the collapse features for DPPC:DPPE control. Here too we observe reversible collapse features, and when ECN is added (Fig 7H), the reversible collapse features are still present. Figures 7B and 7F on the other hand, shows the collapse features in the case of DPPC:POPC control and with 1% ECN. The mechanism of collapse is different in the case of DPPC:POPC. Here too we find the monolayer to be packed, and therefore, the majority of the monolayer appears dark. However, instead of the collapse features that was observed in the case of DPPC:POPG, bright specks appear in the monolayer. These specks in the monolayer of DPPC:POPC control (7B), have been highlighted by circles. When ECN is added to the sample, the

specks appear to increase in number. However, the overall mechanism of collapse remains the same for all the samples when 1% ECN is added.

3.5. DISCUSSION

The present work aims at understanding the impact of ECN on two different collapse mechanisms of lung surfactant monolayers. Previous studies have focused on the effect of nanomaterial on the surface activity and surface morphology of native as well as model lung surfactant monolayers [21, 29, 30]. Additionally, Kodama *et al.,* used multiple compression/expansion cycles to discuss how particle size, ranging from 20 nm to 1.0 μm_s, affect the phase behavior of lung surfactant monolayers [31]. Multiple compression/expansion cycles are relevant for lung surfactants because a loss in the material is encountered after each cycle of breathing. Therefore, greater loss in the material with the addition of nanomaterial suggests a detrimental impact of the particles on the proper functioning of the surfactants. This loss in the material is dependent on both the phase behavior as well as the collapse mechanism of the lung surfactant monolayers. To the best of our knowledge, previous studies have focused on understanding the effect of nanomaterial on the phase behavior of lung surfactants. However, it is of paramount importance to thoroughly evaluate the impact of nanoparticles on the collapse mechanism of lung surfactants, and subsequently, quantify the material loss upon multiple compression/expansion cycles. For this purpose, we systematically looked at experiments that would identify the influence of negatively charged nanoparticles, namely ECN, on the

collapse behavior of the lung surfactants. The phospholipid combinations, which we selected for our study, represent two different mechanisms of collapse. The first method of collapse includes the phospholipid mixtures that collapse with the formation of reversible features like the ones highlighted by arrows in Fig 6. DPPC:POPG (7:3), DPPC:DPPG (7:3) and DPPC:DPPE (7:3) fall under this category. The other method includes the phospholipid mixture, DPPC:POPC (7:3), which collapses with the formation of irreversible collapse features as can be seen in Fig 6B. For neither of the systems, ECN altered the overall mechanism of collapse. However, when we looked at multiple cycles of compressions and expansions, the behavior of ECN changed depending on the lipid tail saturation and charge of the phospholipid mixtures. When DPPC:POPG is compared with DPPC:POPC, where the only difference lies in the charge of the mixture, POPG being negatively charged, whereas POPC being neutral, we observe a greater impact of ECN on POPC than on POPG. This impact has been presented in Fig 5, where positive values for the difference in the integral area under the curve for each cycle between control and ECN implies a greater loss of material. Next, we compared DPPC:POPG with DPPC:DPPG. Thus, the only difference here lies in the saturation of the lipid tail group. Interestingly, from Fig 5 we see that DPPC:DPPG had negative values for the difference in the area under the curve. Thus, we see a favorable impact of ECN on saturated phospholipid groups. However, we also compared DPPC:DPPG with DPPC:DPPE. Here, both the mixtures are saturated, and the only difference lies in the charge of the mixture. DPPC:DPPG is negatively charged, whereas

DPPC:DPPE is a neutral mixture. Between these two mixtures again, DPPC:DPPG shows improved properties when ECN is added. As a result, the charge of phospholipid mixture is also vital when considering the impact of nanodiamonds on the reversibility. Therefore, our data suggest that the impact of ECN on the reversibility of phospholipid monolayers is dependent on both the charge of the monolayer as well as the lipid tail saturation. However, it should be noted that these changes could only be captured with multiple cycles of compressions and expansions. Fluorescence imaging on it's own or even the first cycle of compression/ expansion fail to reveal the subtle changes when ECN interacts with phospholipid mixtures. Even though immediate exposure to the ECN shows minimal changes in the phase behavior of the monolayer, successive cycles point out the loss in the material due to the interaction of the nanomaterial with lung surfactants. Thus, a thorough understanding of the collapse process coupled with the charge of the monolayer as well as the phospholipid saturation is essential to evaluate the effect of the nanoparticles on lung surfactants. We will discuss our results in details in the following sections.

3.5.1. Impact of ECN on the phase behavior and material loss of phospholipids from multiple compression/expansion cycles. Compression/expansion cycles show that the addition of ECN doesn't reflect changes in the phase behavior for DPPC:POPG. The phase transitions remain identical to their control counterpart. However, in the case of DPPC:POPC, we see a change in the phase behavior with the addition of ECN. For the control curve, we observe a plateau around 45 mN/m initially. As we go on compressing

and expanding the monolayer repeatedly, the plateau region shrinks. When ECN is added to DPPC:POPC, the plateau region exists for all cycles. This plateau signifies the squeeze out of material from the monolayer. Thus, the curves indicate a higher loss with the addition of ECN to DPPC:POPC. Additionally, we observe a positive influence of the nanodiamonds with DPPC:DPPG, with the isotherms shifting towards higher area values. This shift also indicates notable insertion of the nanoparticles in the monolayer. To understand material loss in further details, we obtained the area under the curve for each cycle. A continual loss is seen with the progression of compression/expansion cycles for all samples tested. Additionally, we observe that the loss is higher in the case of DPPC:POPG control than DPPC:POPC control. However, with the addition of ECN, we see a steeper initial decrease in the area under the curve for DPPC:POPC. Furthermore, Fig 5 shows that the mean deviation for DPPC:POPC is greater than that of DPPC:POPG when ECN is added. Therefore, the zwitterionic DPPC:POPC is affected more than the negatively charged DPPC:POPG. The role of the saturation of the phospholipid tail was tested next. With DPPC:DPPG we see a beneficial impact of ECN. Furthermore, the zwitterionic as well as saturated DPPC:DPPE showed little impact with ECN. Thus, the charge and saturation both contribute towards the interaction with ECN. In our previous report, we had already demonstrated that the morphology of the LE-C coexistence phase drastically altered in the case of DPPC:POPC with ECN [22], whereas, there was no change when ECN was combined with DPPC:POPG. Moreover, the same study also pointed out that the location of

insertion of the nanodiamonds into the monolayer depended on the saturation of the lipid tail group. Thus, the morphology of the monolayer depends on the headgroup charge and lipid tail saturation. From our combined studies, we can conclude that alterations in the phase behavior eventually affect material preservation.

3.5.2. Volmer's equation to further evaluate material loss. Other than the shift in the integral area under the curve, the loss in the material can also be determined from equations of state that describes the phase transitions in isotherms. Kuo *et al.* used a modified Volmer's equation of state, represented by equation 2, to understand the effect of particle size on SDS-DODAB monolayers [27]. The Volmer's fit accurately describes the LE region of the isotherms and in Kuo's article, a modified Volmer's fit was shown to be effective in relating the total surface area to the surface pressure change in the LE region. Effective molecular area, ω_{eff}, was then extracted from the fit, and this parameter is directly related to the amount of material present on the surface. Thus, a decrease in the value of ω_{eff} when 0.5 μm and 1μm particles were added to the SDS-DODAB monolayer suggests a loss in material. For our work, we used this theoretical model to understand the impact of ECN on the collapse mechanism of lung surfactants. In the case of both the controls, we observe a decrease in the ω_{eff}. This reduction is expected because a material loss occurs after every cycle for all samples, and the data is supported by the information obtained from the area under the curve. Upon the addition of ECN to the lung surfactants, we observe a further decrease in the ω_{eff}. However, we see a sharper drop in ω_{eff} in the case of

DPPC:POPC than DPPC:POPG. This drop has been highlighted in fig 5B by taking the difference between the control and 1%ECN at each cycle. Thus, the conclusion drawn from the area under the curve is further corroborated by the ω_{eff} data. Finally, fluorescence microscopy was used to have a thorough understanding of the collapse mechanism.

3.5.3. Fluorescence Imaging of the monolayer to visualize the mechanism of collapse. Gopal *et al.* have shown that DPPC:POPG monolayers, laterally compressed under conditions, which are similar to our study, collapses via reversible folding mechanism [32]. These reversible folds appear as bright streaks perpendicular to the direction of compression, and range from 100 μms to about 1 mm in length. These reversible structures unfold when the monolayer is expanded, and material reincorporates into the monolayer without notably altering the morphology. Our study shows the occurrence of similar collapse features in the case of DPPC:POPG. With the addition of ECN, we see the monolayer retaining this feature. Bright streaks were again seen spanning across the fluorescence micrograph. Therefore, fluorescence images didn't detect any detrimental impact of the nanoparticle on the DPPC:POPG monolayer. However, we wanted to observe the effect on another mode of collapse to have a better understanding of the interaction. DPPC:POPC monolayers collapses with the formation of vesicles, which appears as bright specks on the monolayer. Large vesicles usually end up detaching from the monolayer making the collapse irreversible. This phenomenon has been observed for DPPC:POPG monolayers at 37^{o}C [32]. At high temperature, the monolayer shows bright specks that are

similar to the ones we observed in the case of DPPC:POPC control at room temperature. These bright specks are globular vesicles that usually detach from the monolayer. However, it has been suggested that some of the globular vesicles do remain attached to the surface and gets reincorporated to the surface once the monolayer is expanded. In the case of DPPC:POPC control, the formation of the vesicles suggests irreversibility of the monolayer. However, further inspection using the area under the curve and equation of state fit methods suggest preservation of material in the case of DPPC:POPC. In fact, in our study, we observed that more material was preserved with DPPC:POPC than with DPPC:POPG. When ECN was added to the DPPC:POPC mixture, more vesicles appeared on the trough. Coupled with the theoretical methods, we do see an initial loss in material for DPPC:POPC and 1% ECN. Thus, some of the vesicles, in this case, fail to get reincorporated to the monolayer. A reason for this failure may be due to the size and density of the vesicles. With DPPC:DPPG, we observe the material retaining the reversible collapse features with the addition of ECN. In fact, area analysis showed a positive impact on the mixture. Finally, In the case of DPPC:DPPE control, we see the formation of reversible collapse features as well. After ECN is added, the collapse features still appear on the monolayer. Therefore, through fluorescence images, we can conclude that ECN doesn’t alter the mechanism of collapse regardless of the phospholipid it encounters.

3.6. CONCLUSION

Composition	Overall Charge	Saturation	Mechanism of collapse for control	Mechanism of collapse with ECN	Impact of ECN on material retention
DPPC:POPG	Negative	Unsaturated	Reversible	Reversible	Some negative influence.
DPPC:POPC	Neutral	Unsaturated	Irreversible	Irreversible	Most negative influence.
DPPC:DPPG	Negative	Saturated	Reversible	Reversible	Material is preserved (Positive influence of ECN).
DPPC:DPPE	Neutral	Saturated	Reversible	Reversible	Similar to control. Shows little impact of ECN.

Table 2. The table summarizes the impact of ECN on the different phospholipid mixtures. The disaturated mixtures have either no effect (DPPC:DPPE) or favorable (DPPC:DPPG) effect when ECN is added depending on the charge of the mixture. On the other hand, some additional loss was recorded for the unsaturated mixtures. However, the most loss on an average was recorded for DPPC:POPC (zwitterionic, unsaturated).

We report the impact of ECN on the collapse mechanism of lung surfactant mixtures. The chosen components of the phospholipid mixtures focus on the role of the lipid headgroup charge, the lipid tail saturation and the subsequent phase behavior under compression when interacting with the nanodiamonds. Our data suggests that a combination of fluorescence images along with multiple compression/expansion cycles and equation of state fit to the isotherms is

required to have a better understanding of the monolayer collapse. This in turn is crucial to gain knowledge on the toxicity of nanomaterial on lung surfactants. We observed that ECN never alters the mode of collapse regardless of the phospholipid mixture it encounters. When the charge of the phospholipid mixtures is considered keeping the composition mono-unsaturated, the zwitterionic component, DPPC:POPC, is the most negatively influenced. Negatively charged, mono-unsaturated phospholipids, DPPC:POPG, also show some loss when coming in contact with ECN. However, when the saturation of the mixture is considered keeping the charge negative, the disaturated component, DPPC:DPPG, shows improved properties when ECN is added. Here, we observe material preservation with the addition of ECN. Therefore, saturated compositions are more favorably affected by ECN than their unsaturated counterpart. Finally, when the charge of the mixture is altered keeping the composition disaturated, we see that the negatively charged, disaturated mixture, DPPC:DPPE, shows very little deviation from control. Thus, we can conclude that ECN has either no or has a beneficial impact when it encounters completely saturated mixtures. When encountering unsaturated components, the negatively charged mixture shows less deviation on the average, which in turn suggests that anionic lipids are less prone to have adverse effects than the zwitterionic ones. Therefore, the composition of the phospholipid mixture plays a valuable role in terms of material retention when coming in contact with ECN. From our studies, we conclude that the overall

charge of the phospholipid composition, as well as the saturation of the tail group, both contribute when the mixtures interact with ECN.

3.7. REFERENCES

1. Vollhardt, D. and V. Fainerman, *Phase transition in Langmuir monolayers.* Colloids and Surfaces A: Physicochemical and Engineering Aspects, 2001. **176**(1): p. 117-124.
2. Lee, K.Y.C., *Collapse Mechanisms of Langmuir Monolayers.* Annual Review of Physical Chemistry, 2008. **59**(1): p. 771-791.
3. Ding, J., et al., *Effects of Lung Surfactant Proteins, SP-B and SP-C, and Palmitic Acid on Monolayer Stability.* Biophysical Journal, 2001. **80**(5): p. 2262-2272.
4. Holten-Andersen, N., et al., *KL4 Peptide Induces Reversible Collapse Structures on Multiple Length Scales in Model Lung Surfactant.* Biophysical Journal, 2011. **101**(12): p. 2957-2965.
5. Takamoto, D.Y., et al., *Interaction of Lung Surfactant Proteins with Anionic Phospholipids.* Biophysical Journal, 2001. **81**(1): p. 153-169.
6. Veldhuizen, E.J.A. and H.P. Haagsman, *Role of pulmonary surfactant components in surface film formation and dynamics.* Biochimica et Biophysica Acta (BBA) - Biomembranes, 2000. **1467**(2): p. 255-270.
7. Goerke, J., *Pulmonary surfactant: functions and molecular composition.* Biochimica et Biophysica Acta (BBA) - Molecular Basis of Disease, 1998. **1408**(2): p. 79-89.
8. Bernhard, W., *Lung surfactant: Function and composition in the context of development and respiratory physiology.* Annals of Anatomy - Anatomischer Anzeiger, 2016. **208**: p. 146-150.

9. Hartog, A., et al., *Improvement of lung mechanics by exogenous surfactant: effect of prior application of high positive end-expiratory pressure.* British Journal of Anaesthesia, 2000. **85**(5): p. 752-756.

10. Han, S. and R.K. Mallampalli, *The Role of Surfactant in Lung Disease and Host Defense against Pulmonary Infections.* Annals of the American Thoracic Society, 2015. **12**(5): p. 765-774.

11. Richard Bayford, T.R., Ivan Roitt1 and Scarlet Xiaoyan Wang, *Emerging applications of nanotechnology for diagnosis and therapy of disease: a review.* Physiological Measurement, 2017. **38**(8): p. R183-R203.

12. Shi, J., et al., *Nanotechnology in Drug Delivery and Tissue Engineering: From Discovery to Applications.* Nano Letters, 2010. **10**(9): p. 3223-3230.

13. Sun, T., et al., *Engineered Nanoparticles for Drug Delivery in Cancer Therapy.* Angewandte Chemie International Edition, 2014. **53**(46): p. 12320-12364.

14. Duncan, T.V., *Applications of nanotechnology in food packaging and food safety: Barrier materials, antimicrobials and sensors.* Journal of Colloid and Interface Science, 2011. **363**(1): p. 1-24.

15. Singh, R. and J.W. Lillard, *Nanoparticle-based targeted drug delivery.* Experimental and Molecular Pathology, 2009. **86**(3): p. 215-223.

16. MICHAEL GOLDBERG, R.L.a.X.J., *Nanostructured materials for applications in drug delivery and tissue engineering.* J. Biomater. Sci. Polymer Edn, 2007. **18**(3): p. 241-268.

17. Heyder, J., *Deposition of Inhaled Particles in the Human Respiratory Tract and Consequences for Regional Targeting in Respiratory Drug Delivery.* Annals of the American Thoracic Society, 2004. **1**(4): p. 315−20.

18. Harishchandra, R.K., M. Saleem, and H.-J. Galla, *Nanoparticle interaction with model lung surfactant monolayers.* Journal of The Royal Society Interface, 2010. **7**(Suppl 1): p. S15.

19. Sachan, A.K. and H.-J. Galla, *Understanding the Mutual Impact of Interaction between Hydrophobic Nanoparticles and Pulmonary Surfactant Monolayer.* Small, 2013. **10**(6): p. 1069-1075.

20. Dwivedi, Mridula V., et al., *Size Influences the Effect of Hydrophobic Nanoparticles on Lung Surfactant Model Systems.* Biophysical Journal, 2014. **106**(1): p. 289-298.

21. Sachan, A.K., et al., *High-Resolution Investigation of Nanoparticle Interaction with a Model Pulmonary Surfactant Monolayer.* ACS Nano, 2012. **6**(2): p. 1677-1687.

22. Chakraborty, A., et al., *Phospholipid Composition Modulates Carbon Nanodiamond-Induced Alterations in Phospholipid Domain Formation.* Langmuir, 2015. **31**(18): p. 5093-5104.

23. Schrand, A.M., S.A.C. Hens, and O.A. Shenderova, *Nanodiamond Particles: Properties and Perspectives for Bioapplications.* Critical Reviews in Solid State and Materials Sciences, 2009. **34**(1-2): p. 18-74.

24. Fainerman, V.B. and D. Vollhardt, *Equations of State for Langmuir Monolayers with Two-Dimensional Phase Transitions.* The Journal of Physical Chemistry B, 1999. **103**(1): p. 145-150.

25. Fainerman, V.B. and D. Vollhardt, *Surface Pressure Isotherm for the Fluid State of Langmuir Monolayers.* The Journal of Physical Chemistry B, 2006. **110**(21): p. 10436-10440.

26. Ghazvini, S., et al., *pH-Induced Changes in the Surface Viscosity of Unsaturated Phospholipids Monitored Using Active Interfacial Microrheology.* Langmuir, 2018. **34**(3): p. 1159-1170.

27. Kuo, C.-C., et al., *Particle Size Effects on Collapse in Monolayers.* Langmuir, 2012. **28**(39): p. 13976-13983.

28. Notter, R.H., *Lung Surfactants: Basic Science and Clinical Applications*. 1st ed. Vol. 149. 2000 New York, USA: CRC Press 464.

29. Harishchandra, R.K., M. Saleem, and H.-J. Galla, *Nanoparticle interaction with model lung surfactant monolayers.* Journal of The Royal Society Interface, 2009.

30. Guzmán, E., et al., *Mixed DPPC–cholesterol Langmuir monolayers in presence of hydrophilic silica nanoparticles.* Colloids and Surfaces B: Biointerfaces, 2013. **105**: p. 284-293.

31. Kodama, Akihisa T., et al., *Investigating the Effect of Particle Size on Pulmonary Surfactant Phase Behavior.* Biophysical Journal, 2014. **107**(7): p. 1573-1581.

32. Gopal, A. and K.Y.C. Lee, *Morphology and Collapse Transitions in Binary Phospholipid Monolayers.* The Journal of Physical Chemistry B, 2001. **105**(42): p. 10348-10354.

Chapter 4: Understanding the Collapse Mechanism of Model Lung Surfactant Mixtures in the Presence of Mini-B

4.1. INTRODUCTION

Lung surfactants are a complex mixture of lipids and proteins that covers the liquid lining of the alveoli [1]. The type II epithelial cells of the alveoli produce the surfactants, and eventually, the surfactants reach the surface of the liquid lining [2]. Other than serving as an innate host defense against pathogens [3, 4], the surfactants are responsible for reducing the energy needed for breathing as well as stabilizing the alveoli by changing the surface tension as a function of the alveolar volume. Low surface tension is necessary while exhaling, failing which, results in the collapse of the alveoli [5]. Therefore, lung surfactants ensure proper breathing, and an absence or dysfunction leads to fatal diseases [6]. At equilibrium, the surface tension is roughly around 20 mN/m in the lungs, whereas upon lateral compression, the value of surface tension goes to 0 mN/m. One other fundamental characteristic of the surfactant is its ability to adsorb rapidly to the surface [7]. Thus, these properties of the surfactants act as the guiding parameters when preparing model surfactant mixtures intended for surfactant replacement therapy in the case of respiratory diseases. However, as stated earlier, the composition of the native surfactants is vast making it challenging to come up with simple model mixtures that can mimic the natural surfactants. The native lung surfactant is a concoction of approximately 90% lipids and 10% proteins [8]. Phospholipids form the majority of the surfactant lipids, and among them, phosphatidylcholines are the most abundant component. Around 70-80% of the total amounts of the lipids are made up of phosphatidylcholine. Furthermore, around 50-70% of these phospholipids are saturated, consisting of

dipalmitoylphosphatidylcholine [DPPC] primarily. The anionic phosphatidylglycerol makes up about 8% of the surfactants. In addition to these components, smaller quantities of phosphatidylserine, phosphatidylinositol, phosphatidylethanolamine, lysophosphatidylcholine, and sphingomyelin are also found in the surfactants. Moreover, neutral lipids also form a part of the surfactant pool. Cholesterol makes up about 2.4 weight% of the total surfactants. The remaining 10% of the surfactants comprises of two hydrophilic and two hydrophobic surfactant proteins. The hydrophilic proteins, SP-A and SP-D serve as a line of defense against inhaled pathogens [3], whereas, the hydrophobic proteins, SP-B and SP-C, enhance the functionality of the lung surfactants [9]. Each component of the surfactant system plays a specific role, and synthetic surfactants are concerned with mimicking the functions and biophysical behavior of the overall surfactant system. One crucial biophysical property of the surfactants at the interface is their ability to go through reversible collapse. Any two-dimensional film at the air/water interface when compressed, undergoes changes in phase. At compression values higher than that of the critical compression pressure, as in the case of exhalation, the monolayer can no longer sustain a film, and instead, yields structures in the third dimension. This phenomenon of destabilization of the monolayer is called collapse [10]. Furthermore, the mechanism of collapse is vital because it determines the reversibility of the monolayer. Reversible Langmuir monolayers are capable of rapidly adsorbing back to the interface. The reversibility arises from the fact that the monolayers collapse through localized, large amplitude buckling [11]. The

buckled areas in the monolayer remain close to the interface, and are capable of being readsorbed rapidly. Besides reversible folding through buckling, the formation of stacked disks has also been shown to reversibly readsorb to the interface upon expansion [12]. Thus, multiple mechanisms have been proposed to explain the reversibility of lung surfactants. On the contrary, monolayers, which are too fluid, or are too rigid, collapse irreversibly by either solubilization or fracture. Therefore, the fluidity of the native surfactant is such that the monolayer undergoes collapse via a reversible pathway. This reversibility of the lung surfactants is attributed to the surfactant proteins, SP-B and SP-C[13, 14]. The behavior of SP-B and SP-C, when interacting with anionic mixtures, has been thoroughly studied [14, 15]. These surfactant proteins eliminate the loss of material from the surface when interacting with the anionic phospholipid mixture. Additionally, multilayered protrusions form when native surfactants are compressed beyond the critical surface pressure. It has also been shown through atomic force microscopy that the formation of these protrusions depends on the concentration of the proteins as well as the phospholipid composition [16]. These protrusions are a result of the monolayers undergoing collapse. Therefore, we hypothesize that the reversibility of the monolayer is a function of the phospholipid mixture under consideration along with their inherent surface viscosity.

The role of phospholipid headgroups was evaluated in our work to determine the reversibility of model lung surfactant monolayers. For this purpose, two lipid compositions were tested, namely, DPPC:POPG and

DPPC:palmitoyloleoyl phosphatidylcholine [DPPC:POPC]. A synthetic analog of SP-B, known as Mini-B was used in this study to evaluate the interaction of the lipids with the surfactant protein. Mini-B is a 34 amino acid residue, which is based on the sequence of the predicted N and C terminal helices of the native SP-B [17, 18]. Mini-B contains a +7 charge, which is the same as that of SP-B. Furthermore, similar to SP-B, oxidized Mini-B also forms disulfide bridges that connect the two helices. Previously, it has been shown that Mini-B is capable of mimicking the biophysical properties of its natural counterpart [19], and thus, it was selected for this work. Here, we have used Langmuir-Blodgett [LB] technique to prepare the monolayers of the phospholipids along with the proteins at the air-water interface. The monolayers were compressed and expanded to observe the change in surface pressure. The LB trough was also coupled with fluorescence microscopy to visualize the monolayer at the interface. Finally, to obtain information on the location of protein insertion, the monolayers were transferred to sheets of mica. These transferred films were then analyzed under the Atomic Force Microscope to obtain topographical information on a nanolevel.

4.2. MATERIAL AND METHODS

4.2.1. MATERIAL

The phospholipids, 1,2-dipalmitoyl-sn-glycero-3-phosphocholine (DPPC), 1-palmitoyl-2-oleoyl-sn-glycero-3-phospho-(1′-rac-glycerol) (POPG), 1,2,-dipalmitoyl-sn-glycero-3-phospho-(1′-rac-glycerol) (DPPG), and 1-palmitoyl-2-oleoyl-sn-glycero-3-phospho-L-serine (POPS) were purchased from Avanti Polar

Lipids, Inc. (Alabaster, Al). The phospholipids were purchased in powdered form. Sample solutions were prepared in organic solvents, and were stored at -20 ^{o}C to avoid any loss of solvent due to evaporation. The synthetic protein Mini-B, prepared via solid phase peptide synthesis as described by A.J. Waring *et al.* [17], was obtained from Biopolymer Core Facility, LA Biomed at Harbor, UCLA Medical center, Torrance, California. The fluorescent dye, 1,2-dihexadecanoyl-sn-glycero-3-phosphoethanolamine-triethylammonium salt (TXR-DHPE), was purchased from Life Technologies (Invitrogen, Grand Island, NY) in powdered form. Additionally, organic solvents, namely acetone, isopropanol, and chloroform, were procured from Thermo Fisher Scientific Inc. (Pittsburgh, PA). The water used in the experiment as well as in the cleaning process was purified to a resistivity of 18.2 MΩ cm with a Direct-Q 3 UV system obtained from EMD Millipore (Billerica, MA).

4.2.3. METHODS

4.2.3.1. Sample Preparation: Binary lipid mixtures of lipids, DPPC:POPG, DPPC:POPC, and DPPC:DPPG were prepared in high performance liquid chromatography (HPLC) grade chloroform. A 7:3 weight ratio was selected for all the mixtures as the DPPC content is the highest in natural surfactants, and model synthetic mixtures contain mostly DPPC. Mini-B solutions were formulated in 3:1 mixture of HPLC grade chloroform and methanol. Subsequently, Mini-B was added to the model phospholipid mixtures.

4.2.3.2. Surface Pressure vs. Mean Molecular Area Isotherm: A Langmuir-Blodgett trough (Biolin Scientific Inc.) was used to evaluate the biophysical properties of the model lung surfactant mixtures. Inside the trough is an area bounded by a moveable ribbon. The moveable ribbon is capable of compressing and expanding, thereby mimicking the breathing process. The bounded area in the trough has a minimum area of 46 cm^2 and a maximum area of 166 cm^2. The difference in area is substantial enough for the compressed monolayer of mixtures to reach zero surface tension values. The model mixtures were added dropwise with a Hamilton glass syringe on purified water sub-phase. We allowed 20 minutes for the organic solvent to evaporate before starting the compression/expansion cycles. For isotherm experiments, we selected a compression rate of 125 cm^2/min. The surface pressure was recorded by a Whilhelmy plate balance (paper filter) that is connected to a pressure sensor device. Experiments were conducted in triplicates.

4.2.3.3. Fluorescence Imaging: The samples were tagged with TXR-DHPE to visualize the monolayer. A Nikon Eclipse Fluorescence Microscope was used to monitor the formation of lipid domains at the air-water interface. For imaging, we used a slower rate of compression (7 cm^2/min). Images were captured at 5 mN/m intervals in the two-phase coexistence region, and around collapse pressure with a CCD camera (Andor LUCA). Five frames for each image sequence was used, and the representative images have been presented in this report. Image J (NIH) was then used to analyze each image. Further analysis of the domains was carried out using Origin (OriginLab, Northampton, MA).

4.2.3.4. Atomic Force Imaging: Due to the difference in charge of the two monolayers, the protein inserts itself in different locations. To determine the location of insertion of Mini-B in the air/water interface, we obtained high-resolution microscopy images using an Atomic Force Microscope. For this imaging technique, the following steps were employed. The monolayers were first compressed to a surface pressure of 20 mN/m, and then transferred to a cleaved mica substrate using a home-built inverse Langmuir-Schaffer technique, a technique developed by Lee et. al [Langmuir, 1998]. Here, the mica sheet sits under the surface while the water is slowly aspirated from the sub-phase. With aspiration, the monolayer drops on the mica sheet. Furthermore, since the mica sheet is under the surface, the film can be visualized constantly during the entire process if the focus is carefully maintained on the interface. The transferred monolayer is then dried in Nitrogen, and the topography of the substrate is observed using a Veeco diMultimode V microscope. For imaging, we used antimony-doped silicon probes (Bruker Scientific) having a resonance frequency of 371 kHz. Also, tapping mode in the air was used for imaging, which has a scanning limit of 125 X 125 μm^2. Snapshots of the surface were taken at a maximum scan rate of 1 μm/s, and a resolution of 512 pixels/line.

4.3. THEORETICAL ANALYSIS

4.3.1. Compressibility Modulus: The modulus of elasticity, also called compressibility modulus (β), describes the ability of monolayers to store

mechanical energy as stress under a compression force. Mathematically it is expressed as:

$$\beta = -A\left(\frac{\partial \Pi}{\partial A}\right)_T = -A\left(\frac{\partial \sigma}{\partial A}\right)$$

… (1)

Additionally, isothermal compressibility, κ, which is the inverse of β, along with β itself are second-order derivatives of the free energy, G, mathematically,

$$\beta = \left(\frac{\partial^2 G}{\partial A^2}\right)_T$$

… (2)

A change in the β vs. A graph implies first order phase transition. Moreover, higher values of β suggest the formation of condensed well-packed films. The development of such condensed films is essential for the proper functioning of the lung surfactants. For our experiments, the compressibility modulus was obtained from the raw isotherm data by calculating the slope of the isotherm at each point. Origin 8.62, with built-in functions for finding derivatives, was used to obtain the compressibility modulus. Furthermore, the derivatives of the π-A isotherms are often noisy because of the fluctuations in the surface pressure readings. Therefore, a five-point Fourier filter, another built-in function of Origin 8.62, was used to smoothen the data.

4.3.2. Area Under the Curve: The hysteresis in the isotherm is an indicator of the amount of material present on the surface. Higher value of the area under the curve implies the presence of more material at the air/water interface. Origin 8.62 with a built-in function for integration was used to obtain the integral area under the curve for each cycle, and a sample set of three was used to calculate the average area under the curve for each cycle.

4.4. RESULTS

4.4.1. ISOTHERMS: DPPC:POPG with and without Mini-B

Fig 1A represents the surface pressure vs. trough area isotherms of DPPC:POPG without Mini-B (control). The sample is added at higher trough area, and gradually compressed to the minimum area possible. When compressed, DPPC:POPG monolayer goes through changes in phase, which appears as changes in slope along the isotherm. This change is a result of the rearrangement of the phospholipids in the monolayer film. In this mixture, DPPC is the primary component, and because of its ability to pack very tightly, DPPC is capable of reaching very high values of surface pressure, which is equivalent to reaching very low values of surface tension. The first cycle of the isotherm shows how the model mixture reaches high surface pressure as expected. However, once the monolayer is expanded, there is loss of phospholipid from the surface of the monolayer, and therefore, a hysteresis is seen in the curve, i.e., upon expansion, the curve no longer retraces the line for compression. This loss is apparent in the subsequent cycles of compression/expansion because of a shift in the isotherm towards lower areas of the trough.

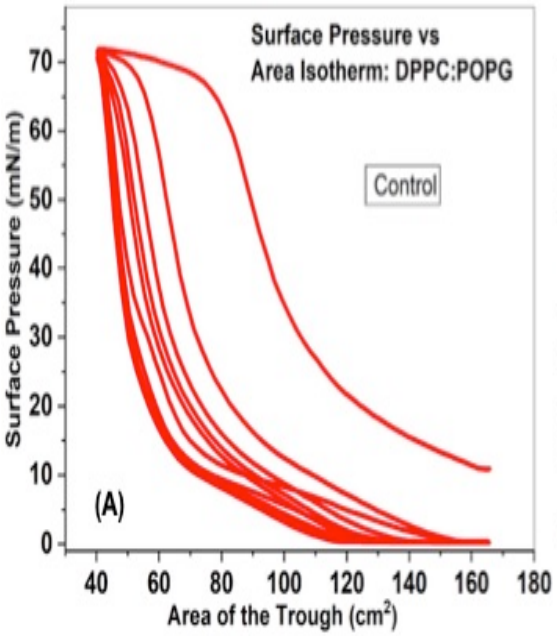
Surface Pressure vs
Area Isotherm: DPPC:POPG
Control
(A)
Surface Pressure (mN/m)
Area of the Trough (cm²)

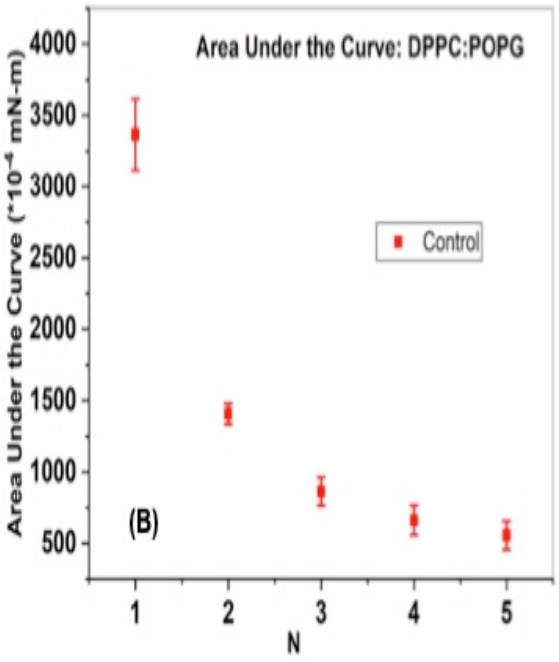
Area Under the Curve: DPPC:POPG
Control
(B)
Area Under the Curve (*10⁻⁴ mN-m)
N

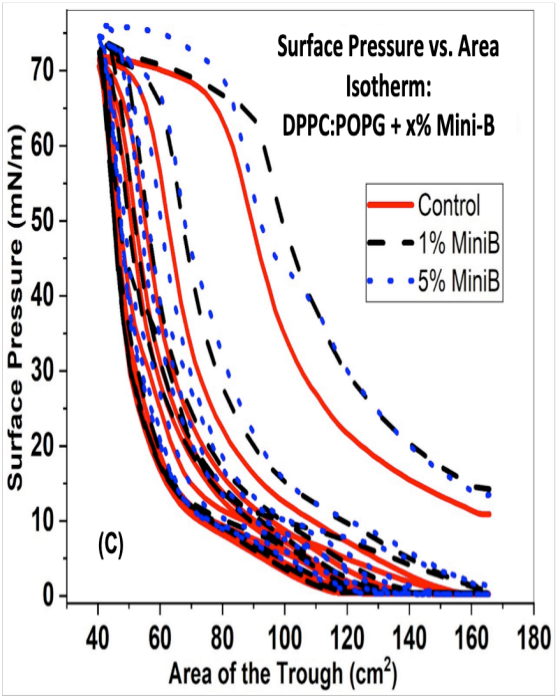
Surface Pressure vs. Area
Isotherm:
DPPC:POPG + x% Mini-B
Control
1% MiniB
5% MiniB
(C)
Surface Pressure (mN/m)
Area of the Trough (cm²)

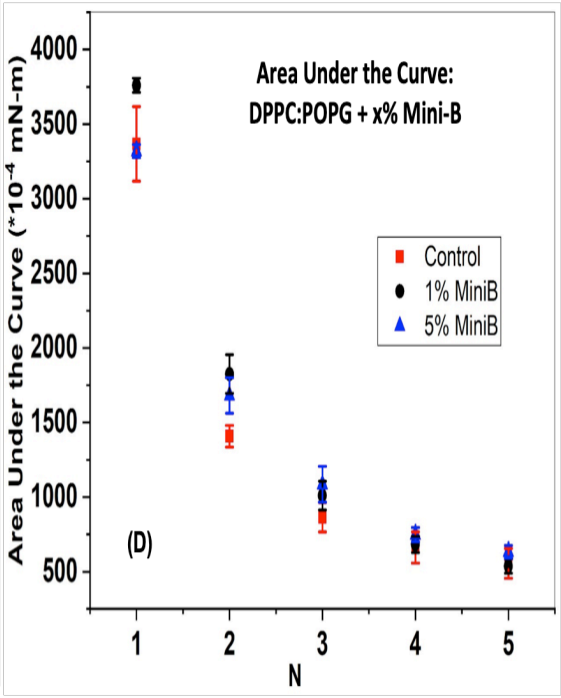
Area Under the Curve:
DPPC:POPG + x% Mini-B
Control
1% MiniB
5% MiniB
(D)
Area Under the Curve (*10⁻⁴ mN-m)
N

Fig 1: (A) *Surface pressure vs. area isotherm recorded for DPPC:POPG. Fig 1A displays multiple compression/expansion cycles to estimate the loss of material from the surface. A constant shift of the isotherm towards the lower area of trough suggests a loss in the material.* ***(B)*** *The area under the curve calculated from surface pressure vs. area isotherm for DPPC:POPG has been shown in Fig 1B. A drastic drop in the area was observed in this case.* ***(C)*** *Surface pressure vs. area isotherm recorded for DPPC:POPG with and without Mini-B: The figure shows multiple compression expansion for DPPC:POPG without (red solid) and with 1% (black dash) as well as 5% (blue dots) Mini-B. With Mini-B, the isotherms were elevated to higher values of surface pressure, which indicates the interaction of the protein with the lipids at the surface. Here, a comparable shift in the isotherms was observed with the addition of Mini-B.* ***(D)*** *The area under the curve calculated from surface pressure vs. area isotherm for DPPC:POPG with 1% (black circle), 5% (blue triangle) and without (red square) Mini-B. The addition of Mini-B shows reversibility similar to that of the DPPC:POPG control surface.*

In the case of DPPC:POPG by itself, we see a formidable loss of material, and a substantial shift of the isotherm towards the lower areas. Further analysis of this loss is represented in Fig 1B, which depicts the area under the curve for each cycle of the isotherm. The first cycle has an area of about 0.35 mN-m, whereas, the second cycle shows a considerable drop in the area to 0.14 mN-M. The subsequent cycles continue to lose material from the surface. Finally, the fifth cycle has an area of 0.05 mN-m. Therefore, from an initial value of 0.35 mN-m, the area drops to 0.05 mN-m, which is an 85% reduction of the area from the first cycle to the fifth cycle. Even from the second cycle to the fifth cycle, there has

been a reduction of about 64% in the area under the curve. Mini-B was then added to DPPC:POPG.

Fig 1C demonstrates multiple cycle isotherms of DPPC:POPG without and with two different concentrations of Mini-B added to the phospholipid mixture. When Mini-B is added, the first cycle for both 1% and 5% shifts to higher areas of the trough. This suggests an interaction of the protein with the phospholipid at the air/water interface. As expected, both the mixtures shows promising results when it comes to lowering the surface tension. After compression, samples containing Mini-B reaches high values of surface pressure, similar to that of the control. For all the samples tested, Fig 1D compares the area under the curve for each cycle. It can be observed that the area under the curve remains the same for all the samples.

4.4.2. ISOTHERM: DPPC:POPC with and without Mini-B

Fig 2A represents the surface pressure versus tough area isotherms of the model mixture DPPC:POPC without Mini-B (control). Here too, the sample is added at a higher trough area and gradually compressed to the lowest area available. Like DPPC:POPG, DPPC:POPC also goes through changes in phase at the surface. Notably, a plateau appears at a surface pressure of about 45 mN/m. This plateau suggests a distinctive collapse of the POPC component of the monolayer, which is known to collapse at surface pressures around 45-50 mN/m. Collapse of the unsaturated POPC lipids causes the film remaining back

at the air/water interface to be DPPC rich. Again, since the primary component is DPPC, this model mixture is also capable of reaching high surface pressure values. Here, multiple cycles do shift the isotherm to lower trough areas. Further analysis with area under the curve, represented by Fig 2B, reveals an area of 0.25 mN-m. With the second cycle, the value in the area decreases to about 0.15 mN-m. Finally, after the fifth cycle, DPPC:POPC has an area of 0.1mN-m. Thus, DPPC:POPC records a 60% reduction in area under the curve from first cycle to the fifth.

Fig 2C shows the multiple compression/expansion cycles of DPPC:POPC without and with Mini-B. At higher trough areas, the isotherms overlaps in the case of DPPC:POPC. However, upon compression, the samples containing 1% and 5% Mini-B both show improvement in surface activity. Furthermore, while the mixture with 1% Mini-B has a similar area under the curve as the control, the multiple cycle isotherms 5% indicate improvement in the reversibility of the monolayer.

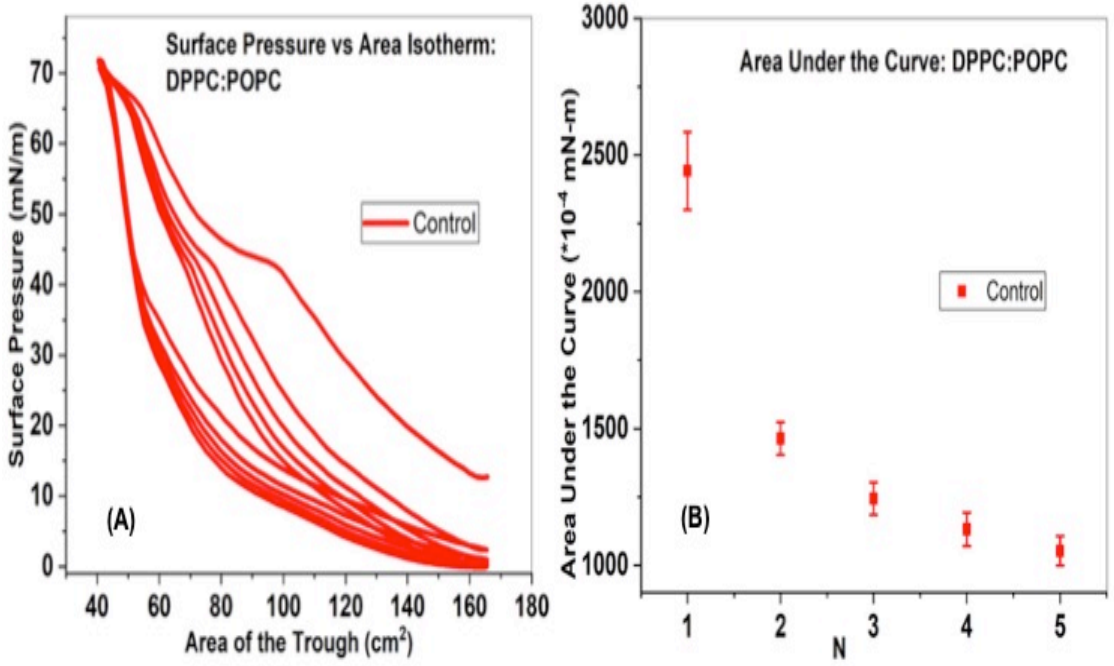
Surface Pressure vs Area Isotherm:
DPPC:POPC
Control
(A)
Surface Pressure (mN/m)
Area of the Trough (cm²)
Area Under the Curve: DPPC:POPC
Control
(B)
Area Under the Curve (*10⁻⁴ mN-m)
N

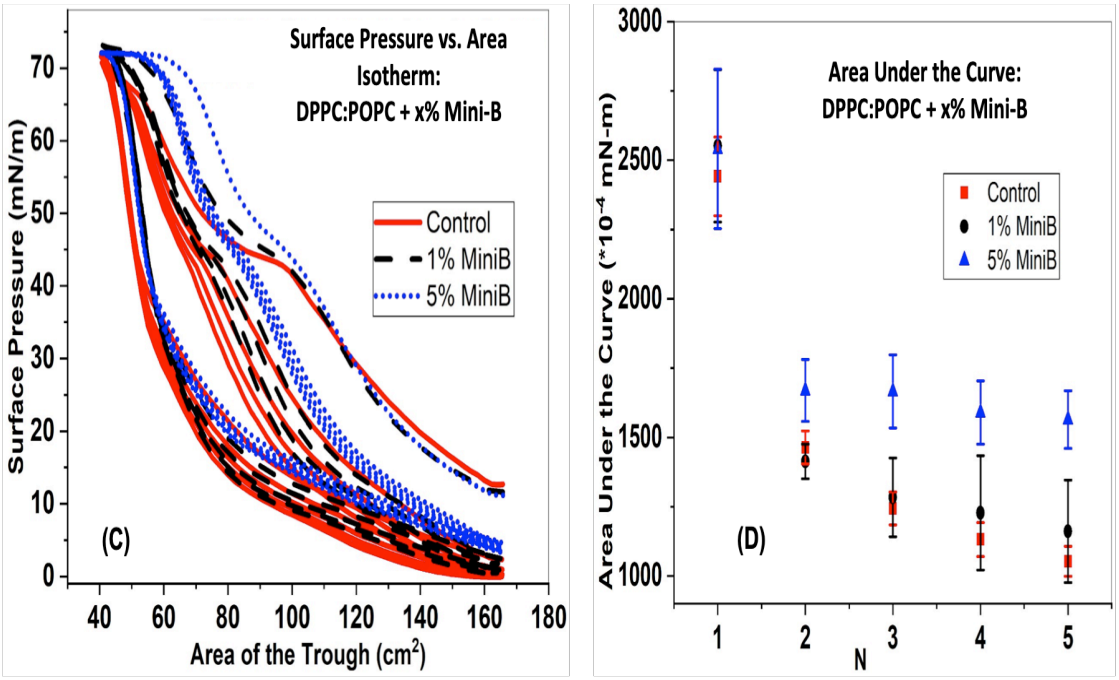
Surface Pressure vs. Area
Isotherm:
DPPC:POPC + x% Mini-B
Control
1% MiniB
5% MiniB
(C)
Surface Pressure (mN/m)
Area of the Trough (cm²)
Area Under the Curve:
DPPC:POPC + x% Mini-B
Control
1% MiniB
5% MiniB
(D)
Area Under the Curve (*10⁻⁴ mN-m)
N

Fig 2: (A) *Surface pressure vs. area isotherm recorded for DPPC:POPC: The figure exhibits multiple cycles of compression and expansion. A constant shift of the isotherm towards a lower area of trough suggests a loss in the material.* ***(B)*** *The area under the curve for DPPC:POPC: A constant drop in the area was observed for DPPC:POPC compression/expansion cycles. However, the reduction in material from the surface is less than that of DPPC:POPG represented in Fig 1.* ***(C)****. Surface pressure vs. area isotherm recorded for DPPC:POPC with and without Mini-B. The figure displays compression and expansion cycles for DPPC:POPC without (red solid) and with 1% (black dash) as well as 5% (blue dots) Mini-B. Again, with Mini-B, the isotherms were elevated to higher values of surface pressure, which indicates the interaction of the protein with the lipids at the surface. 1% Mini-B had a similar loss to that of the control. However, 5% Mini-B showed less reduction of material from the surface.* ***(D)*** *The area under the curve calculated for DPPC:POPC without (red square) and with 1% (black circle) and 5% (blue triangle) Mini-B. DPPC:POPC with 5% Mini-B shows improvement in material retention. In the case of control, there was a 57% reduction in the area under the curve, whereas, in the case of DPPC:POPC with 5% Mini-B around 38% reduction in the area.*

This improvement is more apparent with the area under the curve analysis as can be seen in Fig 2D. Initial areas overlap for both control and 5% Mini-B. However, DPPC:POPC with 5% Mini-B has an area of 0.16 mN-m at the fifth cycle, whereas, DPPC:POPC control has an area of 0.1 mN-m. Thus a 37% difference on the average is seen for the fifth cycle. Moreover, while our results show a shift in the curve and decrease in the area under the curve between the first and second cycles, the subsequent cycles overlap for lipid systems containing 5 wt. % protein.

4.4.3. COMPRESSIBILITY MODULUS: DPPC:POPG with and without Mini-B

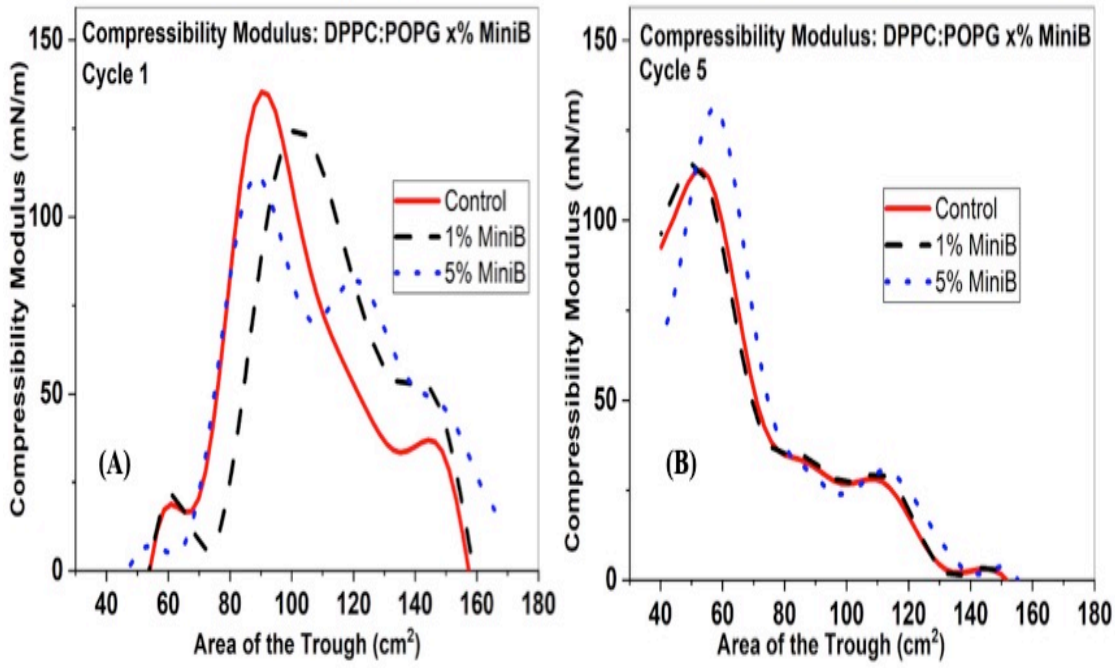

Fig 3: *Compressibility modulus vs. area of the trough for DPPC:POPG without and with varying concentrations of Mini-B.* ***(A)*** *The figure displays the compressibility modulus of the first compression cycle. The red line indicates DPPC:POPG without Mini-B. The dashed line shows the compressibility curve for DPPC:POPG with 1% Mini-B, whereas the dotted line represents the compressibility curve for DPPC:POPG with 5% Mini-B. Addition of Mini-B lowers the compressibility for the first cycle.* ***(B)*** *The compressibility modulus of the fifth cycle of compression has been shown in fig 5B. The compressibility modulus remains the same for 1% and control. However, 5% Mini-B shows an increase from the control.*

Fig 3A plots the compressibility modulus for the first compression cycle for the model DPPC:POPG system. At 150 cm^2 we observe a short peak of 45 mN/m for the control. Beyond this, there is a sharp rise, and the highest peak at 140 mN/m is observed around 87 cm^2. With 1% Mini-B, the shorter peak appears at the same area of the trough as that of the control. However, there is an increase in the compressibility value to 55 mN/m for the 1% Mini-B. The highest peak for 1% can be seen around 105 cm^2. The peak compressibility, corresponding to monolayer collapse, is lower for the 1% Mini-B than that of the control. In the case of the 5% Mini-B, the highest peak is again lower than that of the control. Fig 3B shows the compressibility modulus for the fifth compression cycle. Here, the plot for the 1% Mini-B with DPPC:POPG overlaps with that of the control. The peak for both 1% and control is at 110 mN/m. However, for the fifth cycle, the peak is around 135 mN/m for the 5% sample.

4.4.4.COMPRESSIBILITY MODULUS: DPPC:POPC with and without Mini-B

Fig 4A shows the compressibility modulus for the first cycle of DPPC:POPC with and without Mini-B. For the control, the first peak of 60 mN/m is observed at 120 cm^2 of the trough area. A second peak of 50 mN/m is seen at 60 cm^2. When 1% and 5% Mini-B is added to DPPC:POPC, both the peaks are higher than that of the control. Fig 4B plots the compressibility modulus of the fifth cycle. Here too, both 1% and 5% Mini-B shows an increase in the compressibility over that of the control.

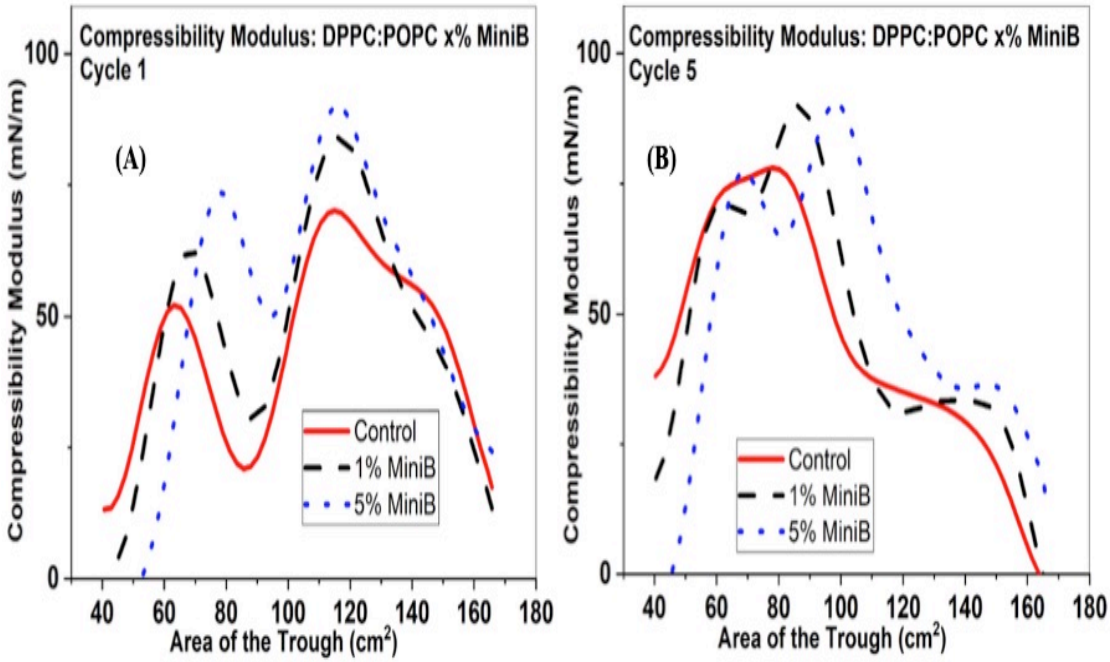

Fig 4: *Compressibility modulus vs. area of the trough for DPPC:POPC without (red solid) and with 1% (black dash) and 5% (blue dots) Mini-B.* ***(A)*** *The compressibility modulus of the first compression cycle has been plotted in Fig 4A. Addition of Mini-B to DPPC:POPC increases the compressibility for the first cycle.* ***(B).*** *The compressibility modulus of the fifth cycle of compression has been shown in fig 5B. The compressibility modulus remains the same for 1% and control. However, 5% Mini-B shows an increase from the control.*

4.4.5. FLUORESCENCE MICROGRAPHS

Fig 5(A-F) puts forward the fluorescence micrographs taken at the collapse pressure of both DPPC:POPG and DPPC:POPC without and with Mini-B. At higher surface pressures, the phospholipid mixtures go through collapse. Fig 5A represents the collapse image of DPPC:POPG control. The image is primarily dark as the monolayer is tightly packed. However, a bright streak, which is a common feature for collapse, runs across the image. The monolayer in the solid phase folds along that streak. With the addition of Mini-B, given in Fig 5B and 5C, the width of the fold increases. These giant collapses are thought to hold phospholipid close to the surface, such that, they can reincorporate within the monolayer with expansion. Fig 5D, for DPPC:POPC control, on the contrary, collapses with the formation of vesicles, which appears as bright specs instead of the bright streaks. Fig 5E and 5F represent the collapse of monolayers containing DPPC:POPC with 1% Mini-B and DPPC:POPC with 5% Mini-B. In both the cases, the monolayer collapses with the formation of vesicles. Similar to the fig 5D, these vesicles appear as bright specs under the fluorescence microscope.

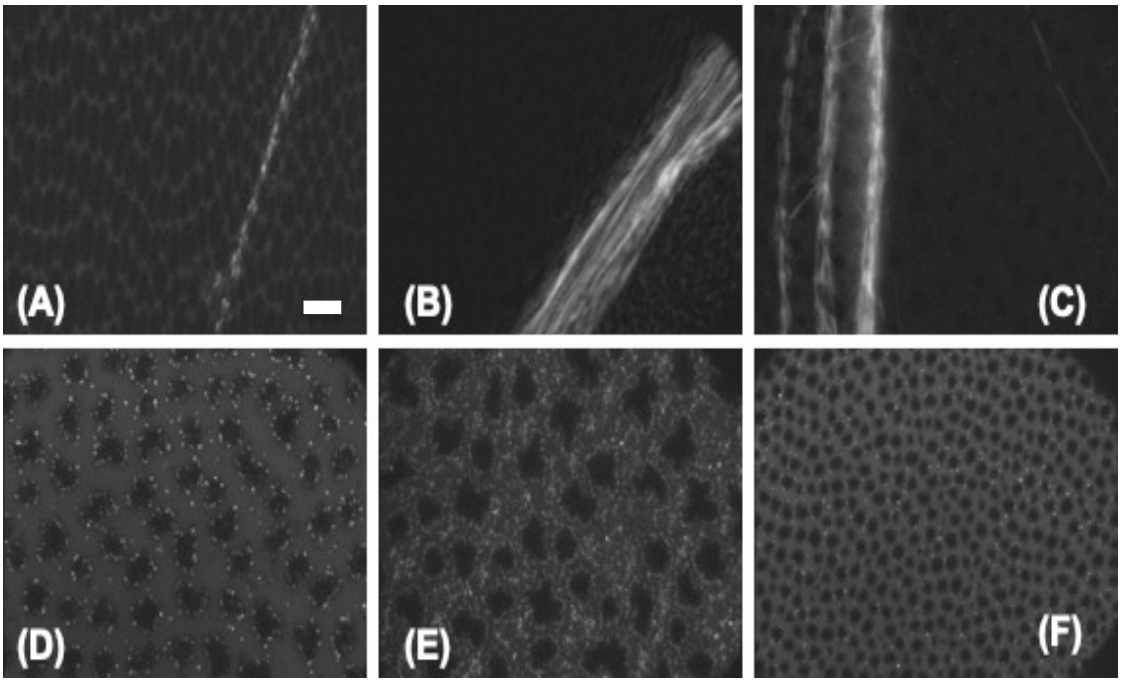

Fig 5: *Images taken at the collapse pressure for (A) DPPC:POPG (7:3) control, (B) DPPC:POPG (7:3) with 1 % Mini-B, (C) DPPC:POPG (7:3) with 5% Mini-B, (D) DPPC:POPC (7:3) control, (E) DPPC:POPC (7:3) with 1% Mini-B and (F) DPPC:POPC (7:3) with 5% Mini-B. Increasing concentration of Mini-B with DPPC:POPG shows the formation of folded collapse features. In the case of DPPC:POPC without or with Mini-B, collapse occurs with the formation of vesicles, which appear as bright dots. The scale bar shown in fig 5A represents 10 µms.*

4.4.6. ATOMIC FORCE MICROGRAPHS

Fig 6(A-D) represents the Atomic force images of the monolayers transferred at 20 mN/m. At this surface pressure, both DPPC:POPG (Fig 6A) and DPPC:POPC (Fig 6C) monolayers are biphasic, i.e., covered by regions containing liquid-expanded phase as well as liquid-condensed phase. The liquid-condensed region is made up of the well-packed DPPC, whereas the liquid-expanded part contains the unsaturated phospholipid. In the AFM images, the lighter color represents taller features on the monolayer. The uniformly raised region is the liquid-condensed part and the increased height results from the alignment of the lipid tail. The rest of the monolayer consists of the liquid-expanded region containing the unsaturated lipids. When comparing the controls for the two lipid systems, we observe the liquid-expanded region of DPPC:POPG monolayer is more packed than that of the DPPC:POPC monolayer. Additionally, in the case of DPPC:POPG the protein inserts itself in the liquid-expanded region, which is observed as the raised feature in fig 6B. However, in the case of DPPC:POPC with 5% Mini-B (fig 6D), the protein inserts itself in both the liquid-expanded region and the boundaries of the liquid-condensed domains.

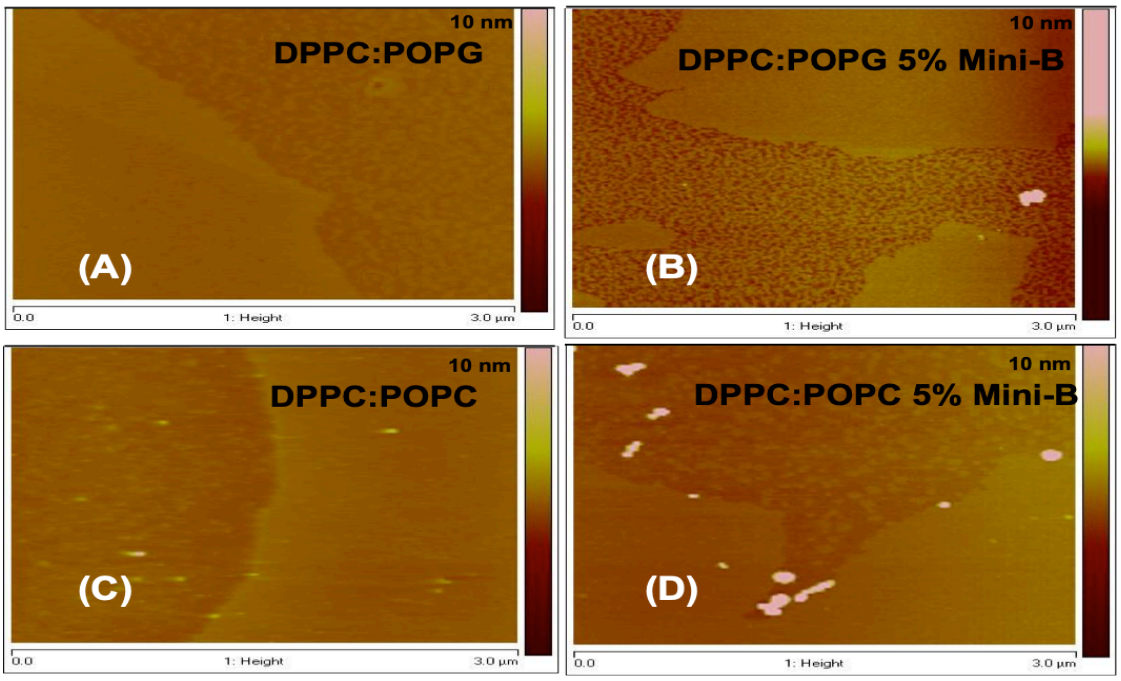

Fig 6: *Atomic Force Micrographs taken at 20 mN/m for* ***(A)*** *DPPC:POPG (7:3) control,* ***(B)*** *DPPC:POPG 5% Mini-B,* ***(C)*** *DPPC:POPC (7:3) control, and* ***(D)*** *DPPC:POPC 5% Mini-B: Here, the height of the monolayer has been indicated by varying shades of color with lighter areas representing higher values. The lighter region is the liquid condensed domain, which is marked by a sharp boundary. Beyond this boundary lies the liquid expanded domain. The lipid here is more scattered containing darker regions in between. These darker regions do not contain any material. In the case of DPPC:POPG, the liquid expanded region has more lipid than that of DPPC:POPC. In figure (B) and (D) the features shown in pink are Mini-B, which demonstrates the insertion of protein at the interface.*

4.5. DISCUSSION

Our research has been motivated by the need to evaluate the role of phospholipid headgroups while interacting with the synthetic surfactant protein, Mini-B. Till date, various compositions of phospholipids have been proposed to serve as model lung surfactant mixtures. The most simplistic models have contained only a single component of the surfactant phospholipids, namely, DPPC [20, 21], or a mixture containing DPPC and surfactant proteins along with it [22, 23]. However, such minimalistic models fail to function adequately owing to the gross omission of the necessary components of the naturally occurring surfactants. Therefore, multiple lipid components are now often introduced to mimic the natural lung surfactants, and this increase in complexity is accomplished using binary mixtures of phospholipids. The properties of the mixtures can then be varied according to the charge and saturation of the phospholipids in use. Models containing both saturated phospholipids have been occasionally used for mimicking the natural surfactants. Since the negatively charged PG lipids form an important part of the native pool, PG lipids have been introduced along with DPPC to serve as models. Thus, binary saturated mixtures of DPPC:DPPG have been used as model candidates [24-26]. However, almost fifty percent of the naturally occurring lung surfactants consist of unsaturated lipids. Therefore, entirely saturated mixtures are not capable of mimicking the functions of the complex surfactants. On the other hand, mixtures containing unsaturated lipids added to the saturated ones form an improved mimic of the native surfactants. DPPC:POPG is one such recurrent combination, where

POPG incorporates both unsaturation and negative charge [27-31]. However, the concentration of PG in the natural mixture is less compared to that of PC. Consequently, some studies have focused on preparing model mixtures that are entirely composed of the PC headgroup. Olżyńska *et al.* studied the structural characteristics of the DPPC:POPC monolayers through comparing Langmuir experiments with Molecular Dynamics simulations [32]. Additionally, Rose *et al.*, also examined the surface properties of different combinations of lipid mixtures, which included the potential candidate DPPC:POPC through Molecular Dynamics simulation [33]. Ternary mixtures comprising of DPPC:POPC:POPG has also been proposed as models for lung surfactants [34]. Thus, different phospholipid mixtures have been used alongside surfactant proteins to prepare formulations for surfactant replacement therapy. On that account, it has become essential to understand the biophysical nature of the interaction of the different lipid mixtures with synthetic proteins. So far, the interplay of the surfactant proteins with the anionic PG headgroup has been discussed in great details [14, 35]. Specifically, it has been hypothesized that the formation of reversible collapse folds, that are enabled due to the presence of anionic PG lipids, are essential for improved reversibility of the material lost from the interface during monolayer collapse. Here, we focus on the collapse and reversibility of both the anionic, DPPC:POPG and the zwitterionic, DPPC:POPC. The primary aim here is to compare the contribution of POPC and POPG. The results from Langmuir experiments combined with Fluorescence imaging and Atomic Force Microscopy, suggests that the material should not only collapse reversibly but also readsorb

quickly to the interface. The following sub-sections discuss the data in further details.

4.5.1. Reversibility of the monolayers through Langmuir Isotherms: Interaction with the anionic mixture: Multiple cycles of isotherms were used to understand the reversibility of the monolayers. The compression/expansion cycle of an entirely reversible monolayer would overlap with every preceding cycle. Any deviation to lower areas of the trough indicates irreversibility and thereby, loss in the material. The isotherms of DPPC:POPG (Fig 1A), in our study, show poor reversibility. This data is similar to the study by Holten-Anderson *et al.*, where the third compression/expansion cycle of DPPC:POPG shifts largely to lower areas of the trough [31]. Additionally, Holten-Anderson reports on the interaction of the peptide KL_4, which is a synthetic analog of SP-B, with DPPC and POPG at the air-water interface. Addition of KL_4, leads to the reversible folding of the monolayer along with an increase in the surfactant robustness when compressed and expanded repeatedly. KL_4 interacts specifically with the anionic POPG, and subsequently, induces the reversible folds in the monolayer, as can be seen through the fluorescent micrographs. The formation of similar reversible folds in the presence of anionic lipids has also been observed with the native surfactant protein, SP-B [14]. The synthetic protein Mini-B used in our study is a functional fragment of SP-B [18]. Having the same positive net charge as that of SP-B, Mini-B is similarly adept at interacting with the negatively charged lipid mixtures, thereby, producing the giant reversible folds, which has

been reported earlier and represented in Fig 7B and 7C [36]. However, at the concentrations (1% and 5%) tested in this study, Mini-B did not show any improvement in the reversibility, when compared to that of DPPC:POPG after five cycles of compression/expansion (Fig 3B). Furthermore, an improvement in the compressibility of the monolayer was only noted for the 5% Mini-B after five cycles of compression/expansion.

4.5.2. Reversibility of the monolayers through Langmuir Isotherms: Interaction with the zwitterionic mixture: As discussed earlier, the zwitterionic lipids form a significant component of naturally occurring lung surfactants. In the case of human surfactants, PC and PG exists at a ratio of 4:1 [37]. However, unlike the anionic counterpart [28], the collapse and reversibility of the binary monolayers containing both saturated and unsaturated PC have not been tested extensively. The isotherms reported in Fig 2A shows that the reversibility of the zwitterionic mixture on its own is superior to that of DPPC:POPG. Vesicles in the form of bright spots (Fig 7D) were observed under the microscope instead of giant folds in the case of DPPC:POPC. The reversibility of the compression/expansion cycles of DPPC:POPC indicates that these vesicles remain close to the interface, and upon the expansion of the monolayer, the vesicles get readsorbed to the surface. Gopal *et al.* showed the formation of budding vesicles when DPPC:POPG went under high compression at 30 ^{o}C [28]. These vesicles reportedly remained attached to the surface and reincorporated at the interface upon expansion. Therefore, it is quite possible that the zwitterionic mixture of DPPC:POPC collapses with the formation of budding

vesicles. One possible explanation for the rapid readsorption and respreading of the material is that the surface viscosity of DPPC:POPC monolayer is lower than that of the DPPC:POPG monolayer, which has been shown by Saba Ghazvini in her dissertation work [38]. Thus, lower viscosity perhaps makes the zwitterionic mixture more reversible than the anionic one. When Mini-B is added to the system, a similar route of collapse is seen, where, unlike producing the giant folds, Mini-B induces the formation of the budding vesicles. Furthermore, the area under the curve suggests that DPPC:POPC with 5% Mini-B is highly reversible (Fig 2B). Again, this enhanced reversibility with the addition of the protein is possible perhaps due to a quick readsorption and respreading of the material at the interface. Additionally, the compressibility modulus also indicates an overall improvement in the mechanical properties of the monolayer.

4.5.3. The topography of monolayers using Atomic Force Micrographs: Self-associated lung surfactant proteins, as well as multilayered structures for lung surfactants at the air/water interface, have been visualized in the past using atomic force microscopy [13, 39, 40]. In the absence of Mini-B, the monolayer is primarily flat for both DPPC:POPG and DPPC:POPC. Hane *et al.* had observed the formation of bilayer stacks when SP-C interacted with DPPC/egg PG mixture [40]. In the case of just the lipid mixture, the bilayer patches were rarely found and were also flatter. However, taller bilayer patches were observed with the addition of SP-C in the mixture. In our case, we observe the raised features when protein is added to either DPPC:POPG or DPPC:POPC mixtures. For DPPC:POPG, we observed fewer number of such features, whereas, a greater

number was seen in the case of DPPC:POPC. We speculate that these raised features are aggregates of protein that may reincorporate into the monolayer, thus making them more reversible. The presence of a greater number of such features in the case of the 5% Mini-B along with DPPC:POPC is then an indicator of enhanced reversibility of the mixture. Furthermore, the LE region is more packed for DPPC:POPG than the DPPC:POPC mixture. The difference in packing is probably an effect of the difference in the molar mass of the lipid headgroups. PG has a lower molar mass than that of PC, and therefore, packs more densely than PC. This contrast in the arrangement of the LE phase of the monolayer may also lead to dissimilarity in the reversibility.

Therefore, when considering the interaction of synthetic proteins with model lung surfactant mixtures, we must include the ability of the monolayers to collapse reversibly, along with their ability to adsorb and respread rapidly at the interface.

4.6. CONCLUSION

Our data addresses the role of lipid headgroup charge when interacting with Mini-B in terms of collapse and reversibility. Giant folds are considered as markers of the reversibility of lung surfactant monolayers. These giant folds when formed with surfactant protein, is believed to hold the collapsed lipids close to the surface, such that, upon expansion, the lipids can reincorporate themselves into the surface. Thus, the reversible mixtures help with material retention at the surface, and this feature is particularly important in the case of Surfactant

Replacement Therapy. However, our study shows that the neutral mixture, DPPC:POPC, is reversible even without the formation of the giant folds. DPPC:POPC along with 5% Mini-B proved to be substantially more reversible than the other samples tested in the report. These mixtures collapse via the formation of vesicles. But some of these vesicles stay close to the surface and upon expansion, reincorporates to the interface. Therefore, the reversibility of the sample is dependent on the ability of the surfactants to re-adsorb and re-spread, which is in turn, dependent on the viscosity of the material. Lower viscosity of DPPC:POPC mixtures allows the vesicles to quickly return to the surface and re-spread. The location of insertion of the protein also plays a part in modifying the viscosity of the mixtures. Thus, while considering the reversibility of phospholipid monolayers in the presence of synthetic proteins, the role of surface viscosity must also be considered along with the formation of giant folds.

4.7. REFERENCES

1. Daniels, C.B. and S. Orgeig, *Pulmonary Surfactant: The Key to the Evolution of Air Breathing.* Physiology, 2003. **18**(4): p. 151-157.
2. Wright, J.R., *Clearance and recycling of pulmonary surfactant.* American Journal of Physiology-Lung Cellular and Molecular Physiology, 1990. **259**(2): p. L1-L12.
3. Crouch, E. and J.R. Wright, *Surfactant Proteins A and D and Pulmonary Host Defense.* Annual Review of Physiology, 2001. **63**(1): p. 521-554.
4. Holmskov, U., S. Thiel, and J.C. Jensenius, *Collectins and Ficolins: Humoral Lectins of the Innate Immune Defense.* Annual Review of Immunology, 2003. **21**(1): p. 547-578.
5. Griese, M., *Pulmonary surfactant in health and human lung diseases: state of the art.* European Respiratory Journal, 1999. **13**(6): p. 1455.
6. Christmann, U., et al., *Role of Lung Surfactant in Respiratory Disease: Current Knowledge in Large Animal Medicine.* Journal of Veterinary Internal Medicine, 2009. **23**(2): p. 227-242.
7. Rugonyi, S., S.C. Biswas, and S.B. Hall, *The biophysical function of pulmonary surfactant.* Respiratory Physiology & Neurobiology, 2008. **163**(1): p. 244-255.
8. L. A. J. M. Creuwels, L.M.G.v.G., H. P. Haagsman, *The Pulmonary Surfactant System: Biochemical and Clinical Aspects.* Lung, 1997. **175**(1): p. 1-39.

9. Weaver, T.E. and J.J. Conkright, *Function of Surfactant Proteins B and C.* Annual Review of Physiology, 2001. **63**(1): p. 555-578.

10. Lee, K.Y.C., *Collapse Mechanisms of Langmuir Monolayers.* Annual Review of Physical Chemistry, 2008. **59**(1): p. 771-791.

11. M. M. Lipp, K.Y.C.L., D. Y. Takamoto, J. A. Zasadzinski, A. J. Waring, *Coexistence of Buckled and Flat Monolayers.* Phys. Rev. Lett., 1998. **81**(9): p. 1650-1653.

12. Schief, W.R., et al., *Liquid-Crystalline Collapse of Pulmonary Surfactant Monolayers.* Biophysical Journal, 2003. **84**(6): p. 3792-3806.

13. Ding, J., et al., *Effects of Lung Surfactant Proteins, SP-B and SP-C, and Palmitic Acid on Monolayer Stability.* Biophysical Journal, 2001. **80**(5): p. 2262-2272.

14. Takamoto, D.Y., et al., *Interaction of Lung Surfactant Proteins with Anionic Phospholipids.* Biophysical Journal, 2001. **81**(1): p. 153-169.

15. Ding, J., et al., *Nanostructure Changes in Lung Surfactant Monolayers Induced by Interactions between Palmitoyloleoylphosphatidylglycerol and Surfactant Protein B.* Langmuir, 2003. **19**(5): p. 1539-1550.

16. Robert V. Diemel, M.M.E.S., Alan J. Waring, *Multilayer formation upon compression of surfactant monolayers depends on protein concentration as well as lipid composition. An atomic force microscopy study.* The Journal of biological chemistry, 2002. **277**(24): p. 21179-21188.

17. Waring, A.J., et al., *The role of charged amphipathic helices in the structure and function of surfactant protein B.* The Journal of Peptide Research, 2005. **66**(6): p. 364-374.

18. Sarker, M., et al., *Structure of Mini-B, a Functional Fragment of Surfactant Protein B, in Detergent Micelles.* Biochemistry, 2007. **46**(39): p. 11047-11056.

19. Walther, F.J., L.M. Gordon, and A.J. Waring, *Design of Surfactant Protein B Peptide Mimics Based on the Saposin Fold for Synthetic Lung Surfactants.* Biomedicine Hub, 2016. **1**(3): p. 3-3.

20. McConlogue, C.W. and T.K. Vanderlick, *A Close Look at Domain Formation in DPPC Monolayers.* Langmuir, 1997. **13**(26): p. 7158-7164.

21. Grunder, R., et al., *Structures of surfactant films: a scanning force microscopy study.* European Respiratory Journal, 1999. **14**(6): p. 1290.

22. Kandasamy, S.K. and R.G. Larson, *Molecular Dynamics Study of the Lung Surfactant Peptide SP-B1–25 with DPPC Monolayers: Insights into Interactions and Peptide Position and Orientation.* Biophysical Journal, 2005. **88**(3): p. 1577-1592.

23. Holm, B.A., et al., *Content of Dipalmitoyl Phosphatidylcholine in Lung Surfactant: Ramifications for Surface Activity.* Pediatric Research, 1996. **39**: p. 805.

24. Nag, K., et al., *Fluorescently labeled pulmonary surfactant protein C in spread phospholipid monolayers.* Biophysical Journal, 1996. **71**(1): p. 246-256.

25. Amrein, M., A. von Nahmen, and M. Sieber, *A scanning force- and fluorescence light microscopy study of the structure and function of a model pulmonary surfactant.* European Biophysics Journal, 1997. **26**(5): p. 349.

26. von Nahmen, A., et al., *The structure of a model pulmonary surfactant as revealed by scanning force microscopy.* Biophysical Journal, 1997. **72**(1): p. 463-469.

27. Zhang, H., et al., *Comparative study of clinical pulmonary surfactants using atomic force microscopy.* Biochimica et Biophysica Acta (BBA) - Biomembranes, 2011. **1808**(7): p. 1832-1842.

28. Gopal, A. and K.Y.C. Lee, *Morphology and Collapse Transitions in Binary Phospholipid Monolayers.* The Journal of Physical Chemistry B, 2001. **105**(42): p. 10348-10354.

29. Koppenol, S., et al., *The interaction of lung annexin I with phospholipid monolayers at the air/water interface.* Biochimica et Biophysica Acta (BBA) - Biomembranes, 1998. **1369**(2): p. 221-232.

30. Pocivavsek, L., et al., *Lateral stress relaxation and collapse in lipid monolayers.* Soft Matter, 2008. **4**(10): p. 2019-2029.

31. Holten-Andersen, N., et al., *KL_4 peptide induces reversible collapse structures on multiple length scales in model lung surfactant.* Biophysical journal, 2011. **101**(12): p. 2957-2965.

32. Olżyńska, A., et al., *Mixed DPPC/POPC Monolayers: All-atom Molecular Dynamics Simulations and Langmuir Monolayer Experiments.* Biochimica et Biophysica Acta (BBA) - Biomembranes, 2016. **1858**(12): p. 3120-3130.

33. Rose, D., et al., *Molecular dynamics simulations of lung surfactant lipid monolayers.* Biophysical Chemistry, 2008. **138**(3): p. 67-77.

34. Diemel, R.V., et al., *Effects of Cholesterol on Surface Activity and Surface Topography of Spread Surfactant Films.* Biochemistry, 2002. **41**(50): p. 15007-15016.

35. Ma, J., et al., *Effects of a Cationic and Hydrophobic Peptide, KL4, on Model Lung Surfactant Lipid Monolayers.* Biophysical Journal, 1998. **74**(4): p. 1899-1907.

36. Chakraborty, A., et al., *Combined effect of synthetic protein, Mini-B, and cholesterol on a model lung surfactant mixture at the air–water interface.* Biochimica et Biophysica Acta (BBA) - Biomembranes, 2016. **1858**(4): p. 904-912.

37. Postle, A.D., E.L. Heeley, and D.C. Wilton, *A comparison of the molecular species compositions of mammalian lung surfactant phospholipids.* Comparative Biochemistry and Physiology Part A: Molecular & Integrative Physiology, 2001. **129**(1): p. 65-73.

38. Ghazvini, S., *Lipid and protein interactions at air-water interface: correlating structural organization with rheological properties*, in *Bioengineering*. 2017, the University of Kansas: Lawrence, Kansas, USA. p. 171.

39. Ruano, M.L., et al., *Comparison of lipid aggregation and self-aggregation activities of pulmonary surfactant-associated protein A.* The Biochemical journal, 1996. **313 (Pt 2)**(Pt 2): p. 683-689.

40. Hane, F., et al., *Effect of SP-C on surface potential distribution in pulmonary surfactant: Atomic force microscopy and Kelvin probe force microscopy study.* Ultramicroscopy, 2009. **109**(8): p. 968-973.

Chapter 5: Summary, Conclusion and Future Directions

5.1.SUMMARY, CONCLUSION & FUTURE DIRECTIONS

This thesis discusses three primary interactions related to lung surfactant research at the air-water interface. These interactions have been presented as three separate chapters.

5.1.1. Chapter 2: The second chapter categorically scrutinizes the interaction of ECN with lung surfactants. Besides being able to lower the surface tension to near zero values, material retention is another major property of the surfactants. Thus, the amount of surfactants retained at the surface in the presence of nanodiamonds has been made the critical focus of this chapter. The major findings include the influence of both lipid head group charge and tail saturation on the said properties when interacting with the nanodiamonds. Saturated lipid mixtures with an overall negative charge shows a positive outcome in terms of the mass retained at the surface when coming in contact with ECN. On the other hand, saturated mixture with a net neutral charge has no effect when ECN is present in the solution. However, the presence of lipid tail unsaturation has a negative outcome. Unsaturation combined with neutral mixture shows the most undesirable result. Therefore, we conclude that the presence of saturated, negatively charged lipids may prove to be beneficial when preparing formulations for drug delivery with engineered carbon nanodiamonds. This thesis primarily deals with binary mixtures coming in contact with the nanodiamonds. However, in the future, it might be lucrative to increase the complexity by preparing ternary lipid mixtures. Because the native surfactant is a cocktail of a variety of lipids and proteins, a ternary mixture may be a better representative of the natural surfactants. It would be interesting to observe the dynamics of the lipid-ECN interaction in the presence of such complex lipid mixtures. Additionally, surfactant

proteins may also be added to possibly counter the effect of nanodiamonds. Therefore, since this thesis reveals the importance of the composition of the surfactants when interacting with ECN, future studies should include the composition of the mixture as one of the key parameters for evaluating the said interaction.

5.5.2. Chapter 3: The third chapter focuses on the interaction of lipids with the synthetic protein Mini-B. Synthetic analogs of native surfactant proteins have been considered for the treatment of respiratory diseases. The synthetic alternatives provide an opportunity for both an increase in production of the replacement formulations as well as a reduction in any undesired impact. However, at the same time, the biophysical behavior of such components must closely mimic that of the native constituent. In this chapter too, the primary goal is to determine the impact of the composition of the surfactants along with Mini-B on material retention. The charge of the mixture plays a role in how the protein interacts with the lipids. Furthermore, with the help of Atomic Force Microscopy we show that a variation in charge of the lipid mixture alters the location of the protein insertion. The location where the protein inserts itself, in turn, may alter the surface properties of the monolayer, affecting the reversibility. Future studies should include more complex lipid mixtures to assess material retention at the air-water interface.

5.5.3. Chapter 4: The fourth chapter puts forward the interaction of Mini-B with cholesterol. Although cholesterol helps in fluidizing the surfactant mixture, it has been associated with diseases. Most commercial replacement surfactants are devoid of cholesterol. Thus, it is a disputed component of the native surfactant mixture. In this chapter, we show that Mini-B can counter the deleterious effects of cholesterol. Even though we see small quantities of cholesterol having noticeable detrimental effect on the

reversible collapse, line tension, and compressibility of the lung surfactants, 1 wt.% to 5 wt.% of Mini-B is capable of countering the negative impacts. In terms of material retention, higher concentration of Mini-B (5 wt.%) with smaller quantities of cholesterol (1 wt.%) had the least loss in material compared to other combinations of the two components. Therefore, our study indicates that small quantities of cholesterol along with the synthetic surfactant protein, Mini-B, may be used in surfactant replacement therapy. The fluidizing properties of cholesterol may be beneficial in preparing formulations that can easily cover the interface upon inhalation, and at the same time, the presence of surfactant protein will ensure that the surfactants are retained at the surface. Future objectives should look towards extending these findings to the lung cells for understanding the effectiveness of the said formulation.